People's Democratic Republic of Algeria
Ministry of Higher Education and Scientific Research
Mohamed El-Bachir El-Ibrahimi University of B.B.A

Faculty of Sciences and Technology
Department of Electromechanical Engineering

Doctoral Thesis LMD in Automation and Industrial Computing

Presented by:

Salah Eddine SAADI

Theme

Advanced Analysis and Robust Control for Chaotic Systems

Analyse Avancée et Commande Robuste des Systèmes Chaotiques

Publicly defended on: April 10th 2025

In front of the jury members:

IRATNI	Abdelhamid	Professor	University of Bordj Bou Arreridj	President
BOUCHAMA	Ziyad	Professor	University of Bordj Bou Arreridj	Supervisor
BEHIH	Khalissa	MCA	University of Setif 1	Co-supervisor
BENHENICHE	Abdelhak	MCA	University of Bordj Bou Arreridj	Examiner
BOUKHALFA	Abdelouahab	MCA	University of M'sila	Examiner

2024/2025

Abstract

Chaos control, chaos analysis, and chaotification in dynamical systems have received increasing attention from research communities and have been extensively studied. Recently, chaotic synchronization and chaotic systems with higher-dimensional attractors, known as hyperchaotic systems, have found a wide range of applications, receiving sustained and fervent attention across several fields. This work focuses primarily on the control, modeling, and synchronization of chaotic systems, using a new family of nonlinear control algorithms based on Lyapunov synthesis, terminal attractor theory, and fuzzy modeling, combined with recent amalgamations of robust control techniques, namely terminal sliding mode control and terminal synergetic control. First, an adaptive terminal sliding mode control law was developed and validated through simulations for controlling certain hyperchaotic systems. Then, fuzzy modeling and its combination with synergetic control were developed to provide a new algorithm for the synchronization of two different hyperchaotic systems. The final part of this work is devoted to the synchronization of chaotic systems using a new concept of terminal synergetic adaptive control. This approach aims to circumvent the drawback of asymptotic convergence in the design of the synergetic control law and to overcome various issues related to chaotic systems, including mathematical model accuracy, parametric uncertainties, and external disturbances, thus enabling easy real-time implementation of the control law. Simulation tests were conducted to assess the effectiveness of the proposed algorithms.

Keywords: nonlinear systems, chaotic systems, sliding mode control, synergetic control, fuzzy modeling, terminal control, finite-time convergence.

Résumé: Le contrôle du chaos, l'analyse du chaos ainsi que la chaotification dans les systèmes dynamiques ont reçu une attention croissante de la part des communautés de recherche et ont été étudiés de manière approfondie. Récemment, la synchronisation chaotique et les systèmes chaotiques avec des attracteurs de dimension supérieure, appelés systèmes hyperchaotiques, présentent un large spectre d'applications, faisant l'objet d'une attention soutenue et fervente dans plusieurs domaines. Dans ce travail, nous nous sommes principalement intéressés au contrôle, à la modélisation et à la synchronisation des systèmes chaotiques, en utilisant une nouvelle famille d'algorithmes de commande non linéaire basée sur la synthèse de Lyapunov, la théorie des attracteurs terminaux et la modélisation floue, combinée avec les récents amalgames des techniques de commande robuste, à savoir la commande par mode glissant terminale et la commande synergétique terminale. Dans un premier temps, une loi de commande adaptative par mode glissant terminale a été développée et validée par simulation pour la commande de quelques systèmes hyperchaotiques. Ensuite, la modélisation floue et sa combinaison avec la commande synergétique ont été élaborées pour fournir un nouvel algorithme de synchronisation de deux systèmes hyperchaotiques différents. La dernière partie de ce travail est consacrée à la synchronisation des systèmes chaotiques par un nouveau concept de commande adaptative synergétique terminale. Celle-ci vise à contourner l'inconvénient de la convergence asymptotique dans la conception de la loi de commande synergétique et à surmonter les différents problèmes liés aux systèmes chaotiques, notamment l'exactitude du modèle mathématique, les incertitudes paramétriques et les perturbations externes, permettant ainsi une implémentation facile de la loi de commande en temps réel. Pour évaluer l'amélioration effective apportée par ces algorithmes, des tests de simulation ont été effectués.

Mots clés : systèmes non linéaires, systèmes chaotiques, commande par mode glissant, commande synergétique, modélisation floue, commande terminale, convergence en temps fini.

ملخص: تحظى دراسة التحكم في الفوضى، وتحليل الفوضى، والفوضوية في الأنظمة الديناميكية باهتمام متزايد من قبل المؤسسات البحثية، وقد تم دراستها بشكل مكثف. وفي الآونة الأخيرة، وجدت المزامنة الفوضوية والأنظمة الفوضوية ذات الجاذبات والأبعاد العليا، والمعروفة بالأنظمة الفائقة الفوضى(hyperchaotic systems) ، مجموعة واسعة من التطبيقات، مما جعل لها اهتمامًا كبيرا عبر عدة مجالات. يركز هذا العمل بشكل أساسي على التحكم، والنمذجة، ومزامنة الأنظمة الفوضوية باستخدام مجموعة جديدة من الخوارزميات غير الخطية للتحكم، تعتمد على تحليل ليابونوف، ونظرية الجاذبات النهائية، والنمذجة الضبابية، بالإضافة إلى دمج تقنيات التحكم القوي الحديثة مثل التحكم الانزلاقي النهائي والتحكم التآزري النهائي. في البداية، تم تطوير قانون للتحكم التكيفي الانزلاقي النهائي وتم اختبار فعاليته من خلال المحاكاة للتحكم في بعض الأنظمة الفائقة الفوضى. بعد ذلك، تم الاعتماد على النمذجة الضبابية ودمجها مع التحكم التآزري لتطوير خوارزمية جديدة لمزامنة نظامين مختلفين فائقي الفوضى. تتناول الجزء الأخير من هذا العمل مزامنة الأنظمة الفوضوية من خلال مفهوم جديد للتحكم التكيفي التآزري النهائي. حيث يهدف هذا النهج إلى التغلب على عيب التقارب غير النهائي في تصميم قانون التحكم التآزري، والتغلب على المشاكل المختلفة المتعلقة بالأنظمة الفوضوية، بما في ذلك دقة النموذج الرياضي، والشكوك في المعاملات، والاضطرابات الخارجية، مما يسمح بالتنفيذ التطبيقي لقانون التحكم. تم إجراء اختبارات المحاكاة لتقييم فعالية الخوارزميات المقترحة في هذا العمل.

الكلمات المفتاحية: الأنظمة غير الخطية، الأنظمة الفوضوية، التحكم بالانزلاق، التحكم التآزري، النمذجة الضبابية، التحكم النهائي، التقارب في الزمن المحدود.

بسم الله الرحمن الرحيم

Acknowledgment

In The Name of Allah, The Most Beneficent, The Most Merciful. Praise be to Allah the Lord of the worlds and may the blessings and peace of Allah be upon the most honored of messengers our master Muhammad and upon all his family and companions.

I would like to share my heartful gratitude and indebtedness to my supervisor and guide Professor Ziad BOUCHAMA for his fruitful guidance and encouragement over the duration of my thesis work. I am very much appreciative of his persistent support and great help and for taking a keen interest in this thesis work. I would also like to thank Dr. Khalissa BEHIH for her help, support, valuable advice, and the occasional push when needed. I have been so happy to work with her on this project.

I would like to thank members of my thesis committee: Professor Abdelhamid IRATNI from the Electromechanics Department, University Mohamed El-Bachir El-Ibrahimi of Bordj Bou Arreridj, Dr. Abdelhak BENHENICHE from the Electromechanics Department, Mohamed El-Bachir El-Ibrahimi of Bordj Bou Arreridj, Dr. Abdelouahab BOUKHALFA from the Electrical Engineering Department, University of M'sila.

I express my profound gratitude to my father Mr. Lakhdar, my Mother Mrs. Khalissa CHIHI, my siblings Sara, Ghada, Habib Allah, Ishak and Yakoub, and my niece Israa for their love, encouragement, understanding, and devotion, for taking care of so many things, and for being there for me at all circumstances. I also would like to thank all members of my extended family and my friends for their encouragement.

Table of Contents

List of Figures

List of Tables

General Introduction

Chaos analysis and chaos control in dynamical systems have been studied broadly and have gained significant interest from research communities. Chaotic behavior can be observed in a range of simple systems [1], in which even a small variation in a single parameter can rise to a behavior indicative of that of complex nonlinear systems. It is an unpredictable system and its trajectories are extremely sensitive on initial conditions [2]. We find that chaos has a broad spectrum of applications in many fields such as cryptography and information processing, biomedical science, laser physics, chemical and electrical engineering [3]–[7]. Due to the fact that nonlinear differential equations rarely have general solutions, this thesis focuses on qualitative methods that reveal chaotic phenomena arising from nonlinear equations and estimate parameters related to stability, periodicity, and chaotic behavior without solving the equations. The objective of chaos control can be divided into two classifications: enhancing or producing chaos when it is desired, and suppressing chaotic behavior when it could be harmful, [8].

Over the past few decades, control techniques for linear and nonlinear dynamical systems have been developed to achieve specific design purposes such as output regulation, local or global stabilization, and synchronization [9]–[12]. When designing controllers, it is frequently important to assume that the system parameters are accurately known. Nevertheless, in numerous control problems, the model parameters could be uncertain. A linear controller based on absolute or inaccurate model parameter's values could encounter considerable degradation in performance or even instability. To deal with model uncertainty, nonlinearities can be intentionally incorporated into the controller function of a control system [13]. There are basically two types of nonlinear controllers for this purpose, which are robust controllers and adaptive controllers. Therefore, efficient control approaches are required to deal with the system's nonlinearity, uncertainty and external disturbance. Various researchers have used hybrid control techniques to benefit from the resulting combination of the advantages of the both approaches [14], [15].

This thesis hands over the lecturer with a wide collection of material from linear dynamic principles such as state-space methods and system stability up to chaos theory and robust control techniques. This work is divided and structured into four chapters.

The objective of the first chapter is to introduce a variety of basic techniques from the dynamical systems theory in a setting as simple as possible. This chapter will provide the fundamentals of the theory of dynamical systems and will serve as a main thrust to understand and

take the picture of what it means for a dynamical system to be chaotic. We start with a generalized 2-D linear system and its phase space analysis. The intuitive notion of stability is discussed based on eigen vectors and eigen values of linear systems, and Lyapunov stability theory. For nonlinear systems, the shift from one set of responses to another often occurs very suddenly as a parameter passes through a critical value, which is referred to as a bifurcation point [16]. Therefore, we shall look at some of the elementary basic properties of bifurcations.

Convergence to an equilibrium point or divergence to infinity are not the only cases in which a nonlinear system can behave; It could include a plenty of possibilities of various degree of complexity of asymptotic stabilities behavior. Limit cycles are important in systems that exhibit self-sustained oscillation and periodic solutions even in the nonexistence of external periodic forcing [2]. Once we have addressed almost completely the dynamical characteristics and properties of nonlinear systems, we can proceed on the topic of chaotic attractors, which have a structure more complicated than that of equilibrium points or periodic orbits. Chaotic orbits are unstable and remain in a restricted region of the state space, never reaching an equilibrium point or periodic point [2]. We start our investigation of chaos with the Lorenz system [17] by analyzing its equations and quantifying the stability and sensitivity to the initial conditions of the system using the Lyapunov Exponents concept. Then, we deal with a simple nonlinear map, which is the logistic map. It is one of the simplest systems, exhibiting order to chaos transition. We discuss the system's properties and analyze the period-doubling phenomenon that eventually leads to chaos. Finally, we give a glimpse of fractional-order chaotic systems that may be useful in future studies.

Nonlinear systems' control is an important subject matter in the field of control, which will be discussed in the second chapter. Modeling inaccuracies and external disturbances can have a significant negative impact on nonlinear control systems. Two major and complementary approaches to dealing with modeling uncertainty and external disturbances are robust control and adaptive control. In the design, we are provided with a nonlinear plant intended to be controlled and some prerequisites of closed-loop system comportment. Therefore, our objective is to design and build a controller that will ensure that the closed-loop system satisfies the desired characteristics. We shall start with a simple approach to robust control, which is named as sliding mode control methodology. In this chapter, we describe an introduction to the main concept and notations of sliding control and illustrate the associated basic controller design. Then we investigate finite-time sliding mode control, which has been applied and studied in many disciplines, giving upthrust to a robust control with adjustable finite-time convergence that provides high precision, fast response, and strong robustness [13]. We also state the synergetic control

approach, which will be investigated in the next chapter. In some control tasks, the system to be governed has parameter uncertainty at the control operation, which may result in inaccuracy or instability for the control system [18]. Therefore, an adaptive finite-time sliding mode control example for synchronizing two hyperchaotic systems will be stated to examine the robustness of the discussed approach.

The third chapter is about fuzzy logic, which is a rule-based system that can be utilized to find solutions to a vast scope of problems, from control, to judgment-making, to modeling, to classification, to forecasting, to diagnosis, etc. [19]. A rule-based system starts out with a particular set of such rules, which can be provided by the knowledge and expertise of the experts or extracted from data of a specific domain. The antecedents of a rule are terms of variables that can be measured or observed. Each rule provides information about a desired decision-making output. We begin with a little bit of history about Zadeh's approach [20] which is based on fuzzy algorithms and fuzzy sets, hands over a general method of expressing linguistic rules. Then we formally make the introduction of the most essential concept in fuzzy theory, which is the concept of fuzzy sets, and then the basic operations on fuzzy sets and linguistic variables. Fuzzy set theory generalizes the original subject matter of a set to allow varying degrees of belonging to the set, that range from complete membership down to full exclusion. To utilize fuzzy sets, a fuzzy rule base should be given and constructed in the first place. Just after the rules have been constructed, the phase that follows can be considered as a mapping of inputs to outputs. Different fuzzy inference techniques are used in fuzzy logic, where max-min and max-product are the most commonly used inference engines. Finally, computing the fuzzy system's output from different rule combinations is needed. A defuzzifier is utilized to calculate the system output through transforming a fuzzy set to a real-valued variable. This chapter will serve as an overview of fuzzy sets and fuzzy logic and as a foundation for how they can be applied to modeling nonlinear systems and control systems design. In addition, we present our contribution that is dedicated to designing a synergetic controller for synchronization purposes between two distinct chaotic systems. Where they are represented by Takagi-Sugeno fuzzy models. The proposed technique grants hyperchaos synchronization utilizing a simple structure, which facilitates simple implementation.

In the last chapter, synchronization and anti-synchronization of two distinct chaotic systems are investigated. Unlike many synchronization approaches for synchronization of chaotic systems based on an exact chaotic model, this chapter addresses the control problem when the exact parameter values are not available while simultaneously taking into consideration the external disturbance. An adaptive terminal convergence using robust synergetic control theory

is explored to achieve synchronization in a finite-time convergence. Furthermore, the synergetic control gain is adaptive and derived, based on the Lyapunov stability theory, to handle the synchronization error system nonlinear terms, the system uncertainty, and the external noise.

Chapter 1. An Overview of Nonlinear Dynamical Systems and Chaotic Systems

1.1 Introduction

A dynamical system is one whose state variables change and move through time. This is frequently achieved through the use of equations that link the variables' values at different, uniformly spaced instances of time [21]. Dynamical systems have two main types which are: differential equations for continuous-time dynamics and iterated maps for discrete-time dynamics. In science and engineering, the differential equations are much more widely used. Therefore, this work will be concerned with them. Also, we show that simple iterated maps are quite useful for exhibiting examples of chaos as well as analyzing periodic or chaotic behaviors.

Ordinary differential equations have a dependent variable, x, which is to be a function of the independent variable t, time variable, in other words $x = x(t)$. We will refer to the derivative of x with respect to time as $\dot{x}$, such that:

$$\dot{x} = \frac{dx}{dt} \tag{1.1}$$

When formulating the general theory of differential equations, it would be useful to establish a system of n first-order equations for n unknown functions $x_1(t),...,x_n(t)$. The following system is a general representation of ordinary differential equations

$$\begin{cases} \dot{x}_1 = f_1(x_1,...,x_n,t) \\ \quad \vdots \\ \dot{x}_n = f_n(x_1,...,x_n,t) \end{cases} \tag{1.2}$$

Here each $f_i(x_1,...,x_n,t)$ represents a defined function of $n+1$ variables, $x_1,...,x_n$ and t. If the right-hand side of the system (1.2) is explicitly dependent on the time variable t, then it is said to be non-autonomous; otherwise, it is said to be autonomous [2].

Furthermore, if every variable on the right-hand side appears to be the first power only, the system is said to be linear; otherwise, it is regarded to be nonlinear. The indicative nonlinear terms include: powers, products, and functions of the x_i. Nonlinear dynamical systems may exhibit distinctive and complex behavior. Therefore, it would be crucial to be cautious when addressing solutions to nonlinear differential equations.

1.2 Trajectories and Phase Portrait

Before dedicating ourselves and diving into chaos phenomena, we will first start with the planar dynamical system, which is a system with two state variables. To analyze nonlinear systems, we begin with an examination of the trajectories of the equation, the flows, and their equilibria in the vicinity of the equilibrium point in the plane. An examination of nonlinear systems' equilibrium points, by linearization around the equilibria's neighborhood, can reveal plenty of information about their qualitative behavior at that point. As a result, we shall commence with a study of the linear systems' phase portraits.

Let a linear system in the plane be in the following form

$$\dot{x} = Ax, \qquad x \in \Re^2 \tag{1.3}$$

The study of the eigenvalues of A will be a useful starting point to examine the system. Let's consider the similarity transformation $T \in \Re^{2\times 2}$, $T^{-1}AT = J$, which states the matrix A's real **Jordan** form. Let $y = T^{-1}x$, then, this coordinate transformation alters the system (1.3) to become the following form

$$\dot{y} = T^{-1}AT\, y = J\, y \tag{1.4}$$

The following three scenarios have qualitatively distinct properties

- *Real Eigenvalues*

$$J = \begin{bmatrix} \lambda_1 & 0 \\ 0 & \lambda_2 \end{bmatrix} \tag{1.5}$$

with $\lambda_1, \lambda_2 \in \Re$ produces the following formula for the relationship between y_1, y_2 from the formulas $y_1(t) = y_1(0)e^{\lambda_1 t}$, $y_2(t) = y_2(0)e^{\lambda_2 t}$ for the system dynamics:

$$\frac{y_1}{y_{10}} = \left(\frac{y_2}{y_{20}}\right)^{\frac{\lambda_1}{\lambda_2}} \tag{1.6}$$

Figure 1.1 depicts the phase portraits for the two scenarios that $\lambda_2 < 0 < \lambda_1$ and $\lambda_1, \lambda_2 < 0$, named a saddle and a stable node, respectively. It is crucial to note that the equation (1.6) stands for both scenarios, with the only difference being the exponent, $\frac{\lambda_1}{\lambda_2}$, is negative for the saddle node, which results in hyperbolic curves, and positive for the stable node, which produces parabolic curves, as illustrated in Figure 1.1. The arrows represent the progress of the

states y_1 and y_2 as time goes on. The stable node case has simple dynamics. All state variables decay and converge toward the origin. The opposite scenario will happen with the unstable node, that corresponds to the case $\lambda_1, \lambda_2 > 0$. All trajectories diverge and move exponentially away from the origin. The term saddle is specifically addressed when describing the dynamics at an equilibrium point that has one negative (stable) and one positive (unstable) eigenvalue. The unique scenario that which the states are asymptotically attracted to the origin is when the initial conditions of states are sitting on the axis of the stable eigenvector. All other initial conditions diverge asymptotically along the hyperbolas determined by the equation (1.6).

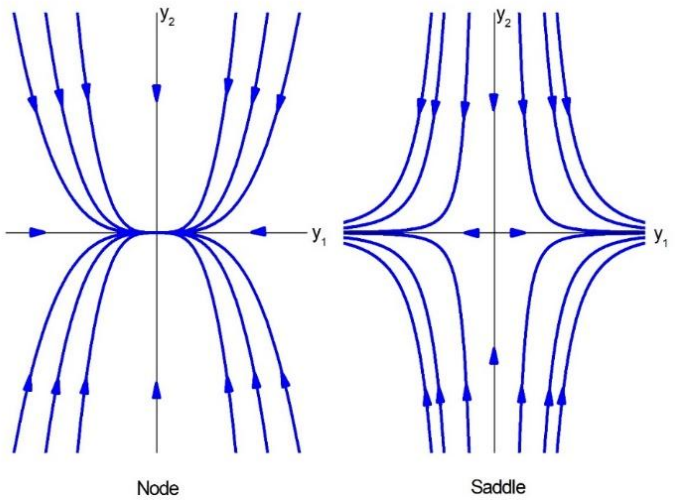

Figure 1.1 A stable node and a saddle-node representation in the y_1 and y_2 coordinates.

Due to the fact that the relationship between x and y is linear, the original x coordinates' phase portrait is slightly modified compared to Figure 1.1.

- *Double eigenvalue*

the Jordan form is not diagonal, due to only one eigenvector, but has the form

$$J = \begin{bmatrix} \lambda & 1 \\ 0 & \lambda \end{bmatrix} \tag{1.7}$$

Hence, the solution is of the form:

$$\begin{aligned} y_1(t) &= y_1(0)e^{\lambda t} + y_2(0)te^{\lambda t} \\ y_2(t) &= y_2(0)e^{\lambda t} \end{aligned} \tag{1.8}$$

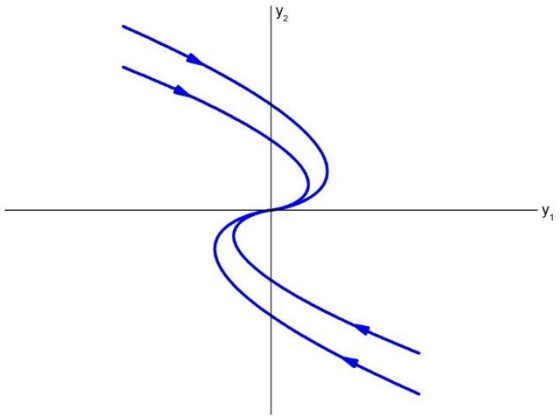

Figure 1.2 An irregular stable node.

We can easily observe that by eliminating the time term, t, the representation of the trajectories in the phase space plan is depicted in Figure 1.2 and is provided by

$$y_1 = \frac{y_{10}}{y_{20}} y_2 + \frac{1}{\lambda} \ln\left(\frac{y_2}{y_{20}}\right) \tag{1.9}$$

therefore, the state trajectories converge toward the origin as shown in Figure 1.2 in a more complex manner. This type of equilibrium point is commonly mentioned as an improper stable node. The improper node is referred to as improper unstable node when $\lambda > 0$.

- *Complex pair of eigenvalues*

Despite having distinct eigenvalues, the A matrix is not able to be diagonalized. Nevertheless, its real Jordan form is

$$J = \begin{bmatrix} \alpha & \beta \\ -\beta & \alpha \end{bmatrix} \tag{1.10}$$

Hence, the transformation matrix T is complex.

To determine the solutions for such cases, it would be convenient to render a polar transformation of coordinates. Therefore, we obtain the following form

$$r = \left(y_1^2 + y_2^2\right)^{1/2}, \quad \phi = \tan^{-1}\left(\frac{y_2}{y_1}\right) \tag{1.11}$$

In polar coordinates, the equations become

$$\begin{aligned} \dot{r} &= \alpha r \\ \dot{\phi} &= -\beta \end{aligned} \tag{1.12}$$

The phase portrait representations are now easier to visualize. ϕ, which is the angular variable, evolves at a steady rate. The trajectory rotates around in a counterclockwise direction if β is negative and clockwise otherwise. When $\alpha > 0$, the state trajectories spiral out from the origin, and the equilibrium is commonly referred to as an unstable focus. furthermore, if $a < 0$, the state trajectories spiral toward the origin in which case the equilibrium is called a stable focus. If the parameter α is zero, an infinite number of circular closed orbits surround the origin and the equilibrium is called as a center. When representing the original x coordinates, the phase portrait is rotated as in the examples of the discussed scenarios, node and saddle cases. Figure 1.3 shows a center and a stable focus.

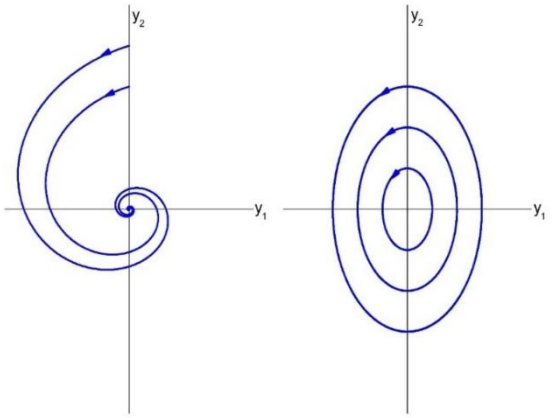

Figure 1.3 A stable focus and center.

1.3 Lyapunov Stability Theory

Let's consider an autonomous system

$$\dot{x} = g(x) \qquad x \in \Re^n \tag{1.13}$$

With an isolated equilibrium point x^* such that $g(x^*) = 0$. If an equilibrium point has a surrounding neighborhood containing no other equilibrium point is called an isolated equilibrium point [2]. Let $x(t)$ be the state of the system at time t, $x(0) = x_0$ the initial point and $\| \cdot \|$ denote the Euclidean distance in $\Re^n$. With this notation, we shall introduce the following definitions of stability.

Definition 1-1[22]:

1) The equilibrium point x^* is stated to be Lyapunov stable, or simply stable, if for any $\varepsilon > 0$ there is a number $\delta(\varepsilon) > 0$ such that if $\|x_0 - x^*\| < \delta$ leads to $\|x(t) - x^*\| < \varepsilon$ for all $t > 0$.

2) The equilibrium point x^* is said to be asymptotically stable if

(a). It is stable; and

(b). There exist an $\eta > 0$ such that whenever $\|x_0 - x^*\| < \eta$, $\lim_{t\to\infty}\|x(t) - x^*\| = 0$.

Definition 1-2 [23]**:**

Let D be a subset domain in $\Re^n$ that includes the origin and let $H : D \to R$ be a continuously differentiable function. The derivative of H along the trajectories of (1.13), referred by $\dot{H}(x)$, is defined by

$$\dot{H}(x) = \sum_{i=1}^{n} \frac{\partial H}{\partial x_i}\dot{x}_i = \left[\frac{\partial H}{\partial x_1}, \frac{\partial H}{\partial x_2}, \ldots, \frac{\partial H}{\partial x_n}\right]\begin{bmatrix} g_1(x) \\ g_2(x) \\ \vdots \\ g_n(x) \end{bmatrix} = \frac{\partial H}{\partial x} g(x) \tag{1.14}$$

A function $H(x)$ stands as to be positive definite if $H(0) = 0$ and $H(x) > 0$ for $x \neq 0$. It is positive semidefinite if it satisfies the weaker condition $H(x) \geq 0$ for $x \neq 0$. A function $H(x)$ stands as to be negative definite or negative semidefinite if $-H(x)$ is positive definite or positive semidefinite, respectively. If $\dot{H}(x)$ is negative, H will decrease along the trajectories of (1.13) passing through x.

In a domain that contains the origin, the stability theorem of Lyapunov determines that the origin is stable if, there is a continuously differentiable positive definite function $H(x)$ such that $\dot{H}(x)$ is negative semidefinite, and it is asymptotically stable if $\dot{H}(x)$ is negative definite. When the condition for stability is satisfied, the function H is a Lyapunov function.

1.4 Bifurcations

Bifurcations have a crucial role in scientific research because they present models of instabilities and transitions as long as some control parameter is varied. As a result, the qualitative structure of the systems' flow can mutate as this latter is adjusted. In other words, an equilibrium point can be destroyed or created, or its stability can change. Bifurcations are qualitative changes in dynamics, and those parameter values at which they occur are referred to as bifurcation points [2].

In this part, we introduce some examples to provide simple comprehension of bifurcations of equilibrium points, with the aid of flows on the line.

1.4.1 Saddle-Node Bifurcation

The basic manner by which equilibrium points are destroyed or created is called the saddle-node bifurcation. We shall start with a simple differential equation that exhibits this type of bifurcation

$$\dot{x} = f(x,\mu) = \mu + x^2 \qquad x \in \Re \tag{1.15}$$

Where μ is a real-valued parameter, which may be negative, zero, or positive.

The system (1.15) has two equilibrium points, which are functions of μ

$$x^*_{1,2} = \pm\sqrt{-\mu} \tag{1.16}$$

Thus, the system (1.15) has two real equilibria for $\mu < 0$. As μ increase through zero and becomes positive, these two points collide and mutually annihilate. As a consequence, a qualitative change in the dynamical properties of (1.15) occurs when μ is null, which is called a saddle-node bifurcation. This kind of bifurcation is also known as a tangent bifurcation in one-dimensional systems [2].

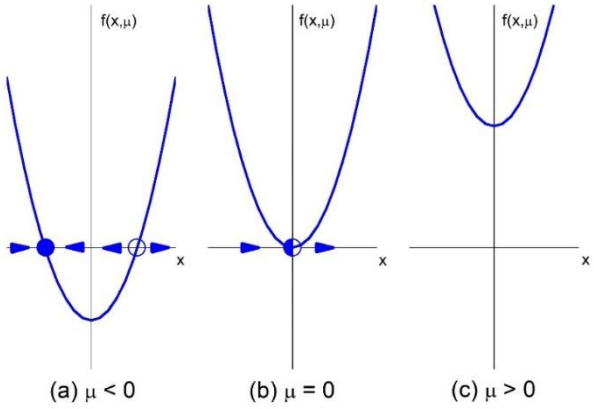

Figure 1.4 Saddle-node bifurcation.

To determine the stability of discussed equilibrium points from the plot of the system (1.15) for the case where $\mu < 0$, it is transparent that the equilibrium point $x^*_2 = -\sqrt{-\mu}$ is stable, because the flow direction for both, the right and left, sides is toward that equilibrium. Whereas the second fixed point is unstable.

In the second case where $\mu = 0$, the equilibrium point is half-stable (saddle).

To obtain a quantitative measure of stability, for instance, the rate of divergence from an unstable equilibrium point, this sort of measure can be collected by linearizing these equilibria, as we shall explain.

Let us define $\varepsilon(t) = x(t) - x^*$ as a tiny perturbation away from the equilibrium point x^*. We derive a differential equation for ε to reveal whether the perturbation decays or grows. Differentiation gives

$$\dot{\varepsilon} = \frac{d}{dt}(x - x^*) = \dot{x} \tag{1.17}$$

since x^* is constant. Hence, $\dot{\varepsilon} = \dot{x} = f(x) = f(x^* + \varepsilon)$. Now using the expansion of Taylor, we get

$$f(x^* + \varepsilon) = f(x^*) + \varepsilon f'(x^*) + O(\varepsilon^2) \tag{1.18}$$

Where $O(\varepsilon^2)$ denotes quadratically small terms in ε. Finally, note that $f(x^*) = 0$ since x^* is an equilibrium point.

Therefore

$$\dot{\varepsilon} = \varepsilon f'(x^*) + O(\varepsilon^2) \tag{1.19}$$

Now if $f'(x^*) \neq 0$, the $O(\varepsilon^2)$ terms are negligible and we may write the approximation

$$\dot{\varepsilon} \approx \varepsilon f'(x^*) \tag{1.20}$$

(1.20) represents a linear equation in function of δ. It is referred to as the linearization about x^*. That equation showcases that the perturbation $\delta(t)$ decays if $f'(x^*)$ is strictly negative, and grows exponentially if $f'(x^*)$ is strictly positive. The $O(\varepsilon^2)$ terms are not negligible if $f'(x^*) = 0$; Thus, a nonlinear analysis is required to determine stability.

1.4.2 Transcritical Bifurcation

Let's check out the following equation

$$\dot{x} = f(x, \mu) = \mu x - x^2 \tag{1.21}$$

It is obvious that the system (1.21) has two equilibrium points, $x^*_1 = 0$ (which exists for all values of μ) and $x^*_2 = \mu$.

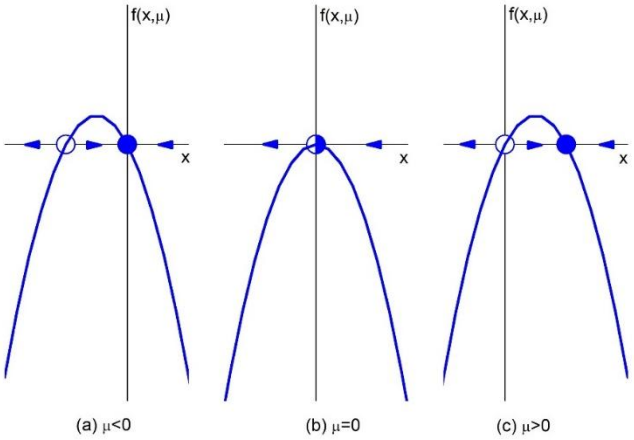

Figure 1.5 Vector field as μ varies of (1.21).

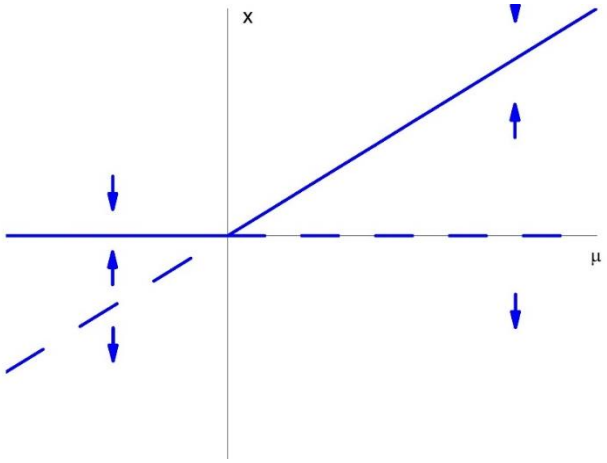

Figure 1.6 Transcritical bifurcation.

For $\mu < 0$, if we apply a linearization around our fixed points, we notice that the perturbation decays (due to $\partial f(x^*, \mu)/\partial x = \mu - 2x^*$) for the fixed point x^*_1 (then, x^*_1 is locally stable) and it grows for the fixed point x^*_2 (then, x^*_2 is locally unstable). As μ increases, the unstable equilibrium point approaches the origin and merges with it when $\mu = 0$. Finally, when $\mu > 0$, x^*_2 has become stable, and x^*_1 is now unstable. Despite that μ passes through zero, no equilibrium point appears or disappears, only its stability property changes. The transcritical bifurcation is the standard mechanism for such a change in stability [2].

1.4.3 Pitchfork Bifurcation

Another category of local bifurcation is known as pitchfork bifurcation. This type of bifurcation arises in one-dimensional systems that have one parameter.

$$\dot{x} = f(x, \mu) = x(\mu - x^2) \tag{1.22}$$

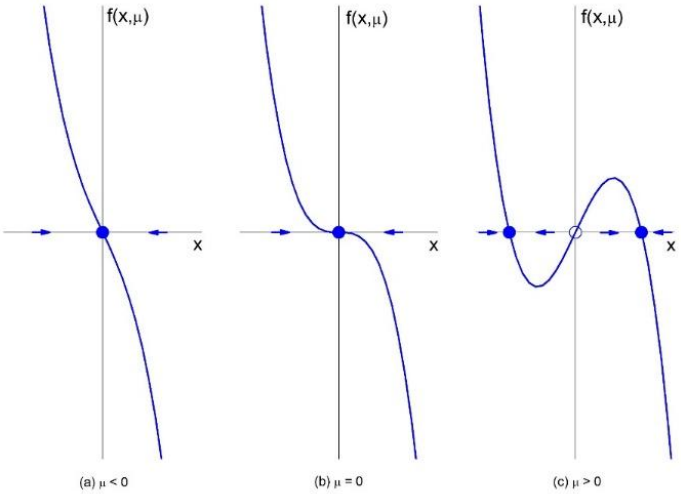

Figure 1.7 Vector field as μ varies for (1.22).

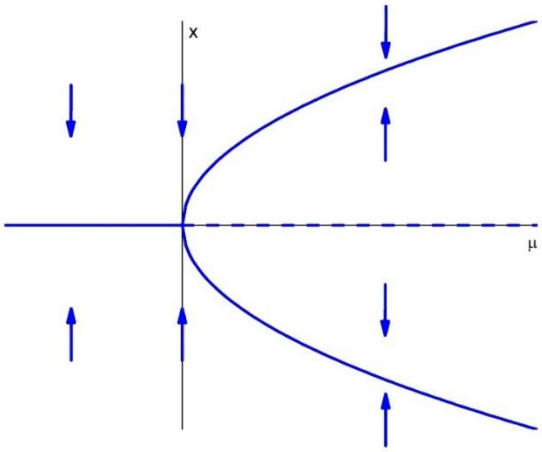

Figure 1.8 Pitchfork bifurcation.

The equilibrium solution $x^* = 0$ is independent of the parameter μ. when μ is strictly positive, there are two supplemental equilibria $x^*_{2,3} = \pm\sqrt{\mu}$. By considering that $\partial f / \partial x = \mu - 3x^2$ and $x(\mu - x^2) > 0$, we could infer that for $\mu < 0$, $x^*_1 = 0$ is the unique equilibrium which is stable. For $\mu > 0$, the point x^*_1 becomes unstable, whereas the two nonzero equilibria are both stable. Hence, a qualitative change becomes clearly visible in the orbit structure of (1.22) when the value of the parameter μ is zero. This circumstance is called pitchfork bifurcation, in which both the disappearance or appearance of equilibria and stability changes take place [2].

1.4.4 Hopf Bifurcation

In a two-dimensional system, the eigenvalues of the Jacobian are the key to spotting all possible ways that the system can lose stability as the value of a parameter varies which are:

- Either the eigenvalues are real and negative, and then one of them passes through $\lambda = 0$. These were just discussed in the tangent, pitchfork, and transcritical bifurcations.
- The other possible scenario is that the eigenvalues are complex conjugates and they cross the imaginary axis at the same time into the right half-plane. This kind of bifurcation is referred to Hopf bifurcation.

Hopf bifurcations come in both subcritical and supercritical types. A small, nearly elliptical limit cycle encircling an unstable spiral is known as a supercritical Hopf bifurcation. In engineering applications, the subcritical scenario is considerably more potentially dangerous and dramatic. Resulting of the bifurcation, the system's trajectories have to move to a distant attractor, which could be an equilibrium point, a different limit cycle, infinity, or a chaotic attractor (in three and higher dimension continuous differential equations).

1.5 Limit Cycles

As we discussed previously in the Trajectories and Phase Portrait section, linear systems in $\Re^n, n \geq 2$ space characterized by a set of two purely imaginary eigenvalues, the center's case, have an infinite number of periodic solutions, associated with every initial condition. A linear system $\dot{y} = Ay$ can have closed orbits, periodic orbits or cycle; If $y(t)$ is a periodic solution, similarly for $k\,y(t)$ with any constant $k \neq 0$, but they will not be isolated. An isolated closed trajectory is often referred to as a limit cycle; where isolated means that the nearby trajectories are not closed; they spiral either toward or away from the limit cycle [2]. Only nonlinear differential equations can have isolated periodic solutions (limit cycles).

A limit cycle can be structurally stable, which means that if it exists for a particular system of differential equations, it will persist even if the system's parameters are significantly perturbed.

Let's consider the following model

$$\begin{cases} \dot{r} = r - r^3 \\ \dot{\theta} = 1 \end{cases}, r \geq 0 \tag{1.23}$$

The angular and radial dynamics are unconnected and so can be analyzed separately.

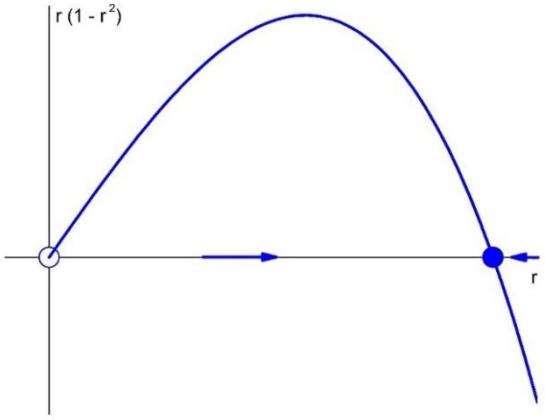

Figure 1.9 Vector field of (1.23).

Tackling $\dot{r} = r - r^3$ as a vector field on the line, we infer that $r^* = 1$ is stable and $r^* = 0$ is an unstable equilibrium, as the Figure 1.9 illustrates.

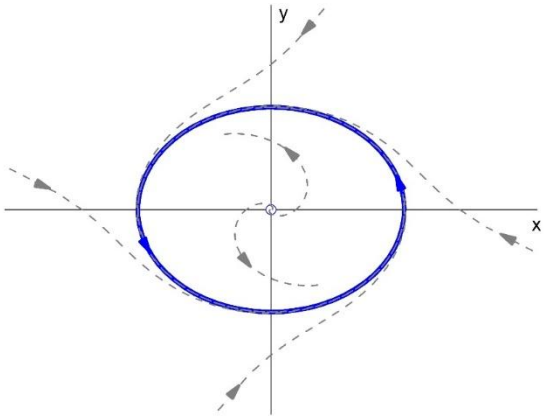

Figure 1.10 Limit cycle.

On the other hand, when we plot the phase plane of the discussed system. We notice that all trajectories approach the unit circle $r^* = 1$ except the case when $r^* = 0$. As a conclusion, at $r = 1$, all trajectories spiral asymptotically toward a limit cycle.

1.6 Conservative and Dissipative Systems

Dissipative and Conservative systems are two sorts of dynamical systems characterized by the concept of attractiveness and stability. A system is considered conservative if the volumes in the phase space remain consistent throughout time. Dissipative dynamical systems, unlike conservative systems, exhibit phase space volume contraction. The dynamics of a system will ultimately be confined to a subset of fractal smaller than n, which is the dimension of the system's state space, and possibly zero due to the dissipation. Chaotic sets are frequently

characterized by a particular geometry structure commonly referred to by the term fractal dimension [24].

Where the volume is expressed with

$$V_{olume}(t+dt) = V_{olume}(t) + \Delta(V_{olume}(t))$$

where $\Delta(V_{olume}(t))$ is the volume resulting from the swept-out tiny patch of surface, integrated over all areas. let $\dot{x} = g(x)$ and $g.n$ is the outward velocity's normal component. hence, in time dt a patch of area dA, of a closed surface $S(t)$ of initial conditions for trajectories, sweeps out a volume $(g.n\ dt)\ dA$. so, we can get

$$V_{olume}(t+dt) = V_{olume}(t) + \int_S (g.n\,dt)\,dA$$

Hence

$$\dot{V}_{olume} = \frac{V_{olume}(t+dt) - V_{olume}(t)}{dt} = \int_S g.n\,dA$$

By using the divergence theorem, we rewrite the integral above and get

$$\dot{V}_{olume} = \int_V \nabla.g\ dV_{olume} \tag{1.24}$$

If the divergence is considered as a constant, (1.24) reduces to $\dot{V}_{olume} = (\nabla.g)V_{olume}$, which possesses the solution $V_{olume}(t) = V_{olume}(0)e^{(\nabla.g)t}$. Therefore, volumes in phase space decay exponentially if $\nabla.g < 0$.

1.7 Chaotic Systems

The first chaotic attractor has been developed from a famous model first proposed by Edward Lorenz in 1963 which provides a mathematical description of atmospheric turbulence [17]. He made a simpler convection rolls' model in the atmosphere and then he derived a three-dimensional system for it. When Lorenz plotted the trajectories in the phase space, he observed that they settle onto a strange and complex set. He showed that tiny differences in the initial conditions amount to dramatic differences in the system behavior over time. Also, he indicated that the solutions swing irregularly, never exactly visiting the same point but for all future time, they maintain within a bounded region of phase space. The work of Lorenz handed over strong numerical indicates that a low-dimensional system of differential equations with simple nonlinearities can produce extremely complex orbits.

Chaos theory is the qualitative study of unstable aperiodic behavior in deterministic nonlinear dynamical systems. we will cover in this part signatures of chaos with some dynamical systems examples simulated on MATLAB software.

1.7.1 Lorenz System

Lorenz simplified his twelve-dimensional equations into a three-dimensional model describing the convective motion of the atmosphere heated by the ground below and cooled from above. The air rises and falls along opposite edges of long rotating cylinders.

$$\begin{cases} \dfrac{dx(t)}{dt} = \sigma(y(t) - x(t)) \\ \dfrac{dy(t)}{dt} = x(t)(\rho - z(t)) - y(t) \\ \dfrac{dz(t)}{dt} = x(t)y(t) - \beta z(t) \end{cases} \tag{1.25}$$

The variable x is the speed of rotation, positive representing clockwise and negative representing counterclockwise motion. The variable y is proportional to the temperature difference between the ascending and descending fluids. The variable z is proportional to the distortion of the vertical temperature profile from linearity, a positive value indicating that the strongest gradients occur near the boundaries. While the parameters σ and ρ are proportional to the $Prandtl\ number$ and the $Rayleigh\,number$, respectively. The parameter is the aspect ratio of the convection cylinders.

According to the system, we can obtain

$$\nabla V = \frac{\partial \dot{x}}{\partial x} + \frac{\partial \dot{y}}{\partial y} + \frac{\partial \dot{z}}{\partial z} = -\sigma - 1 - \beta \tag{1.26}$$

Thus

$$\frac{dV}{dt} = -(\sigma + 1 + \beta)V \tag{1.27}$$

Which may be solved to yield

$$V(t) = V(0)e^{-(\sigma+1+\beta)t} \tag{1.28}$$

The system is dissipative, since $\sigma = 10$ and $\beta = 8/3$.

If we apply the transformation $[x, y, z] \to [-x, -y, z]$, we can notice that the system (1.25) is symmetrical. By setting $\frac{dx}{dt} = \frac{dy}{dt} = \frac{dz}{dt} = 0$, its equilibria represent the real solutions to the equation

$$x^*\left[b(\rho - 1) - x^{*2}\right] = 0$$

For $0 < \rho < 1$ the only equilibrium is $S_1 : (0,0,0)$. There exist two other equilibria when $\rho > 1$, namely $S_2 : \left(+\sqrt{\beta(\rho-1)}, +\sqrt{\beta(\rho-1)}, \rho - 1\right)$ and $S_3 : \left(-\sqrt{\beta(\rho-1)}, -\sqrt{\beta(\rho-1)}, \rho - 1\right)$.

Local stability of the equilibria, S_1, S_2 and S_3, is depending on assessing the eigenvalues, the real part's sign, of the Jacobian matrix at equilibrium

$$Df(x, y, z) = \begin{pmatrix} -\sigma & \sigma & 0 \\ \rho - z & -1 & -x \\ y & x & -\beta \end{pmatrix}$$

The trivial equilibrium S_1 is stable for $0 < \rho < 1$; And, we say the origin is globally stable for these parameters. And for $\rho > 1$, the origin becomes a saddle equilibrium point (it has two negative eigenvalues and one positive eigenvalue).

Bifurcations of the S_2 and S_3 equilibria can be found by identifying the parameter values' combinations that lead them to become nonhyperbolic, that is, for which the corresponding characteristic equation for either of these points

$$\lambda^3 + (\sigma + \beta + 1)\lambda^2 + \beta(\sigma + \rho)\lambda + 2\beta\sigma(\rho - 1) = 0 \tag{1.29}$$

has a solution $\lambda = 0$ or an imaginary pair $\lambda_{1,2} = \pm ib \;\; b \in \Re$.

Substituting $\lambda = 0$ into (1.29) and gives $2\beta\sigma(\rho - 1) = 0$ whence $\rho = 1$. At $\rho = 1$, a pitchfork bifurcation occurs, two new stable equilibria come to being whereas the previous stable equilibrium point, S_1, becomes unstable. S_2 and S_3 are stable nodes until $\rho \approx 1.34561$.

Whereupon, if we substitute $\lambda = ib$ into (1.29) and evaluate both real and imaginary parts to be zero of the obtained equation we get

$$\begin{aligned} -(\beta + \sigma + 1)b^2 + 2\beta\sigma(\rho - 1) &= 0 \\ -b^3 + \beta(\rho + \sigma)b &= 0 \end{aligned}$$

when

$$b^2 = \frac{2\beta\sigma(\rho-1)}{\beta+\sigma+1} = \beta(\rho+\sigma)$$

and since b is real, $b^2 > 0$ implying $\rho > 1$, then as long as $\sigma > \beta + 1$, there is a *subcritical Hopf bifurcation* at $\rho_H = \frac{\sigma(\sigma+\beta+3)}{\sigma-\beta-1} = 24.7368421$. In other words, S_2 and S_3 equilibria points are stable spiral nodes where the parameter ρ satisfy the condition $1.34561 < \rho < \rho_H$, whereupon they possess two complex conjugate eigenvalues with $\mathrm{Re} > 0$ (unstable spiral saddle points) and one real negative eigenvalue.

The usual parameters used by Lorenz, $\sigma = 10$, $\rho = 28$, $\beta = 8/3$, give chaos in which the direction of rotation occasionally changes. the strange attractor of the Lorenz system is illustrated in Figure 1.11.

Although we set very close two nearby initial conditions $\begin{pmatrix} x1_0 \\ y1_0 \\ z1_0 \end{pmatrix} = \begin{pmatrix} 7 \\ 2 \\ 30 \end{pmatrix}$ *and* $\begin{pmatrix} x2_0 \\ y2_0 \\ z2_0 \end{pmatrix} = \begin{pmatrix} x1_0 + 0.001 \\ y1_0 \\ z1_0 \end{pmatrix}$, the sensitive dependence on initial conditions property of chaos appears, which causes the divergence of the x state trajectory in Figure 1.12.

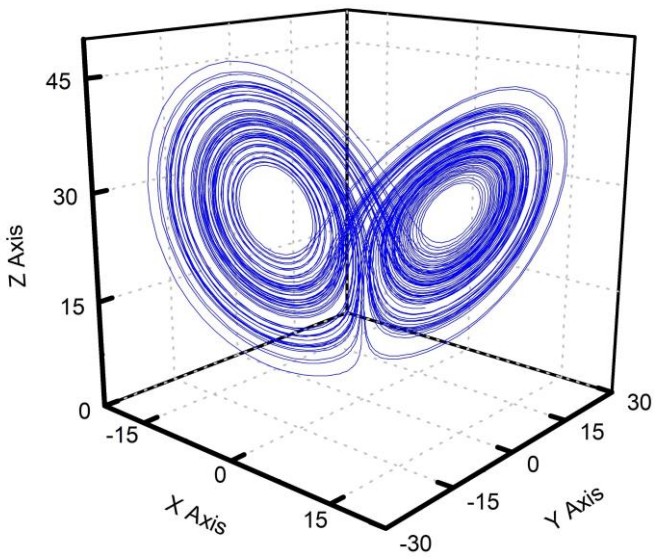

Figure 1.11 Lorenz attractor on a 3D plane.

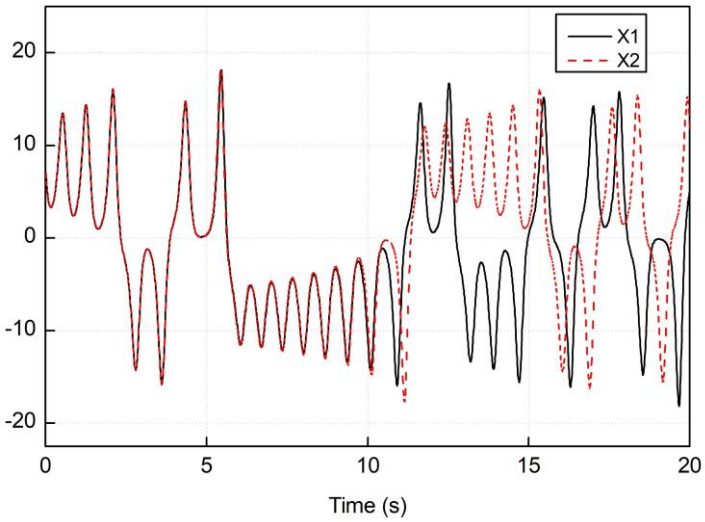

Figure 1.12 Evolution of the X state trajectories of Lorenz system with small deviation on the initial condition.

1.7.1.1 Lyapunov Exponents

Lyapunov exponents are an essential concept of nonlinear dynamics and important statistics for quantifying stability and deterministic chaos. they are commonly used to quantify local stability features of attractors and to define the exponential rates at which nearby trajectories diverge (or converge) on an average as the system evolves in time [2]. For the purpose of quantifying the sensitivity of Lorenz system orbit on initial conditions, we use one of the famous methods that is based on Gram-Schmidt Reorthonormalization (GSR) of the tangent vectors [25].

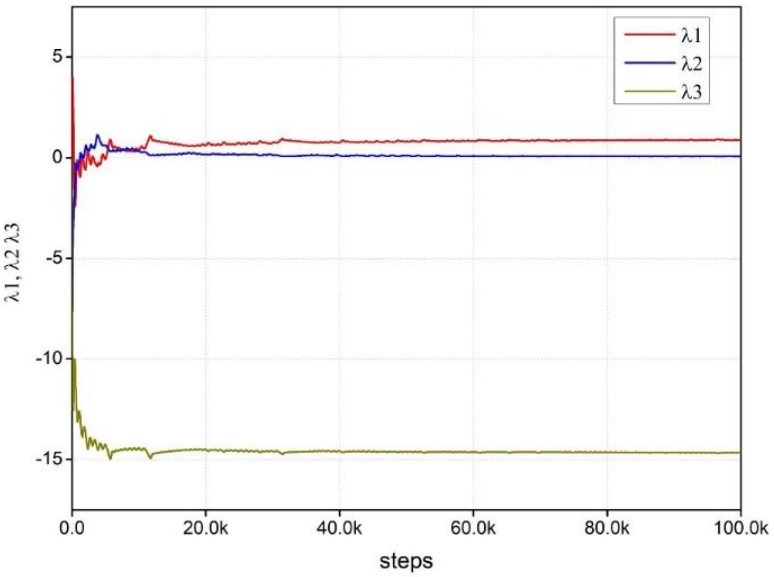

Figure 1.13 Lyapunov exponents spectrum of Lorenz system.

Figure 1.13 illustrates the Lyapunov exponents spectrum of the Lorenz system for the usual parameters with step time $Ts = 10^{-3} s$. The average exponents are $\lambda_1 \approx 0.9053,\ \lambda_2 \simeq 0,\ \lambda_3 \approx -14.6673$.

1.7.1.2 Lyapunov Dimension

According to the concept of *Lyapunov Dimension* suggested by Kaplan and Yorke [26] for estimating the Hausdorff dimension of attractors. Where the Lyapunov exponents of a system with n-dimension are $\lambda_1 \geq \lambda_2 \geq ... \geq \lambda_n$.

$$D_L = \begin{cases} 0 & \text{if } j \text{ doesn't exist} \\ n & \text{if } j = n \\ j + \dfrac{\sum_{i=1}^{j} \lambda_i}{|\lambda_{j+1}|} & \text{if } j < n \end{cases} \quad , j = \max\left\{ m : \lambda_1 + \lambda_2 + ... + \lambda_m \geq 0 \right\} \tag{1.30}$$

Therefore, the Lyapunov dimension of the Lorenz attractor is: $D_L = 2 + \dfrac{\lambda_1 + \lambda_2}{|\lambda_3|} \approx 2.0617$, so the Lorenz system is fractal.

1.7.2 Logistic Map

Robert May emphasized in his paper that a simple nonlinear map may exhibit extremely complex dynamics [27]. The logistic map is one of the simplest and most transparent systems exhibiting order-to-chaos transition. The logistic map is a discrete dynamical system defined by:

$$x_{n+1} = G(x_n) = x_n\, \mu (1 - x_n) \quad \text{such that } 0 < \mu \leq 4 \text{ and } 0 \leq x_n \leq 1 \tag{1.31}$$

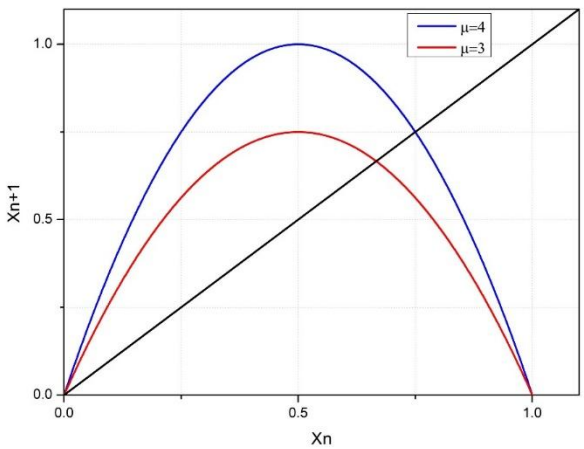

Figure 1.14 Logistic map.

The first term represents the reproduction tendency that is proportional to the nth-generation, and the second term, $1-x_n$, denotes the need for coexistence and the sharing of limited resources.

The graph of the Logistic map illustrated in Figure 1.14, is a parabola with a maximum value of $\mu/4$ at $x_n = 1/2$.

The fixed points of the equation (1.31) that satisfy $G(x^*) = x^*$ *i.e,* $x^* = x^*\mu(1-x^*)$ are:

$$\begin{cases} x^* = 0 & \text{for all values of } \mu \\ x^* = 1-1/\mu & \text{for } \mu \geq 1 \end{cases} \tag{1.32}$$

The stability of each fixed point depends on $G'(x^*) = \mu - 2\mu x^*$, such that, it's stable only if $|G'(x^*)| < 1$. Since $G'(x^* = 0) = \mu$, then the origin is unstable for $\mu > 1$ and is stable for $\mu < 1$, Hence the population always proceeds to extinct as $n \to \infty$, $(x_n \to 0)$, for a small growth rate $\mu < 1$. Whereas for the other fixed point since $G'(x^* = 1-1/\mu) = 2-\mu$, then it is stable as long as $1 < \mu < 3$, and unstable for $\mu > 3$, therefore the population reaches a nonzero steady state for $1 < \mu < 3$.

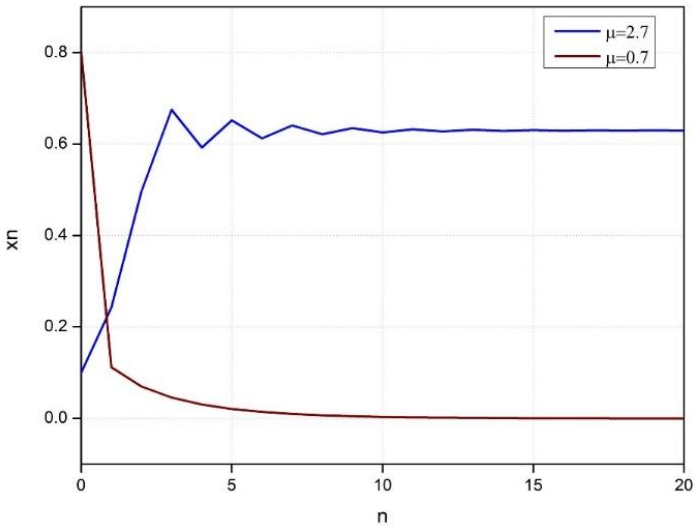

Figure 1.15 Population growth of logistic map x_n vs. n.

At $\mu = 3$ the slope $G'(x^* = 1-1/\mu) = -1$, this resulting bifurcation is referred to as a flip bifurcation [2]. Such that if we make a slight change in the parameter μ above the value 3, a stable period-2 cycle appears close to the fixed point $x^* = 1-1/\mu$. the cobweb diagram in Figure 1.16 reveals the oscillation between two points (p, q) of the iterated logistic map for $\mu = 3.1$

Those stable period-2 points are solutions of a quadratic equation of the second iterate map $G^2(x_n) = G(G(x_n))$ besides the previous fixed points $(x^* = 0 \; and \; x^* = 1 - 1/\mu)$.

Where the point $p \; (or \; q)$ is stable period-2 as long as the value of $\left|\left(G^2(p)\right)'\right| < 1$ i.e., $\left|G'(G(p))G'(p)\right| = \left|G'(p)G'(q)\right| < 1$. where $p, q = \dfrac{\mu + 1 \pm \sqrt{(\mu - 3)(\mu + 1)}}{2\mu}$

From these observations and explanations, we can extrapolate that as the height of the logistic map's convexity is increased, the period-2 cycle loses stability at $\mu = 1 + \sqrt{6}$, the $G'^2(p)$ is equal to -1. Beyond this parameter value, a stable period-4 limit cycle replaces the period-2.

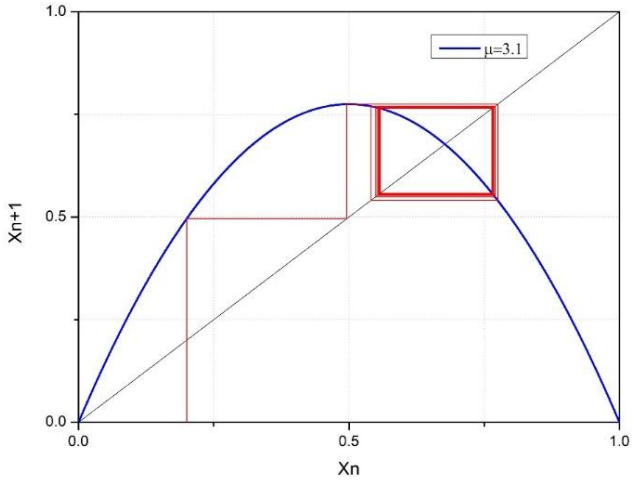

Figure 1.16 Cobweb diagram of the logistic map.

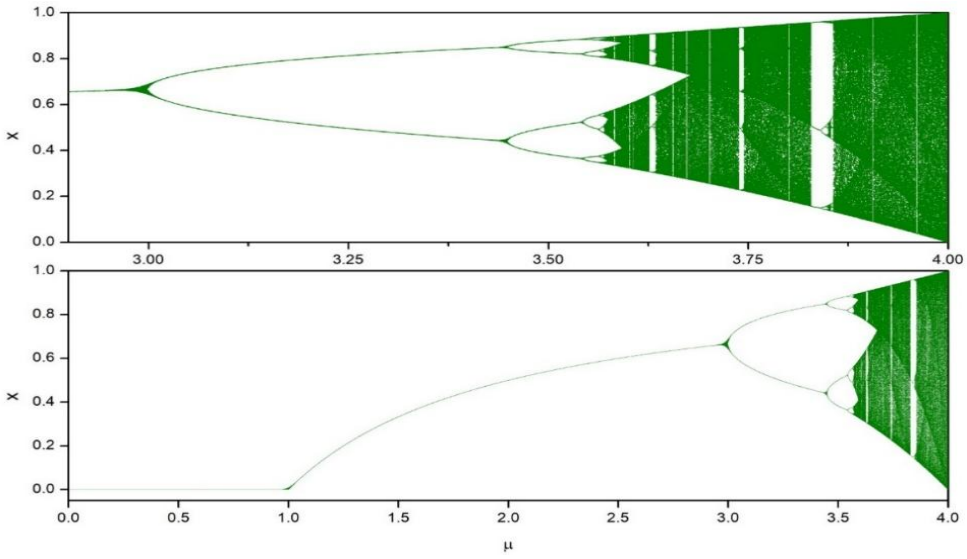

Figure 1.17 Bifurcation diagram of the logistic map.

The mechanism that produced period-4 from period-2 is repeated as the parameter μ

increase. This period doubling eventually leads to an infinite cascade of periodic orbits (as Figure 1.17 illustrate) at $\mu \approx 3.5699456...$. Just beyond this parameter value, a periodic region occurs with period-3. In the same manner that happened to the period-2 orbit, a period-doubling cascade for period-3 becomes chaotic [28].

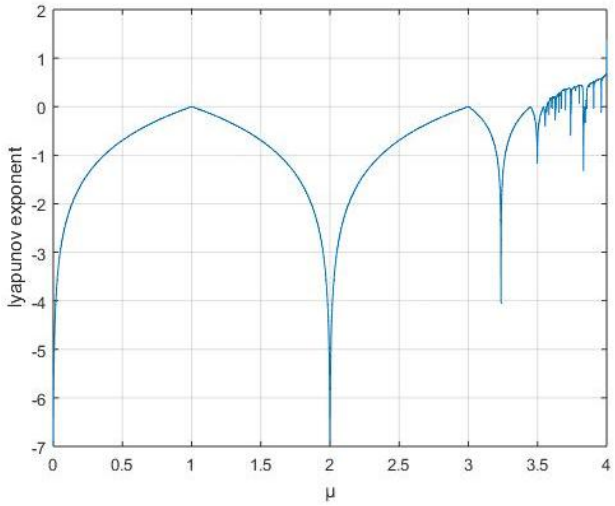

Figure 1.18 Logistic map Lyapunov exponent spectrum.

Figure 1.18 reveals that the logistic map exhibits sensitive dependence on initial conditions when the parameter μ gives a positive Lyapunov exponent value.

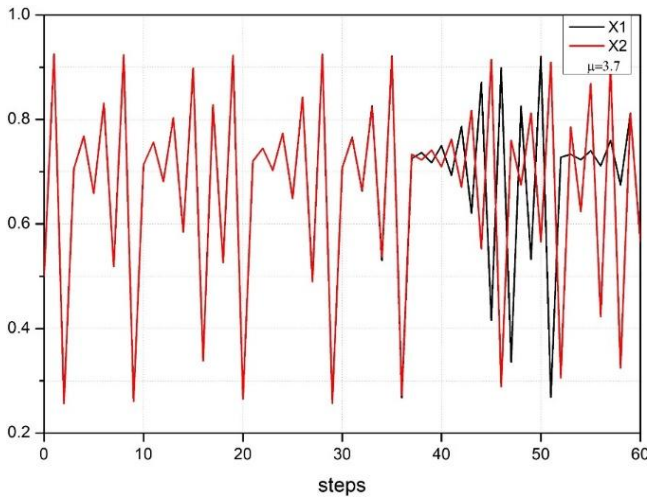

Figure 1.19 Logistic map's initial conditions sensitivity.

As it's shown in Figure 1.19, a very tiny perturbation on the initial condition, leads to a separation of trajectories after some iterations, where $X_1(n=0)=\frac{1}{2}, X_2(n=0)=\frac{1}{2}+10^{-4}$ and μ=3.7 .

1.7.3 Hyperchaotic Systems

Hyperchaotic systems are typically classified as chaotic systems that have more than one positive Lyapunov exponent. Due to the expansion in more than one direction, it leads to more complex attractors and strange behavior of the system dynamics. Where the minimum space dimension of coupled first-order autonomous ordinary differential equations that embed the hyperchaotic attractor should be at least four and the order of the state equation is at least two [29].

Hyperchaos was firstly reported by Rössler in 1979 [30]. Several four-dimensional hyperchaotic systems were designed from some well-known three-dimensional chaotic systems by adding some simple feedback control techniques such as on the Lü system [31], the generalized Lorenz system [32], Chen system [33]. Hyperchaotic systems are broadly applied in nonlinear circuits, secure communications, lasers, biological systems, neural networks, and so on.

The 4-D hyperchaotic Lü system described in [8] is constructed by introducing a state feedback controller on Lü system as follows:

$$\begin{cases} \dot{x} = a(y - x) + u \\ \dot{y} = -xz + cy \\ \dot{z} = xy - bz \\ \dot{u} = xz + du \end{cases} \tag{1.33}$$

The system (1.33) is symmetrical about z-axis for its invariance under the coordinate transformation $(x, y, z, u) \to (-x, -y, z, -u)$. Where the parameters $a = 36, b = 3, c = 20$ are the constants of the Lü system and d is a control parameter.

According to system (1.33), we can obtain the following equilibrium point;

$$p_1 = (0, 0, 0, 0)$$

$$P_2 = \left(\sqrt{bc}, \frac{ad\sqrt{bc}}{ad - c}, \frac{acd}{ad - c}, -\frac{ac\sqrt{bc}}{ad - c} \right)$$

$$P_3 = \left(-\sqrt{bc}, -\frac{ad\sqrt{bc}}{ad - c}, \frac{acd}{ad - c}, \frac{ac\sqrt{bc}}{ad - c} \right)$$

Such that P_2 and P_3 exist only if $ad - c \neq 0$

The Lyapunov exponents illustrated in Figure 1.20 show that the dynamic behavior of the system (1.33) has :

1) A hyperchaotic attractor for $-0.35 < d \leq 1.30$

2) A chaotic attractor for $-0.46 < d \le -0.35$

3) A periodic orbit for $-1.03 \le d \le -0.46$

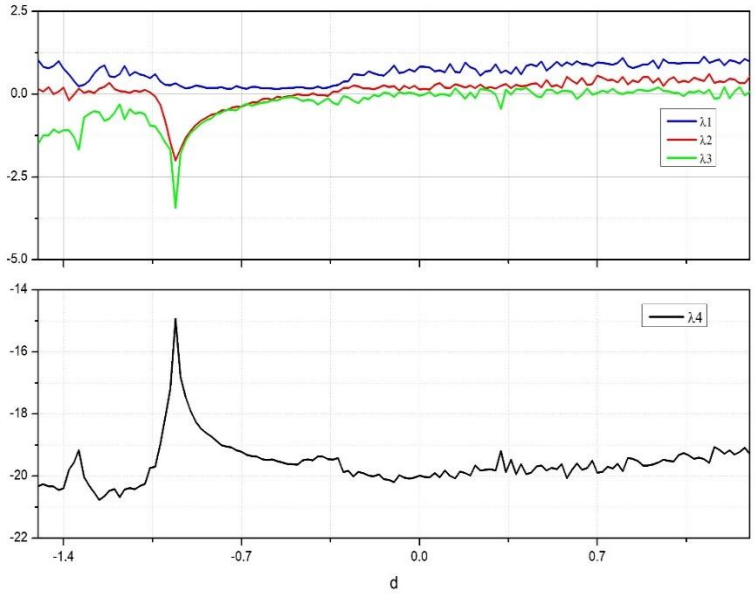

Figure 1.20 Lü hyperchaotic system Lyapunov exponents spectrum versus control parameter d .

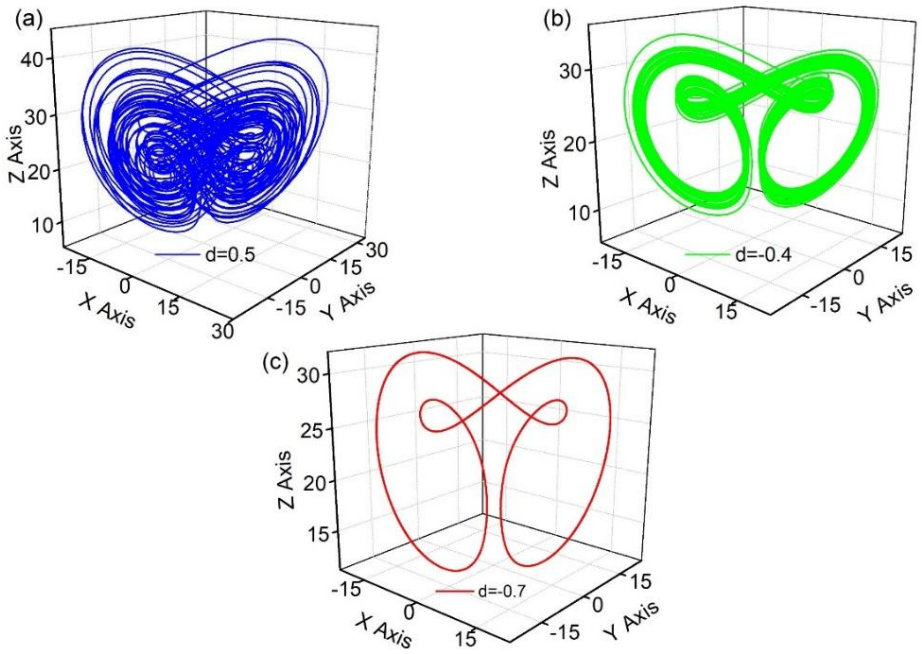

Figure 1.21 Different dynamical behaviors of the system (1.33): (a) Hyperchaotic ; (b) Chaotic ; (c) Periodic.

The phase spaces depicted in Figure 1.21 emphasize that the system's dynamic behaviors (1.33) alternate among periodic obit, chaotic state, and hyperchaotic state when adjusting the value of the parameter d , as the numerical analysis of the Lyapunov exponents spectrum emphasizes.

1.7.4 Fractional-order Chaotic Systems:

The fractional calculus history was born with a letter dated in 30th September 1695, from Leibniz to l'Hopital which was about the meaning of the derivative of order one-half. Despite the old of this mathematical topic for more than 300 years, the studies on the dynamics of fractional-order differential systems and their applications to physics and engineering have been attracted lots of attention only in recent years. For example: fractional derivatives have been widely used in the mathematical modeling of viscoelastic materials [34], [35], Rivero et al. reported population models with fractional dynamics [36].

The generalization of integration and differentiation to joint non-integer $q-order$ operator ${}_{b_1}D_{b_2}^{q}$, where b_1 and b_2 represent the bounds of the operation, can be found widely in research topics associated with fractional calculus. Due to the difficulty of writing the exact solutions of most of the fractional-order differential equations, finding accurate and efficient analytical and numerical methods for solving them has been active research.

By using non-integer order differential equations, chaotic systems can be accurately modeled [37]. To investigate fractional-order chaotic and hyperchaotic systems, it is often necessary to solve fractional-order differential equations. Three frequently used definitions of the fractional-order differential operator are [38]:

1. The Grunwald-Letnikov (GL) definition is described by

$$ {}_{a}D_{t}^{q} f(t) = \lim_{h\to 0} h^{-q} \sum_{i=0}^{(t-a)/h} (-1)^{i} \binom{q}{i} f(t-ih) \qquad (1.34) $$

2. The Riemann-Liouville (RL) definition is given by

$$ D_{t}^{q} f(t) = \frac{1}{\Gamma(n-q)} \frac{d^{n}}{dt^{n}} \int_{0}^{t} \frac{f(\tau)}{(t-\tau)^{q+1-n}} d\tau \qquad (1.35) $$

Where n is the first integer which is not less than q, i.e. $n-1 \le q < n$ and $\Gamma(\cdot)$ is the well-known Euler's gamma function, such that

$$ \Gamma(s) = \int_{0}^{\infty} t^{s-1} e^{-t} dt \qquad (1.36) $$

3. The Caputo definition is written as

$$D_t^q f(t) = \begin{cases} \dfrac{1}{\Gamma(n-q)} \int_0^t \dfrac{f^{(n)}(\tau)}{(t-\tau)^{q+1-n}} d\tau & n-1 < q < n, \\ \dfrac{d^n f(t)}{dt^n} & q = n, \end{cases} \tag{1.37}$$

In our work, to solve the fractional differential equation that is defined as follows

$$\begin{cases} D_t^q x(t) = f(x(t), t), & 0 < q \le 1, \\ x(t_0) = x_0, \end{cases} \tag{1.38}$$

We use a Predictor-Corrector (PECE Predict, Evaluate, Correct, Evaluate) approach for the numerical solution of fractional differential equations provided by Diethelm et al. [39], which is one of the most popular methods for the chaotic analysis of fractional differential equations. This approach is based on the analytical property that the initial value problem in the equation (1.38) is identical to the Volterra integral equation

$$x(t) = \sum_{k=0}^{\lceil q \rceil - 1} x_0^{(k)} \frac{x^k}{k!} + \frac{1}{\Gamma(q)} \int_0^t (t-\tau)^{q-1} f(x(\tau), \tau) d\tau \tag{1.39}$$

Where $\lceil q \rceil$ is just the value q rounded up to the nearest integer and the real numbers $y_0^{(k)}, k = 0,1,...,\lceil q \rceil - 1,$ are assumed to be given.

In our case $0 < q \le 1$ and by working on a uniform grid on some interval $[0,T]$, such that $\{t_n = nh : n = 0,1,..., N\}$ with some integer N and $h = T/N$, then the equation (1.39) becomes

$$x(t_n) = x_0 + \frac{1}{\Gamma(q)} \int_{t_0}^{t_n} (t_n - \tau)^{q-1} f(x(\tau), \tau) d\tau \tag{1.40}$$

let

$$\int_{t_0}^{t_n} (t_n - \tau)^{q-1} f(x(\tau), \tau) d\tau = \sum_{i=0}^{n-1} \int_{t_i}^{t_{i+1}} (t_n - \tau)^{q-1} f(x(\tau), \tau) d\tau \tag{1.41}$$

On each sub-interval $[t_i, t_{i+1}]$, the function $f(x,t)$ is approximated by a piecewise linear function as follows:

$$f(x(t),t)\big|_{[t_i, t_{i+1}]} \approx \tilde{f}(x(t),t)\big|_{[t_i, t_{i+1}]} = \frac{(t_{i+1} - t) \times f(x(t_i), t_i) + (t - t_i) \times f(x(t_{i+1}), t_{i+1})}{t_{i+1} - t_i} \tag{1.42}$$

Then, the equation (1.40) will be written

$$x(t_n) = x_0 + \frac{1}{\Gamma(q)} \sum_{i=0}^{n-1} \int_{t_i}^{t_{i+1}} (t_n - \tau)^{q-1} \left(\frac{(t_{i+1} - \tau) \times f(x(t_i), t_i) + (\tau - t_i) \times f(x(t_{i+1}), t_{i+1})}{t_{i+1} - t_i} \right) d\tau$$

(1.43)

$$x(t_n) = x_0 + a_{n,n} f(x_p(t_n), t_n) + \sum_{i=0}^{n-1} a_{i,n} \ f(x(t_i), t_i) \tag{1.44}$$

where

$$a_{i,n} = \frac{1}{\Gamma(q)} \begin{cases} \int_{t_0}^{t_1} (t_n - \tau)^{q-1} \dfrac{(t_1 - \tau)}{t_1 - t_0} d\tau & \text{if } i = 0 \\ \int_{t_{i-1}}^{t_i} (t_n - \tau)^{q-1} \dfrac{(\tau - t_{i-1})}{t_i - t_{i-1}} d\tau + \int_{t_i}^{t_{i+1}} (t_n - \tau)^{q-1} \dfrac{(t_{i+1} - \tau)}{t_{i+1} - t_i} d\tau & \text{for } 1 \le i \le n-1 \\ \int_{t_{i-1}}^{t_i} (t_n - \tau)^{q-1} \dfrac{(\tau - t_{i-1})}{t_i - t_{i-1}} d\tau & \text{if } i = n \end{cases} \tag{1.45}$$

By doing the integration and take $t_n = nh$

$$a_{i,n} = \frac{h^q}{\Gamma(q+2)} \begin{cases} (n-1)^{q+1} - (n-1-q)n^q & \text{if } i = 0 \\ (n-i+1)^{q+1} + (n-1-i)^{q+1} - 2(n-i)^{q+1} & \text{for } 1 \le i \le n-1 \\ 1 & \text{if } i = n \end{cases} \tag{1.46}$$

This gives us our corrector formula. While the predicted value of $x_p(t_n)$ that used in the right-hand side of the equation (1.43) and equation (1.44) is determined by the fractional Adams-Bashforth method

$$x_p(t_n) = x_0 + \frac{1}{\Gamma(q)} \sum_{i=0}^{n-1} b_{i,n} f(x(t_i), t_i) \tag{1.47}$$

and

$$b_{i,n} = \frac{h^q}{q} ((n-i)^q - (n-i-1)^q) \tag{1.48}$$

Figure 1.22 illustrate a comparison between the numerical solution of the Lorenz system in the equation (1.25) using MATLAB ODE45 solver and PECE method to solve Lorenz fractional order for $q_1 = q_2 = q_3 = 1$(ordinary differentiation). The figure reveals that by using more small step time in the PECE method we get a more accurate numerical approximation solution (due to the property of sensitivity on initial conditions of chaotic systems, the divergence of trajectories appears after a considerable time).

Where the Lorenz fractional-order system is described as follows

$$\begin{cases} D_t^{q_1} x(t) = \sigma(y(t) - x(t)) \\ D_t^{q_2} y(t) = x(t)(\rho - z(t)) - y(t) \\ D_t^{q_3} z(t) = x(t)y(t) - \beta z(t) \end{cases} \tag{1.49}$$

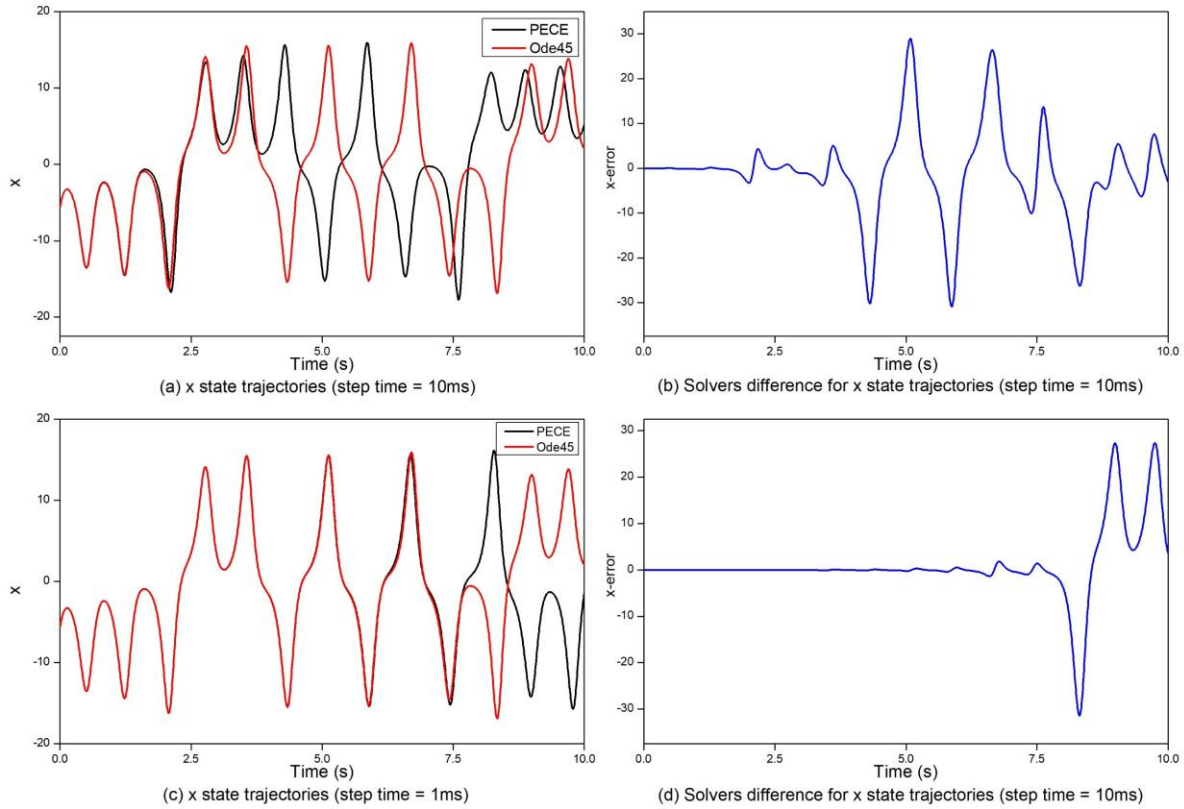

Figure 1.22 Comparison between ODE45 MATLAB solver and the PECE method for q=1 of the X state of Lorenz system.

The stability of each equilibrium point of a fractional order system depends on the fractional order q and the argument of the complex eigenvalues. In other words, an equilibrium point is said to be stable if and only if all its corresponding eigenvalue arguments satisfy [40] $\left|\arg(\lambda_i)\right| > (q\pi)/2$.

Table 1: Equilibrium point analysis of the Lorenz fractional order system (1.49).

Equilibrium Points	**Jacobian Matrix**	**Eigen Values**	$\arg(\lambda_i)$
$E_1 = \begin{pmatrix} 6\sqrt{2} \\ 6\sqrt{2} \\ 27 \end{pmatrix}$	$J_1 = \begin{bmatrix} -10 & 10 & 0 \\ 1 & -1 & -6\sqrt{2} \\ 6\sqrt{2} & 6\sqrt{2} & -8/3 \end{bmatrix}$	$\lambda_1 \approx -13.8545$ $\lambda_2 \approx 0.09395 + 10.1945i$ $\lambda_3 \approx 0.09395 - 10.1945i$	$\arg(\lambda_1) = \pi$ $\arg(\lambda_2) \approx 1.5616$ $\arg(\lambda_3) \approx -1.5616$
$E_2 = \begin{pmatrix} 0 \\ 0 \\ 0 \end{pmatrix}$	$J_2 = \begin{bmatrix} -10 & 10 & 0 \\ 28 & -1 & 0 \\ 0 & 0 & -8/3 \end{bmatrix}$	$\lambda_1 \approx -22.8277$ $\lambda_2 \approx 11.8277$ $\lambda_3 \approx -8/3$	$\arg(\lambda_1) = \pi$ $\arg(\lambda_2) = 0$ $\arg(\lambda_3) = \pi$
$E_3 = \begin{pmatrix} -6\sqrt{2} \\ -6\sqrt{2} \\ 27 \end{pmatrix}$	$J_3 = \begin{bmatrix} -10 & 10 & 0 \\ 1 & -1 & 6\sqrt{2} \\ -6\sqrt{2} & -6\sqrt{2} & -8/3 \end{bmatrix}$	$\lambda_1 \approx -13.8545$ $\lambda_2 \approx 0.09395 + 10.1945i$ $\lambda_3 \approx 0.09395 - 10.1945i$	$\arg(\lambda_1) = \pi$ $\arg(\lambda_2) \approx 1.5616$ $\arg(\lambda_3) \approx -1.5616$

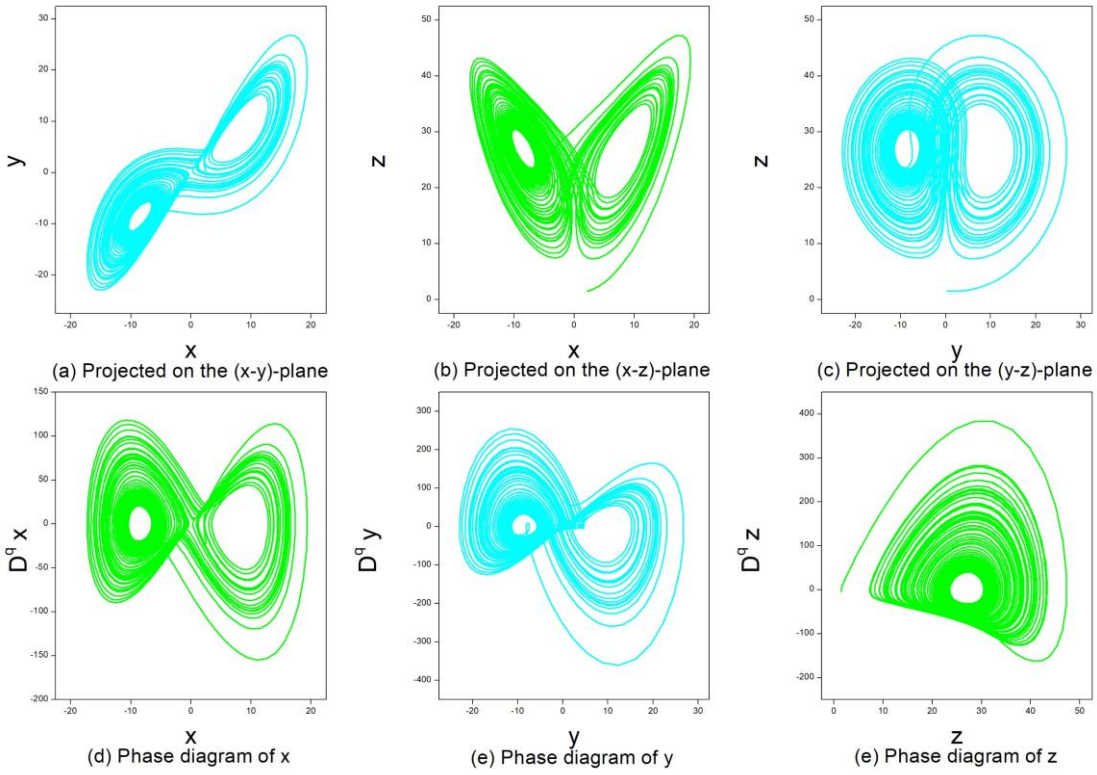

Figure 1.23 Numerical results for the Lorenz fractional order system at q=0.995 and T=50s.

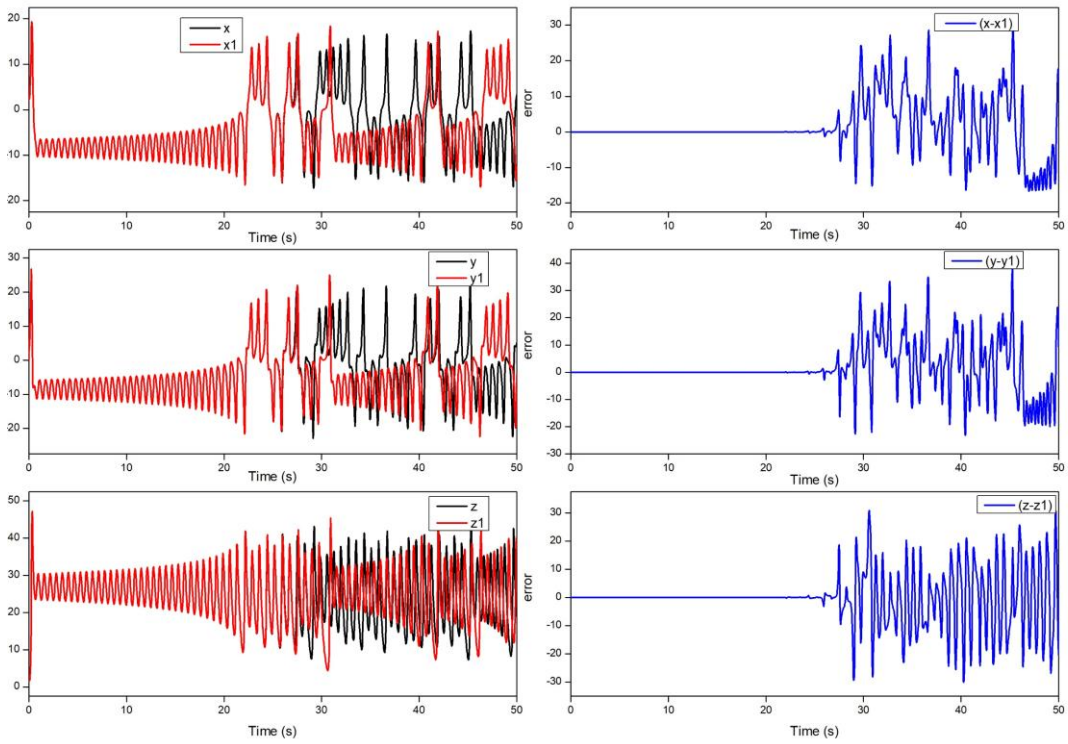

Figure 1.24 Evolution of the state trajectories of fractional order Lorenz system with small deviation on the initial conditions.

1.8 Conclusion

There are many different tools available to express the characteristics of a non-linear dynamical system such as time-series, phase portrait, bifurcation diagram, Poincare map, etc. General chaotic behavior is characterized by two properties. The first one is stretching, which causes a separation of very close neighborhoods of initial conditions that leads to exponential separation of trajectories, this separation is quantified by the Lyapunov exponent. The second one is the mixing and bending property where the stretched trajectories fold back unto themselves. The most important signature of the chaos phenomena is the sensitive dependence on initial conditions besides the boundness and aperiodicity properties. Where the Lyapunov exponent is a tool that provides an examination and a quantification of the sensitivity of the system attractor on initial conditions and helps to classify the system to which behavior it belongs to.

Table 2: Different attractors types based on Lyapunov exponents.

Lyapunov exponents	Dynamical behavior of system
$\lambda_1 > \lambda_2 > 0, \lambda_3 = 0, \lambda_4 < 0$ and $\lambda_1 + \lambda_2 + \lambda_4 < 0$	Hyperchaotic
$\lambda_1 > 0, \lambda_2 = 0, \lambda_4 < \lambda_3 < 0$ and $\lambda_1 + \lambda_3 + \lambda_4 < 0$	chaotic
$\lambda_1 = 0, \lambda_4 < \lambda_3 < \lambda_2 < 0$	periodic
$\lambda_4 < \lambda_3 < \lambda_2 < \lambda_1 < 0$	Equilibrium point

Chapter 2. Robust Controllers for Nonlinear Systems

2.1 Introduction

In the conception of any practical control problem, there will always be a variance between the mathematical model used for the controller design and its actual plant. These differences arise from unknown external disturbances, plant parameters, and unmodeled dynamics. In the presence of these disturbances/uncertainties, a control engineer faces a difficult problem when developing control laws that guarantee the prerequisite performances of the closed-loop system. This has motivated significant excitement about the development of robust control approaches, which are intended to tackle this problem.

In this part of the work, we study the sliding mode control (SMC) technique, which is a particular method for robust controller design. The major advantage of SMC, in addition to finite-time convergence and robustness, is that its foundation is built on the principle of the Lyapunov theory which guarantees asymptotic stability. Then, a synergetic control approach is introduced to prevent the mentioned problems in the next chapters.

2.2 Sliding Mode Control Theory

The variable structure control was suggested in the fifties of the last century by former Soviet scholars. It is innovated from Bang-Bang control and relay control. The discontinuity of control is the main difference that resides in between it and conventional control. Sliding mode control, which is a branch of variable structure control, belongs to nonlinear control, which is performed by switching functions, and switches the structure of the controller (control law or controller parameters) according to the amount of how much the system state deviates from the sliding surface, so that the system operates depending on the law specified by the sliding mode. Sliding mode control has evolved into a relatively full theoretical framework that is frequently used in a variety of industrial control applications. Principle reasons for sliding mode control's widespread application include high control performance for nonlinear systems, adaptability for multiple-input and multiple-output systems, and good design criteria for discrete-time systems. The sliding mode control's main advantage is its robustness. On the condition that the system operates on the sliding surface, this controller has excellent insensitivity to the model error of the controlled object, external disturbances, and changes in object parameters.

2.2.1 Main Concept of Sliding Control

Consider the nonlinear autonomous system of the form [41]

$$\begin{aligned} \dot{x}_1 &= x_2 \\ \dot{x}_2 &= f(x_1, x_2) + u \end{aligned} \tag{2.1}$$

where $x(t) = [x_1, x_2]^T$ is the state of the system, $f : \Re^n \to \Re$ is the nonlinear part of the system and $u \in \Re$ is the control input. The tracking control challenge aims to find a control law that ensures that, given a desired trajectory $x_d(t)$, the tracking error $e(t) = x_1(t) - x_d(t)$ tends to zero. Choose a manifold $S(e)$ where $S \in \Re$, so that if the system trajectories are on the manifold, the systems' behavior meets a prespecified control target. Assume that the control signal is designed to drive system trajectories from any starting state point to attain the manifold (sliding surface $S(e) = 0$) in finite time and slide on it. This approach is generally referred to as sliding mode control (SMC) or, in some literature, may called variable structure control.

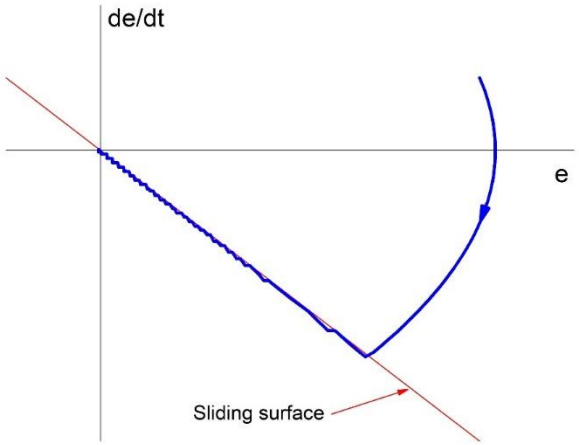

Figure 2.1 Portrait phase and sliding surface.

The sliding surface is determined by

$$S = \left(d/dt + \lambda\right)e \tag{2.2}$$

such that, λ is chosen to be a positive constant scalar. Hence, the dynamic error $e(t)$ is uniformly asymptotically stable once the sliding surface is reached ($S = 0$), i.e. the error e decreases asymptotically with time.

The next design process is to establish a control law that is capable to bring the drive system (2.1) into the sliding surface and maintains it on this surface once it has been reached. Thus, we first calculate the time derivative of (2.2)

$$\begin{aligned}\dot{S} &= \frac{d^2e}{dt^2} + \lambda\frac{de}{dt} = \dot{x}_2 - \ddot{x}_d + \lambda\left(x_2 - \dot{x}_d\right) \\ &= f(x_1, x_2) + u - \ddot{x}_d + \lambda\left(x_2 - \dot{x}_d\right)\end{aligned} \tag{2.3}$$

With the aim to derive such a control, we choose the following Lyapunov function

$$V(t) = \tfrac{1}{2}S(t)^2 \tag{2.4}$$

so that,

$$\begin{aligned}\dot{V}(t) &= S(t)\dot{S}(t) \\ &= S\left(f(x_1, x_2) + u - \ddot{x}_d + \lambda\left(x_2 - \dot{x}_d\right)\right)\end{aligned} \tag{2.5}$$

In practice, the control rule is commonly represented as $u = u_e + u_d$, where u_e represents the equivalent control, which allows us to eliminate the known terms on the right-hand side of (2.3) , and u_d is the discontinuous component that ensures the condition $\dot{V} < 0$ for $S \neq 0$ to achieve an asymptotic stability about the equilibrium point $S = 0$.

$$\begin{aligned}u_e &= -\left(f(x_1, x_2) - \ddot{x}_d + \lambda\left(x_2 - \dot{x}_d\right)\right) \\ u_{d=} &- k\,sign(S) \;\;, k > 0\end{aligned} \tag{2.6}$$

Thus, the right-hand-side of (2.5) will be written as follows

$$\begin{aligned}S\dot{S} &= -k\,S\,sign(S) \\ &< 0\end{aligned} \quad \text{for } S \neq 0 \tag{2.7}$$

If we replace u_d in (2.6) by $u_d = -k\,S$. Therefore, $\dot{S} = -k\,S$ leads to an asymptotic convergence to $S = 0$ since $S(t) = S(0)e^{-kt}$. To guarantee a finite time convergence to the chosen surface, let

$$S\dot{S} \leq \eta|S| \tag{2.8}$$

(2.8) is called η-reachability condition [42]. by integrating $|S(t)| - |S(0)| \leq -\eta t$, it indicates that the needed time to reach the surface, starting from an initial condition $S(0)$, is constrained by

$$t_e = \frac{|S(0)|}{\eta}$$

2.3 Sliding Mode Control for a Second Order System with Disturbance

Let us introduce a second-order system, which is represented by

$$\begin{cases} \dot{x} = y \\ \dot{y} = g(x, y, t) + u \end{cases} \tag{2.9}$$

where u is the control input, and the disturbance term $g(x, y, t)$ is presumed to be bounded, i.e. $g(x, y, t) \le H > 0$. For the purpose of achieving an asymptotic convergence of the state variables to zero, i.e. $\lim_{t \to \infty} x, y = 0$, in the existence of the bounded disturbance $g(x, y, t)$, we will want to be sure to conduct the variable S in (2.10) to zero in finite time with the aid of the control u.

$$S = S(x, y) = y + \lambda x, \qquad \lambda > 0 \tag{2.10}$$

This task can be attained by applying the Lyapunov function to the S-dynamics that are derived using (2.9) and (2.10). Thus

$$\dot{S} = g(x, y, t) + u + \lambda y, \qquad S(0) = S_0 \tag{2.11}$$

where the candidate Lyapunov function takes the form

$$V = \frac{1}{2} S^2 \tag{2.12}$$

In order to provide the asymptotic stability of (2.11) about the equilibrium point $S = 0$, the following condition must be satisfied:

$$\dot{V} < 0 \ \text{ for } \ \mathrm{S} \neq 0 \tag{2.13}$$

Furthermore, if we want to achieve global finite-time stability, i.e. finite-time convergence, (2.13) can be modified to be

$$\dot{V} \le -\alpha V^{1/2} \tag{2.14}$$

where $\alpha > 0$. then, by separating variables and integrating the inequality in (2.14) over the time interval $[0, t]$, we claim

$$V^{1/2}(t) \le -\frac{1}{2} \alpha t + V^{1/2}(0) \tag{2.15}$$

This results that the Lyapunov function (2.12) attains zero in a finite-time t_r, which is defined by

$$t_r \le \frac{2V^{1/2}(0)}{\alpha} \tag{2.16}$$

The time derivative of (2.12) is computed as

$$\dot{V} = S\dot{S} = S(g(x,y,t) + u + \lambda y) \tag{2.17}$$

By assuming that $u = u_e + u_d$, where $u_e = -\lambda y$, and substituting it into (2.17) we obtain

$$\dot{V} = S(g(x,y,t) + u_d) = S\,g(x,y,t) + S\,u_d \le |S|H + S\,u_d \tag{2.18}$$

selecting $u_d = -\rho sign(S)$, where $\rho > 0$, and substituting it into (2.18) we get

$$\dot{V} \le |S|H - |S|\rho = -|S|(\rho - H) \tag{2.19}$$

Taking into account (2.12), (2.14) can be rewritten as

$$\dot{V} \le -\alpha V^{1/2} = -\frac{\alpha}{\sqrt{2}}|S| \quad ,\alpha > 0 \tag{2.20}$$

Combining (2.19) and (2.20) we obtain

$$\dot{V} \le -|S|(\rho - H) = -\frac{\alpha}{\sqrt{2}}|S| \tag{2.21}$$

As a final point, the control gain ρ is quantified as

$$\rho = H + \frac{\alpha}{\sqrt{2}} \tag{2.22}$$

such that, the first element of the control gain, H, is responsible for compensating the bounded external noise $g(x,y,t)$, while the second the second term, $\frac{\alpha}{\sqrt{2}}$, is designed to determine the time by which the sliding surface is reached illustrated by (2.16) . the largest α, the shortest reaching time.

Consequently a control law u that conducts the sliding surface S to zero in finite-time (2.16) is

$$u = u_e + u_d = -\lambda y - \rho\, sign(S) \tag{2.23}$$

2.4 Terminal Sliding Mode Control (TSMC)

The classical sliding mode control is based on the possibility of making and keeping the sliding variables on the sliding surface by means of a discontinuous control acting on the first-time derivative of the sliding variable. Where, at time t_r the sliding surface $S = y + \lambda x = 0$ is reached and the trajectories x, y remain on the sliding surface; This means that $S = \dot{S} = 0$ for

all $t \geq t_r$. The dynamic of the variable x_1 is uniformly asymptotically stable ($\lim_{t\to\infty}(x_1) = 0$) once the sliding surface is reached ($S = 0$). In order to make the state variables settle into origin in finite time (x, y) instead of being exponentially decreasing, we shall assay the following nonlinear sliding variable

$$S = S(x, y) = y + \lambda |x|^{\beta} \operatorname{sign}(x) \tag{2.24}$$

where $\lambda > 0$ and $0 < \beta < 1$. Note that in some works, for analytical convenience, β was selected as $\beta = p_1 / p_2$ where p_1 and p_2 are positive odd integers. The sliding variable in (2.24) is called terminal sliding mode (TSM) [43].

The sliding manifold, it doesn't perform the function of a straight line in the current circumstance due to its nonlinearity, that associates with the sliding variable (2.24) is continuous, as Figure 2.2 reveals.

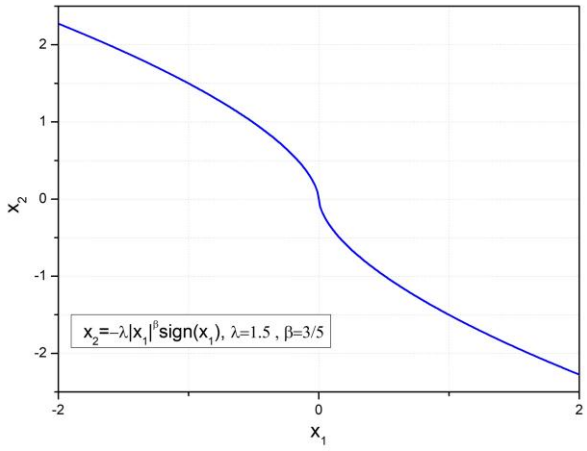

Figure 2.2 TSM manifold.

The sliding mode equations that correspond to the systems (2.1) and (2.24) are defined for all $t \geq t_r$ as

$$\begin{cases} \dot{x} = y \\ y = -\lambda |x|^{\beta} \operatorname{sign}(x) \end{cases} \quad x(t_r) = x_r \tag{2.25}$$

Equation (2.25) can be written as one nonlinear differential equation:

$$\dot{x} = -\lambda |x|^{\beta} \operatorname{sign}(x) \tag{2.26}$$

By integration, we get

$$t - t_r = -\frac{|x(t)|^{1-\beta} - |x_r|^{1-\beta}}{\lambda(1-\beta)} \tag{2.27}$$

We would to set a time instant $t = t_f$ so that $x_1(t_f) = x_2(t_f) = 0$. This is

$$t = \frac{|x_{1r}|^{1-\beta}}{\lambda(1-\beta)} + t_r \tag{2.28}$$

From this result, we can infer that the state variables $x, y \to 0$ in finite time quantified by $t_f - t_r$ while the system (2.1) is in the sliding surface represented by the equation (2.25). Whereas, the overall reaching time from the initial condition $x(t=0)$ and $y(t=0)$ to zero will be $t \le t_f$.

2.5 Synergetic Control (SC)

A perfect sliding mode does not exist in reality since it would require that the control switches at an infinite frequency. In the presence of commuting imperfection, for instance, switching time delays, the discontinuity in the feedback control causes a particular dynamic behavior in the neighboring of the surface, which is typically referred to as chattering. Chattering leads to high heat wastes in electrical power circuits and causes significant corrosion on moving mechanical parts. Several solutions and procedures have been designed to eliminate or reduce the discontinuity in the control function by estimating the discontinuous function $u_d = -k\,\text{sign}(S)$ using some continuous/smooth function such as hyperbolic tangent function, sigmoid function, saturation function, and so on. Due to the mentioned sliding mode control drawback, a recent, and promising, approach to the chattering problem is synergetic control [44].

Let us consider a nonlinear dynamics system, with n-dimension, that can be expressed as follows

$$\frac{dy(t)}{dt} = f(y,u,t) \tag{2.29}$$

where y represents the system state variable vector, u is the control input vector, and t symbolizes the time.

The theory of synergetic control is founded on state-space theory, which is used for designing and controlling complicated nonlinear systems. This control strategy initiates by stating a macro-variable defined in the following equation:

$$\varphi = \varphi(y) \tag{2.30}$$

The control approach allows the system's state variables to evolve on a predefined manifold, macro-variable φ function, achieving desired performance despite uncertainties and external disturbances. The synergetic control's objective is to drive the system to perform on the manifold $\varphi = 0$.

The macro-variable evolves in the desired way by placing a constraint that its dynamic evolution can be described by the following equation

$$\dot{\varphi} + \tau\varphi = 0 \tag{2.31}$$

where τ represents a controller argument that signifies the convergence rate speed of the closed-loop system to the given manifold toward $\varphi = 0$. Such that, its value should be greater than zero.

Regarding the chain rule of differentiation, the derivative of the equation (2.30) is

$$\dot{\varphi} = \frac{d\varphi(y)}{dy}\frac{dy(t)}{dt} = \frac{d\varphi(y)}{dy} f(y,u,t) \tag{2.32}$$

Then equation (2.31) will be rewritten as follows

$$\frac{d\varphi(y)}{dy} f(y,u,t) + \tau\varphi = 0 \tag{2.33}$$

Upon solving equation (2.33) for u, the control law is stated as

$$u = g(y,t,\varphi(y),\tau) \tag{2.34}$$

The control output depends on both system state variables and selected macro-variable, as well as the time constant τ. The designer can choose the controller's attributes by picking an appropriate macro-variable and a time constant τ.

Traditional control theory requires linearization and simplification of the system model, whereas this approach, as seen in the synthesis technique above, does not require any. The system is not supposed to leave the manifold once it has been reached. This indicates that the SC law ensures the manifold's global stability but does not assure the global stability of the system itself. The designer must select a suitable manifold to guarantee the new constrained system has the required stability characteristics. By selecting an appropriate macro-variable, designers can achieve the following desirable system characteristics: global stability, parameter insensitivity, and noise suppression.

2.6 Adaptive Terminal Sliding Mode Control for Synchronizing Two Hyperchaotic Systems.

Many research investigations focused on the potential applications of chaos and chaos synchronization in various fields of engineering and sciences. A well-designed controller will ensure that the trajectory of the response system follows and aligns with the trajectory of the drive system dynamics. In the following section, we shall demonstrate using an example and simulation plots to successfully achieve a global chaos synchronization of hyperchaotic systems using the TSMC technique.

Suppose a chaotic system with n dimension, which its dynamics are represented as follows

$$\dot{x} = Ax + f(x) \tag{2.35}$$

where $x \in \Re^n$ is the state of the system, $f : \Re^n \to \Re^n$ represents the nonlinear part of the system and A is the $n \times n$ matrix of the system parameters. The system (2.35) is regarded as the master system.

Let the slave system be described by the dynamics

$$\dot{y} = By + g(y) + u \tag{2.36}$$

with the controller $u = \left[u_1, u_2, \ldots, u_n\right]^T$, such that $u \in \Re^n$. $y \in \Re^n$ represent the state vector of the system, $g : \Re^n \to \Re^n$ is the nonlinear part of the slave system, and B is the $n \times n$ matrix of the system parameters.

If $A = B$ and $f = g$, then the systems, (2.35) and (2.36), are said to be identical chaotic systems; otherwise, x and y are the state vectors of two distinct chaotic systems.

The synchronization error vector dynamics is determined as

$$e = y - x \tag{2.37}$$

Hence, the synchronization error dynamics derivative is defined as

$$\dot{e} = \dot{y} - \dot{x} = By - Ax + g(y) - f(x) + u \tag{2.38}$$

The main challenge is to construct a nonlinear feedback controller u that will stabilize the error dynamics (2.37) for all initial conditions $e(t_0)$ in $\Re^n$, i.e. $\lim_{t \to \infty} \|e(t)\| = 0$ for every starting conditions $e(t_0) \in \Re^n$.

The Lyapunov stability approach starts with defining a candidate Lyapunov function is taken as

$$V(e(t)) = e(t)^T P e(t) \tag{2.39}$$

Where P is a $n \times n$ positive definite matrix.

$V : \Re^n \to \Re$ is a positive definite function by definition. The design presumes that the parameters of (2.35) and (2.36) systems are known beforehand that both systems' states, master and slave, are measurable.

If a controller u is designed such that the derivative of (2.39) is negative, i.e. $\dot{V}(e) < 0$, then based on Lyapunov stability theory, the tracking error dynamics (2.37) is said to be globally asymptotically stable, which leads to the condition $\lim_{t\to\infty} \|e(t)\| = 0$ to be achieved for all initial conditions $e(t_0) \in \Re^n$. As a consequence, the states of the drive system (2.35) and the response system (2.36) will be globally asymptotically synchronized.

The synthesis of an adaptive terminal sliding mode control is applied to synchronize a hyperchaotic (slave) Zhou system that has unknown parameters with another hyperchaotic (master) Zhou system.

The Master Hyperchaotic Zhou is defined by the following equation

$$\begin{cases} \dot{x}_1 = a(x_2 - x_1) + x_4 \\ \dot{x}_2 = cx_2 - x_1 x_3 \\ \dot{x}_3 = -bx_3 + x_1 x_2 \\ \dot{x}_4 = dx_1 + 0.5 x_2 x_3 \end{cases} \tag{2.40}$$

The response system dynamics are as follows

$$\begin{cases} \dot{y}_1 = \hat{a}(y_2 - y_1) + y_4 + u_1 \\ \dot{y}_2 = \hat{c}y_2 - y_1 y_3 + u_2 \\ \dot{y}_3 = -\hat{b}y_3 + y_1 y_2 + u_3 \\ \dot{y}_4 = \hat{d}y_1 + 0.5 y_2 y_3 + u_4 \end{cases} \tag{2.41}$$

Where the estimated errors of the parameters are defined by

$$\begin{cases} \tilde{a} = \hat{a} - a \\ \tilde{b} = \hat{b} - b \\ \tilde{c} = \hat{c} - c \\ \tilde{d} = \hat{d} - d \end{cases}$$

Let us consider the following sliding surface

$$S_i = e_i + \lambda_i \int_0^t e_i^{\frac{p_i}{qi}}(\tau)d\tau \ , \quad \lambda_i > 0 \tag{2.42}$$

Such that $\dot{e}_i = \dot{y}_i - \dot{x}_i$ and $i = 1,..,4$.

To accomplish a synchronization concerning the drive and the response systems in (2.40) and (2.41), respectively. The control laws are designed as follows

$$\begin{cases} u_1 = -\hat{a}(e_2 - e_1) - e_4 - \lambda_1 e_1^{\frac{p_1}{q_1}} - k_1 \operatorname{sgn}(S_1) - \eta_1 S_1 \\ u_2 = -\hat{c}e_2 + y_1 y_3 - x_1 x_3 - \lambda_2 e_2^{\frac{p_2}{q_2}} - k_2 \operatorname{sgn}(S_2) - \eta_2 S_2 \\ u_3 = \hat{b}e_3 - y_1 y_2 + x_1 x_2 - \lambda_3 e_3^{\frac{p_3}{q_3}} - k_3 \operatorname{sgn}(S_3) - \eta_3 S_3 \\ u_4 = -\hat{d}e_1 - 0.5 y_2 y_3 + 0.5 x_2 x_3 - \lambda_4 e_4^{\frac{p_4}{q_4}} - k_4 \operatorname{sgn}(S_4) - \eta_4 S_4 \end{cases} \tag{2.43}$$

Theorem 2.1

The evolution of the hyperchaotic Zhou system, which is described in the equation (2.41) with the arbitrary initial conditions $y(0) \in \Re^4$ and unknown parameters, tends toward the drive system (2.40) in a finite-time utilizing the control laws in the equation (2.43) with $\lambda_i, k_i, n_i > 0$, where the unknown parameters are adjusted by

$$\begin{cases} \dot{\hat{a}} = -S_1 (x_2 - x_1) \\ \dot{\hat{b}} = S_3 x_3 \\ \dot{\hat{c}} = -S_2 x_2 \\ \dot{\hat{d}} = -S_4 x_1 \end{cases} \tag{2.44}$$

Proof. Select the following Lyapunov function candidate

$$V = \frac{1}{2}\sum_{i=1}^{4} S_i^2 + \frac{1}{2}\tilde{a}^2 + \frac{1}{2}\tilde{b}^2 + \frac{1}{2}\tilde{c}^2 + \frac{1}{2}\tilde{d}^2$$

Taking the time derivative of the Lyapunov function yields

$$\dot{V} = \sum_{i=1}^{4} S_i \left(\dot{e}_i + \lambda_i e_i^{\frac{p_i}{qi}} \right) + \tilde{a}\dot{\tilde{a}} + \tilde{b}\dot{\tilde{b}} + \tilde{c}\dot{\tilde{c}} + \tilde{d}\dot{\tilde{d}} \tag{2.45}$$

By substituting the above control laws (2.43) and the parameters adaptation laws (2.44) into (2.45), we obtain

$$\dot{V} = -k_1 |S_1| - \eta_1 S_1^2 - k_2 |S_2| - \eta_2 S_2^2 - k_3 |S_3| - \eta_3 S_3^2 - k_4 |S_4| - \eta_4 S_4^2$$
$$\leq 0$$

Since $\dot{V}$ is negative, then the stability is proven. As a result, when $S_i = 0$, the dynamical errors e_i will converge to the origin in the following finite-time

$$t = \frac{|e_i(t_r)|^{1-\frac{p_i}{q_i}}}{\lambda(1-\frac{p_i}{q_i})} + t_r \tag{2.46}$$

Therefore, the proof is complete.

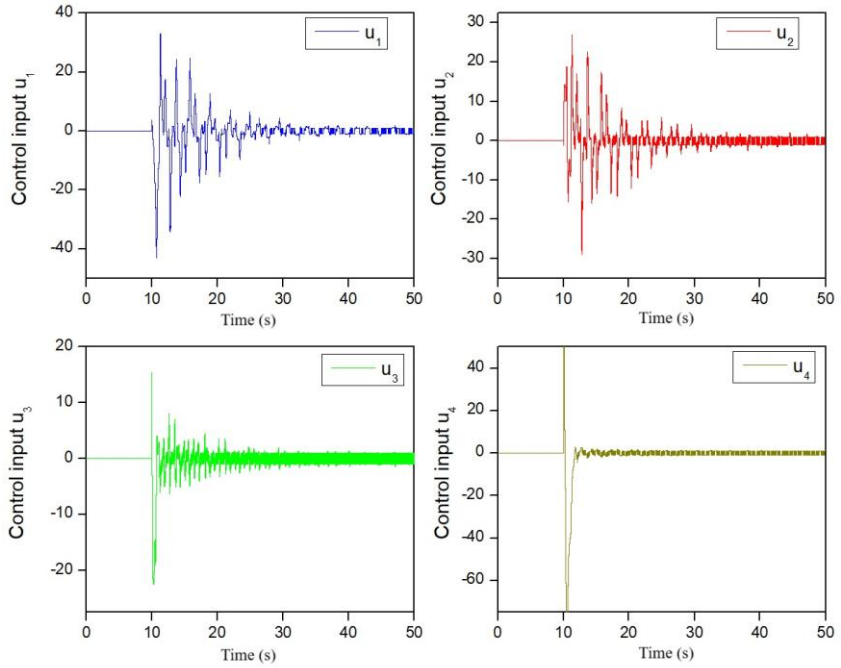

Figure 2.3 Control inputs based adaptive TSMC.

Simulation results in Figure 2.3 show the control inputs for the response system using the adaptive TSMC, where the control signal is disabled for $t < 10s$ and is enabled for $t \geq 10s$. Figure 2.4 reveals the fast convergence of the response system state space trajectories toward the trajectories of the drive system. The results depicted in Figure 2.5 reveals that with the performance of the proposed method, the parameter $\hat{a}(t)$ exhibits a slow convergence rate in attempting to reach the reference parameter, which means $a = 35$, in the master system. On the other hand, the other unknown parameters, $\hat{b}, \hat{c}$ and $\hat{d}$, in the slave system move towards the master system's parameters with faster response.

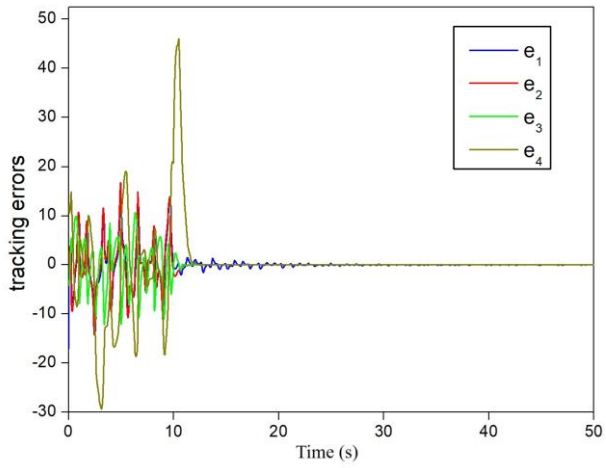

Figure 2.4 Trajectories of synchronization errors.

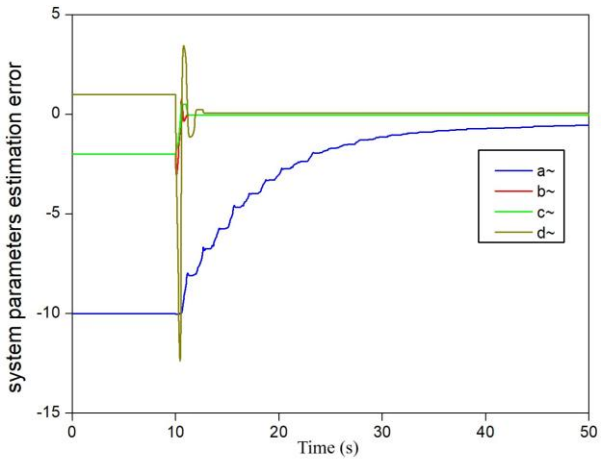

Figure 2.5 Parameters convergence evolution error.

2.7 Conclusion

Due to the fact that there is always a dissimilarity between the mathematical model of a system and its actual plant dynamics, in this chapter, we introduced some robust control techniques that are intended to provide the desired closed-loop system performance by taking into consideration the system parameter uncertainties and the external disturbances. Then, we demonstrated the robustness of the sliding mode control technique by synchronizing two hyperchaotic systems with unknown parameters.

Chapter 3. Takagi-Sugeno Fuzzy Model Based Synergetic Control Theory

3.1 Introduction

Modeling, synchronization, and control of chaotic dynamical systems are fields of study that have attracted more interest recently [45]–[47]. In the current effort devoted to these subjects, the approach presented here uses a methodology based on fuzzy logic extended and integrated into synergetic control (SC) to enhance performances resulting from the combination of both techniques' advantages.

Fuzzy modeling [48] uses the concept of fuzzy set theory to construct multi-models of the process based on the original mathematical model of the system or uses the input-output data. The main advantage of creating sub-models is to represent the local dynamics by a linear system model and facilitate the design of their controller.

In this section, we begin with intuitive and preliminaries to fuzzy logic. Next, a fuzzy synergetic controller is designed to synchronize two distinct hyperchaotic systems obtained through the Takagi-Sugeno fuzzy modeling technique. Finally, in comparison to the sliding mode control technique, the newly proposed controller's performances are examined on the synchronization of Lorenz and Lu hyperchaotic systems.

3.2 Preliminaries to Fuzzy Logic

Most of the physical dynamical systems in reality exhibit nonlinearities and uncertainties that are difficult to precisely describe with mathematical models. In addition, in the design of the algorithm of controllers, it is necessary that the mathematical system model and the parameters of the system are well-known and achievable. Unfortunately, in many nonlinear plans, building a mathematical model is quite complex and sometimes only the yielded input-output data from operating the process is reachable for estimation.

Fuzzy Logic was founded in 1965 by Lotfi Zadeh [20] as a broadening of the Boolean logic to handle situations when we cannot determine whether the state is completely true or completely false. The fuzzy logic offers valuable adaptability for reasoning to deal with imprecise or uncertain information, where the partial truth can be any real number in the region between the value 0 and 1, rather than fully true or false.

Based on fuzzy sets and fuzzy algorithms that are introduced by Lotfi Zadeh, its approach

provides a general method to incorporate strategies based on an experienced operator for controlling or modeling a system using linguistic variables by a set of rules to be used in different situations.

3.2.1 Fuzzy Sets

With the aim of introducing fuzzy sets, let's start by discussing whether the elements of the universal set belong to or do not belong to particular sets, whereas the traditional sets are founded by two-valued logic. In other words, due to the factuality that two-valued logic requires us to assign and classify an object into one of two groups, for example, odd or even, true or false, 0 or 1, etc. This sort of classification type of the objects can be quite easily performed on processes that are accurate and well-defined. However, many terms that are used in engineering like slow, warm, good, far, turbulent …, are all relative and their classification could be considered differently by an individual and another individual.

From the above discussion, it is obvious that we need to determine the degree of belonging of an ill-defined object to a set. For this purpose, Lotfi Zadeh introduced and formulated the concept of a fuzzy set.

3.2.1.1 Definition of Fuzzy Sets

The main concept of fuzzy logic is the membership function, which assigns the degree of membership of each element y in the universe of discourse D to a certain set by a value included in the range of zero and one instead of from the two-values set, which is absolute zero or absolute one, in classic set theory. Such an extended membership function is referred to as a Fuzzy set [20].

For a fuzzy set S , The membership function μ_S is a function

$$\mu_S : D \to [0,1] \tag{3.1}$$

That every item y in D has a membership degree $\mu_S(y) \in [0,1]$. S is completely expressed by the set of tuples. The greater the value of a particular item's membership, y , to the fuzzy set S , $\mu_S(y)$, the strongest link of y to the category defined by S .

A fuzzy set S can be illustrated by an ordered pair

$$S = \{(y, \mu_S(y) | y \in D)\} \tag{3.2}$$

When D is continuous, S is commonly written as

$$S = \int_D \mu_S(y)/y \tag{3.3}$$

where the integral sign in (3.3) does not signify integration, it indicates the set of all points $y \in D$ and their associated membership function $\mu_S(y)$.

When the universe of discourse D is finite. Then, the fuzzy set is commonly represented as

$$S = \sum_D \mu_S(y)/y \tag{3.4}$$

The summation sign in (3.4) does not signify arithmetic addition, it indicates the collection of all points $y \in D$ with the associated membership function $\mu_S(y)$.

Hence, a fuzzy set is possible to be viewed by plotting y versus $\mu_S(y)$. Trapezoidal and triangular are commonly used forms as membership functions in fuzzy applications. Also, there are other membership functions such as Piecewise linear, Gaussian, monotonically increasing and decreasing functions. In addition, for discrete D, a table can also be used to represent a fuzzy set.

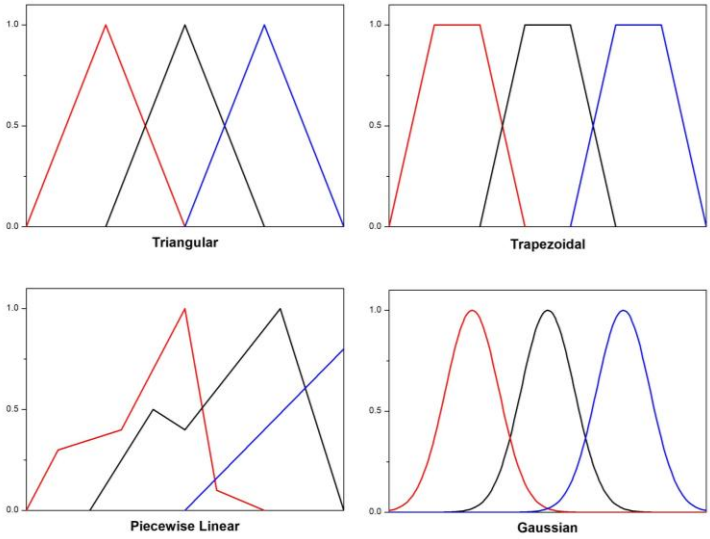

Figure 3.1 Membership Functions.

3.2.1.2 Fundamental Operations of Fuzzy Sets

Lotfi Zadeh established the following definition of the classical operators.

Union of fuzzy sets S_1 and S_2, $S_1 \cup S_2$, is expressed by the following membership function:

$$\mu_{S_1 \cup S_2}(y) = \mu_{S_1}(y) \cup \mu_{S_2}(y) \tag{3.5}$$

where

$$\mu_{S_1}(y) \cup \mu_{S_2}(y) = \begin{cases} \mu_{S_1}(y) & if\ \mu_{S_1}(y) \geq \mu_{S_2}(y) \\ \mu_{S_2}(y) & else \end{cases}$$
$$= \max\left\{\mu_{S_1}(y), \mu_{S_2}(y)\right\}$$

Intersection of fuzzy sets S_1 and S_2, $S_1 \cap S_2$, is by the following membership function:

$$\mu_{S_1 \cap S_2}(y) = \mu_{S_1}(y) \cap \mu_{S_2}(y) \tag{3.6}$$

where

$$\mu_{S_1}(y) \cap \mu_{S_2}(y) = \begin{cases} \mu_{S_1}(y) & if\ \mu_{S_1}(y) \leq \mu_{S_2}(y) \\ \mu_{S_2}(y) & else \end{cases}$$
$$= \min\left\{\mu_{S_1}(y), \mu_{S_2}(y)\right\}$$

Complement of fuzzy set S_1, $\bar{S}_1$, is expressed by the following membership function

$$\mu_{\bar{S}_1}(y) = 1 - \mu_{S_1}(y) \tag{3.7}$$

Let S_1, S_2 and S_3 be fuzzy sets on the universe of discourse D.

1. The following properties are specific for both crisp and fuzzy sets.

Associativity law:

$$S_1 \cap (S_2 \cap S_3) = (S_1 \cap S_2) \cap S_3,\ S_1 \cup (S_2 \cup S_3) = (S_1 \cup S_2) \cup S_3 \tag{3.8}$$

Distributivity law:

$$\begin{aligned} S_1 \cap (S_2 \cup S_3) &= (S_1 \cap S_2) \cup (S_1 \cap S_3), \\ S_1 \cup (S_2 \cap S_3) &= (S_1 \cup S_2) \cap (S_1 \cup S_3) \end{aligned} \tag{3.9}$$

De Morgan's laws:

$$\begin{aligned} \overline{S_1 \cup S_2} &= \bar{S}_1 \cap \bar{S}_2 \\ \overline{S_1 \cap S_2} &= \bar{S}_1 \cup \bar{S}_2 \end{aligned} \tag{3.10}$$

2. Properties that are specific for crisp sets, nonetheless mostly not for fuzzy sets.

The contradiction's law:

$$S_1 \cap \bar{S}_1 = \varnothing \tag{3.11}$$

Where $\varnothing$ means an empty set.

The law of excluded middle:

$$S_1 \cup \overline{S}_1 = D \tag{3.12}$$

A $t-norm$ is a function $t:[0,1]\times[0,1]\to[0,1]$ that meets the bellow conditions:

a) Boundary condition: $t(0,0)=0$, $t(y,1)=t(1,y)=y$.

b) Commutativity: $t(y,z)=t(z,y)$.

c) Monotonicity: if $y\le y'$ and $z\le z'$ then $t(y,z)\le t(y',z')$ .or

d) Associativity: $t(t(y,z),w)=t(y,t(z,w))$.

In addition to the previously stated classical min operator, other $t-norm$ comprise:

a) Algebraic product: $t_a:(y,z)\to yz$.

b) Bounded product: $t_b:(y,z)\to \max(0,y+z-1)$.

c) Drastic product: $t_d:(y,z)\to\begin{cases} y, \text{ if } z=1 \\ z, \text{ if } y=1 \\ 0, \text{ for other cases} \end{cases}$

A $s-norm$ (or $t-conorm$) is a function $s:[0,1]\times[0,1]\to[0,1]$ that meets the bellow conditions:

a) Boundary condition: $s(1,1)=1$, $s(y,0)=s(0,y)=y$.

b) Commutativity: $s(y,z)=s(z,y)$.

c) Monotonicity: if $y\le y'$ and $z\le z'$ then $s(y,z)\le s(y',z')$ .or

d) Associativity: $s(s(y,z),w)=s(y,s(z,w))$.

In addition to the previously stated classical max operator, other $s-norm$ comprise:

a) Algebraic sum: $s_a:(y,z)\to y+z-yz$.

b) Bounded sum: $s_b:(y,z)\to \min(y+z,1)$.

c) Drastic sum: $s_d:(y,z)\to\begin{cases} y, \text{ if } z=0 \\ z, \text{if } y=0 \\ 1, \text{ otherwise} \end{cases}$

3.2.1.3 Linguistic Variables

If a variable is capable of accepting natural language words as values, it is referred to as a linguistic variable, with the words specified by fuzzy sets in the universe of discourse in which the variable is defined [49].

A linguistic variable is fully characterized by (X,T,D,M), on which X is the name of the variable, T is the set of linguistic terms of X that refer to a base variable whose values range over the actual physical domain D, whereas M is a semantic rule that relates each linguistic value in T with a fuzzy set in D.

A hedge is a word that acts on a term and modifies its meaning. In other words, we use more than one word to describe the linguistic variable. For example, in 'very young', here the term "young" is the main term, and "very" is a hedge. A hedge operates on a membership function, and the result is a membership function.

Some hedges examples: very, more or less, slightly, etc.

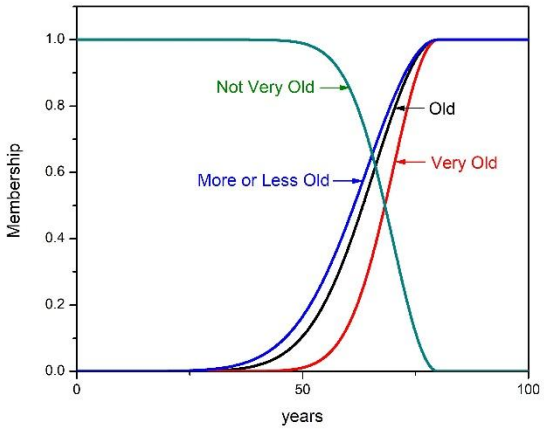

Figure 3.2 The membership functions for different hedges of the primary linguistic variable "old".

3.2.2 Fuzzifier

Producing a map from a crisp (real-valued) point $y \in D \subset \Re^n$ into a fuzzy set S in the universe of discourse D is referred to as a fuzzifier. There are many proposed choices of fuzzifiers in literature like Singleton fuzzifier, Gaussian fuzzifier, Triangular, etc. Figure 3.1 reveals some forms of the fuzzifiers maps.

3.2.3 If-Then Rules

A fuzzy model or controller contains the set of rules and the If-Then conditions provided by the knowledge and experience of the experts to govern the decision-making system and link the linguistic statements (the input variables to the output variable or variables).

A fuzzy IF-THEN rule is a conditional statement expressed as

$$IF < \text{premise (Antecedent)} >, THEN < \text{conclusion (Consequent)} > \tag{3.13}$$

There are two types of fuzzy propositions in the "premise" part

1. Atomic fuzzy propositions are single statements.
2. Compound fuzzy propositions combine atomic fuzzy propositions with the connectives "or", "and", and "not" to describe the fuzzy union, fuzzy intersection, and fuzzy complement, respectively.

Rule-based fuzzy systems can be distinguished according to the types of fuzzy IF-THEN rules. Two major canonical structures are available, namely Takagi-Sugeno (T-S) and Mamdani fuzzy systems [49].

3.2.4 Mamdani Fuzzy Systems:

For each of the two fuzzy modeling and fuzzy control, a general Mamdani fuzzy rule is most likely defined as

$$\text{Rule}^{(l)}\text{: IF } y_1 \text{ is } S_1^l \text{ and ... and } y_n \text{ is } S_n^l \text{ ,THEN o}^1 \text{ is } H^l.\ \ l = 1,2,3,... \tag{3.14}$$

Where S_i^l and H^l are fuzzy sets, $y = (y_1,...,y_n)^T \in D$ and $o \in V$ represents the inputs and outputs, respectively. This sort of fuzzy IF-THEN rules hands over a comfortable framework and helpful system to join human experts' knowledge and experience.

3.2.5 Fuzzy Inference of Mamdani Fuzzy System

Fuzzy inference is required to compute the result for output variables at each rule consequence when a particular state or data is appointed to input variables in the rule antecedent. Max-min inference and Max-product inference are methods that are used for defuzzification and transform the fuzzy results of the inference into a crisp output [50]. They are the major typically used fuzzy inference engine in fuzzy control and fuzzy systems due to their computational simplicity.

3.2.5.1 Max-min Inference

Let us consider a simple 2 rule system where each has 2 antecedents and one consequence as follows:

$$\begin{aligned} &\text{Rule}^{(1)}\text{: IF } y_1 is S_1^1 \text{ and } y_2 is S_2^1 \text{ ,THEN o}^1 is H^1 \\ &\text{Rule}^{(2)}\text{: IF } y_1 is S_1^2 \text{ and } y_2 is S_2^2 \text{ ,THEN o}^2 is H^2 \end{aligned} \tag{3.15}$$

From the equation (3.15) we get:

$$\begin{aligned} \mu_{H^1}(y^*) &= \mu_{S_1^1}(y_1) \cap \mu_{S_2^1}(y_2) = \min\left\{\mu_{S_1^1}(y_1), \mu_{S_2^1}(y_2)\right\} \\ \mu_{H^2}(y^*) &= \mu_{S_1^2}(y_1) \cap \mu_{S_2^2}(y_2) = \min\left\{\mu_{S_1^2}(y_1), \mu_{S_2^2}(y_2)\right\} \end{aligned} \tag{3.16}$$

Where $\mu_{H^i}(y^*)$ is the overall inferred truth value of the i-th rule.

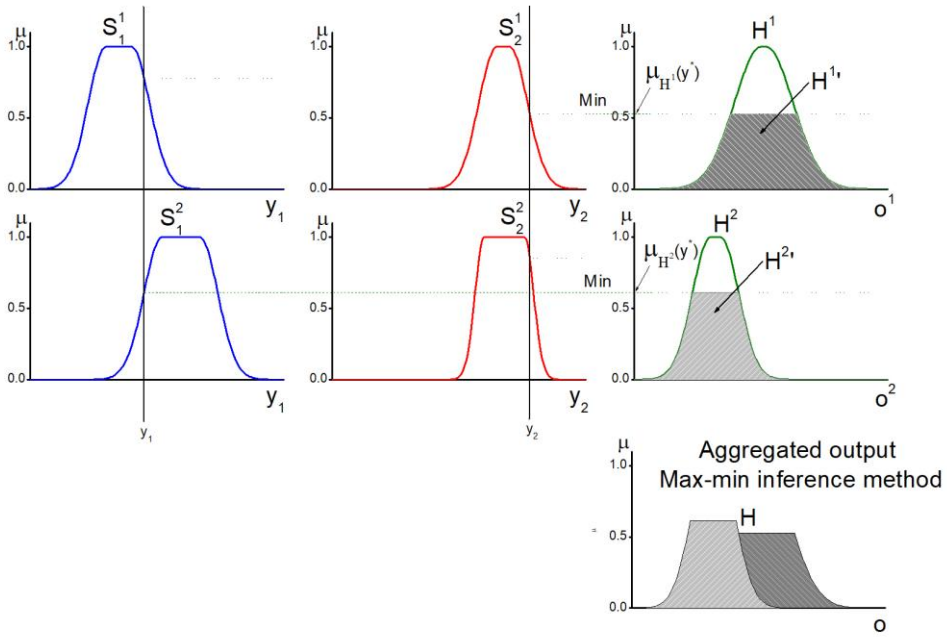

Figure 3.3 Graphical representation of Max-min inference method.

Then, the output of each rule is as follow:

$$\begin{aligned} \mu_{H^{1'}}(o^1) &= \min(\mu_{H^1}(y^*), \mu_{H^1}(o^1)) \\ \mu_{H^{2'}}(o^2) &= \min(\mu_{H^2}(y^*), \mu_{H^2}(o^2)) \end{aligned} \tag{3.17}$$

The union of these two membership functions resulting from $\text{Rule}^{(1)}$ and $\text{Rule}^{(2)}$ are used to produce the aggregated output that is depicted in Figure 3.3.

$$\mu_H(o) = \mu_{H^{1'}}(o^1) \cup \mu_{H^{2'}}(o^2) = \max\left\{\mu_{H^{1'}}(o^1), \mu_{H^{2'}}(o^2)\right\} \tag{3.18}$$

3.2.5.2 Max-product Inference

Figure 3.4 reveals the aggregated output using the Max-product inference method, which utilizes the standard product of the input membership functions.

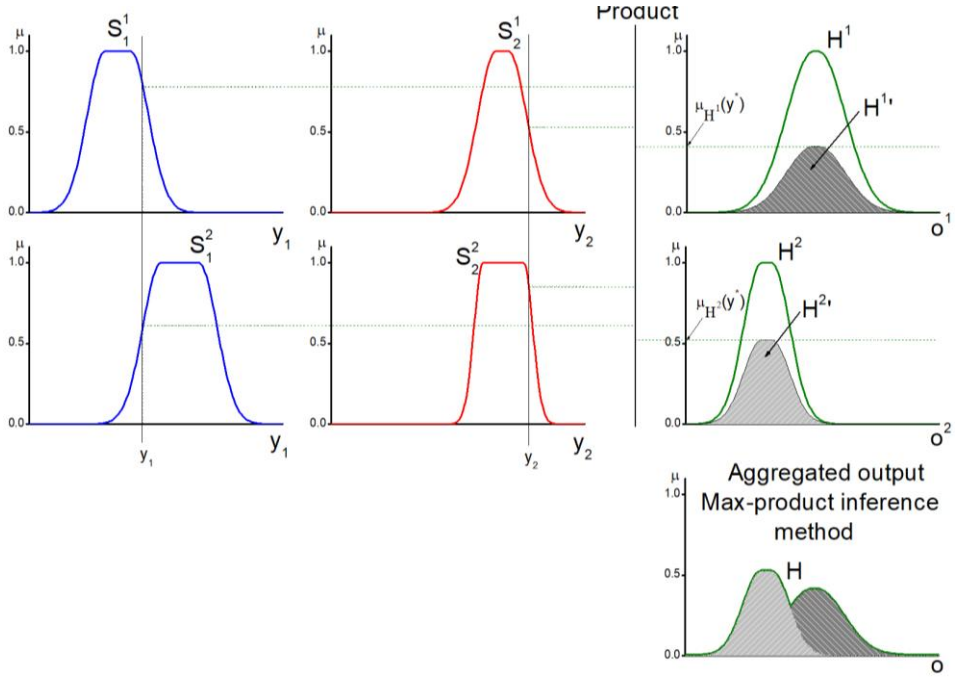

Figure 3.4 Graphical representation of Max-product inference method.

$$\begin{aligned}\mu_{H^{1'}}(o^1) &= \mu_{H^1}(y^*)\,\mu_{H^1}(o^1)\\ \mu_{H^{2'}}(o^2) &= \mu_{H^2}(y^*)\;\mu_{H^2}(o^2)\end{aligned} \tag{3.19}$$

Where:

$$\begin{aligned}\mu_{H^1}(y^*) &= \mu_{S_1^1}(y_1)\,\mu_{S_2^1}(y_2)\\ \mu_{H^2}(y^*) &= \mu_{S_1^2}(y_1)\,\mu_{S_2^2}(y_2)\end{aligned} \tag{3.20}$$

Then, the aggregated output is:

$$\mu_H(o) = \mu_{H^{1'}}(o^1) \cup \mu_{H^{2'}}(o^2) = \max\left\{\mu_{H^{1'}}(o^1), \mu_{H^{2'}}(o^2)\right\} \tag{3.21}$$

3.2.5.3 Defuzzification of Mamdani Fuzzy System

Defuzzification is a necessary step to produce a crisp output for our fuzzy logic system from the fuzzy set that is the inferenced output. It is a mapping from fuzzy sets (one or more) into corresponding real value numbers in the universe of discourse.

Many different defuzzifiers have been proposed. The most commonly used methods for defuzzification are:

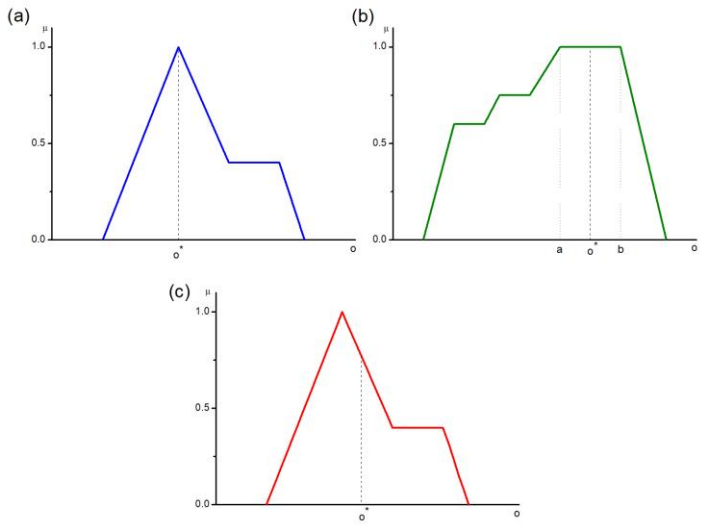

Figure 3.5 Defuzzication methods: (a) Maximum defuzzifier, (b) Mean of maxima defuzzifier, and (c) Centroid defuzzifier.

(a). Maximum defuzzifier

This defuzzifier selects the o^* as the point in the discourse V at which the membership of this point ($\mu_H(o)$) achieves its maximum value.

Where the set of all points in V at which $\mu_H(o)$ achieves its maximum value is defined as

$$hgt(H) = \left\{ o \in V \middle| \mu_H(o) = \sup_{o \in V} \mu_H(o) \right\} \tag{3.22}$$

If $hgt(H)$ consists of a single point, then o^* is uniquely defined, otherwise, we may use any point in $hgt(H)$, or use the smallest of maxima or the largest of maxima.

(b). Mean of maxima defuzzifier

The defuzzifier inspects the fuzzy set H and first identifies the values of o for which it is a maximum, then calculates the mean of these values as its output.

(c). Centroid defuzzifier

This defuziifier is the most commonly used method, due to its output result being sensitive to all the rules executed. It calculates the o^*, which is the center of the area covered by the membership function of H . Such that

$$o^* = \frac{\int_V \mu_H(o)\, o\, do}{\int_V \mu_H(o)\, do} \tag{3.23}$$

Where $\int_V$ is the conventional integral.

3.2.6 Takagi-Sugeno Fuzzy System

A Takagu-Sugeno fuzzy rule is characterized as

$$\text{Rule}^{(l)}\text{: IF } y_1 \text{ is } S_1^l \text{ and ... and } y_n \text{ is } S_n^l \text{ ,THEN } o^l = f^l(y_1, y_2, ..., y_n) = c_0^l + c_1^l y_1 + ... + c_n^l y_n \text{ .} \tag{3.24}$$

Where S_i^l represent fuzzy sets, o^l expresses the system output and c_i^l are real-valued parameters. Where the IF part (premise) is fuzzy sets. But rather than using fuzzy sets in the consequence part, the THEN part in TS is crisp, in other words the output comprises a linear input variables' combination.

The corresponding output value of TS fuzzy system is given by

$$o^* = \frac{\sum_{i=1}^{l} w^i o^i}{\sum_{i=1}^{l} w^i} \tag{3.25}$$

Such that, the weight w^i represents the premise's overall truth value of the ith rule.

3.2.7 Takagi-Sugeno Fuzzy Models of Nonlinear Systems

The foremost attribute of a Takagi-Sugeno fuzzy model is that at each fuzzy rule it states a system and represents its local dynamics using a linear state space system model. By combining of these local linear system models, an aggregated fuzzy model of the system is obtained by employing some suitable membership functions.

The form of continuous time nonlinear systems is described as follows

$$\dot{y}(t) = f(y(t)) + g(y(t))u(t) \tag{3.26}$$

Where $y(t) \in \Re^n$ represents the state vector, $f(y(t)) \in \Re^n$ and $g(y(t)) \in \Re^{n \times m}$ are nonlinear vector functions, and $u(t) \in \Re^m$ expresses the control input vector,.

The goal is to derive TS model from the above given nonlinear system equation. To determine its corresponding local model, the ith rule of the continuous Takagi-Sugeno fuzzy model is formulated in the following form:

$$\begin{aligned} \text{Ru}^{(i)}\text{: IF } & y_1(t) \text{ is } \Gamma_1^i \text{ and ... and } y_n(t) \text{ is } \Gamma_n^i \\ \text{THEN } & \dot{y}(t) = A_i y(t) + B_i u(t) \quad , i = 1, 2, ..., q \end{aligned} \tag{3.27}$$

where q represents the number of rules of this Takagi-Sugeno model, Γ_j^i is a fuzzy set, $y(t) \in \Re^n, y(t) = [y_1(t)\ y_2(t)\ ...\ y_n(t)]^T$ is the system state, $A_i \in \Re^{n\times n}$ and $B_i \in \Re^{n\times m}$ are system matrix and input matrix, respectively, $u(t) \in \Re^m, u(t) = [u_1(t)\ u_2(t)\ ...\ u_m(t)]^T$ represents the control input vector.

Then, the defuzzified output of the Takagi-Sugeno fuzzy system described in equation (3.27) is represented as follows:

$$\dot{y}(t) = \sum_{i=1}^{q} \mu_i(y(t))(A_i y(t) + B_i u(t)) \tag{3.28}$$

Where:

$$\mu_i(y(t)) = \frac{w_i(y(t))}{\sum_{i=1}^{q} w_i(y(t))} \tag{3.29}$$

Such that, the weight w_i represents the premise's overall truth value of the ith rule. It is described by

$$w_i(y(t)) = \prod_{j=1}^{n} \Gamma_j^i(y_j(t)) \tag{3.30}$$

In which $\Gamma_j^i(x_j(t))$ is the grade of membership of $x_i(t)$ in Γ_j^i.

Due to some basic properties of $w_i(y(t))$, which are:

$$w_i(y(t)) \geq 0 \text{ and } \sum_{i=1}^{q} w_i(y(t)) > 0,\ i = 1,2,...,q \tag{3.31}$$

It is obvious that

$$\mu_i(y(t)) \geq 0, \text{and } \sum_{i=1}^{q} \mu_i(y(t)) = 1,\ i = 1,2,...,q \tag{3.32}$$

Using the same manner for the discrete time nonlinear system, which is in the form

$$y(k+1) = f(y(k)) + g(y(k))u(k) \tag{3.33}$$

Where k and $k+1$ signify the pointers of the time steps.

Then, Takagi-Sugeno fuzzy model for the discrete time case is formulated as follows:

$$\begin{aligned} &\text{Rule}^{(i)}\text{: IF } y_1(k) \text{ is } \Gamma_1^i \text{ and ... and } y_n(k) \text{ is } \Gamma_n^i \\ &\qquad \text{THEN } y(k+1) = C_i y(k) + D_i u(k) \quad ,\ i = 1,2,...,q \end{aligned} \tag{3.34}$$

3.3 Synchronization of Hyperchaos Systems Using Takagi-Sugeno Fuzzy-Model Based Synergetic Control Theory

The Takagi-Sugeno fuzzy system is extremely used as a tool for modeling and controlling highly complex nonlinear system [51]. A Takagi-Sugeno fuzzy model has been widely utilized for mathematical simplicity in analysis. This fuzzy model combines linear models represented by local dynamics across state space regions. Since the Takagi-Sugeno fuzzy model can give a representation of a hyperchaotic system with a small number of implications of rules, we have applied fuzzy control to synchronizing two different hyperchaotic systems [14]. The main idea is to utilize the well-known Takagi-Sugeno fuzzy model to express a typical hyperchaotic system and then construct a synergetic controller for the fuzzy model.

3.3.1 Takagi-Sugeno Fuzzy Modeling of Hyperchaotic Systems

In our work, we proposed a fuzzy rule-based T-S model that describes the Hyperchaotic Lu system represented in chapter 1 (section 1.7.3) by assuming that $y_1(t) \in [-\beta\ \beta]$, then, the dynamic fuzzy model can be presented as follows

$$\begin{aligned} &\text{Rule1: if } y_1(\text{t}) \text{ is } \xi_1, \text{ Then } \dot{y}(t) = A_1 y(t) \\ &\text{Rule2: if } y_1(\text{t}) \text{ is } \xi_2, \text{ Then } \dot{y}(t) = A_2 y(t) \end{aligned} \tag{3.35}$$

where $\dot{y}(t) = A_i y(t)$ represents the output from the i-th if-then rules. While ξ_1 and ξ_2 are the fuzzy sets and. Therefore, the inferred output of the fuzzy system can be inferred as follows

$$\dot{y}(t) = \sum_{i=1}^{2} \xi_i(y_i) A_i y(t) \tag{3.36}$$

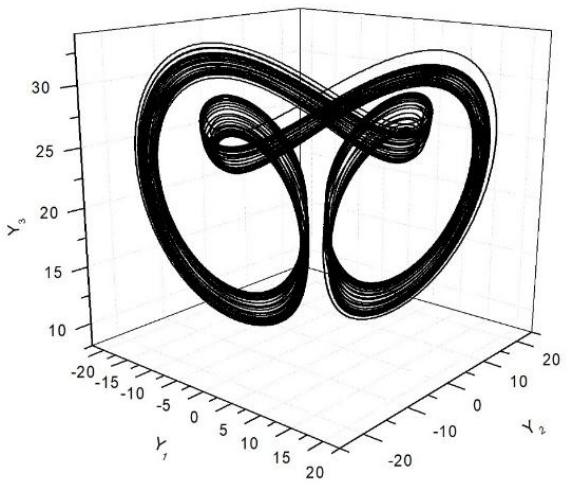

Figure 3.6 Hyperchaotic attractor of fuzzy system (3.36) for $a = 36, b = 3, c = 20$ and $d = -0.345$.

such that

$$A_1 = \begin{bmatrix} -a & a & 0 & 1 \\ 0 & c & -\beta & 0 \\ 0 & \beta & b & 0 \\ 0 & 0 & \beta & d \end{bmatrix}, \quad \xi_1 = 0.5 + \frac{y_1(t)}{2\beta}$$

and

$$A_2 = \begin{bmatrix} -a & a & 0 & 1 \\ 0 & c & \beta & 0 \\ 0 & -\beta & b & 0 \\ 0 & 0 & -\beta & d \end{bmatrix}, \quad \xi_2 = 0.5 - \frac{y_1(t)}{2\beta}$$

The system response depicted in Figure 3.6 is identical to the results discussed and obtained in [8], [52]. Hence, for any region of interest, the fuzzy system (3.35) can model exactly the hyperchaotic Lu system (1.33). Through this fuzzy model, the final form of the fuzzy model turns out to be very simple and is attained by fuzzy blending of the two linear subsystem models. In this section, we illustrated that the selected model represents the real model, and we showed the effectiveness and advantages of the Takagi-Sugeno fuzzy model.

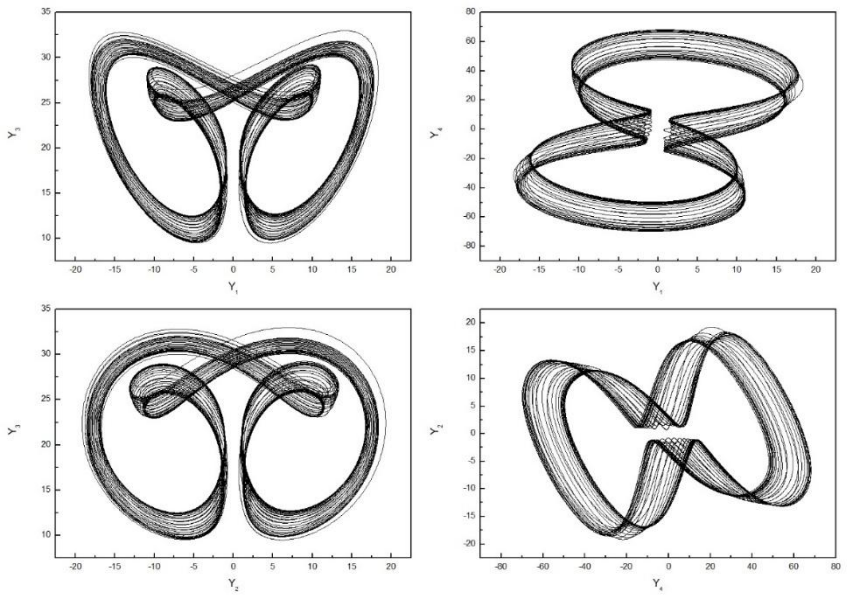

Figure 3.7 Phase portraits of the fuzzy system (3.35); (a) the $y_1 - y_2$ space; and projected on (b) the $y_2 - y_3$ plane; (c) the $y_1 - y_4$ plane.

3.3.2 Synergetic Synchronization of Hyperchaotic Systems Modeled by Takagi-Sugeno Fuzzy Technique

In the following, we will focus our attention on the control of a linear controllable system of the form

$$\dot{x}(t) = Ax(t) + Bu(t) \tag{3.37}$$

where $x \in \Re^{n\times 1}$ is system state $A \in \Re^{n\times n}$ and $B \in \Re^{n\times n}$ are constant matrices, while the synergetic control to be designed is $u \in \Re^{n\times 1}$. As we mentioned in the section 2.5, the synergetic control synthesis begins by choosing a macro-variable φ , which is a function of the system variable, that needs to be zero. Let it be chosen as

$$\varphi(x) = M\,(x - x_d) \tag{3.38}$$

where $x_d = [x_{1d}, x_{2d}, \cdots, x_{nd}]^T \in \Re^{n\times 1}$ is the desired or the reference output signal. M represents a constant matrix to be defined.

To assure the stability and convergence of the state trajectories toward their prerequisite intended manifolds and remain on them in the future, we shall define the evolution dynamic of the macro-variable as follows

$$\dot{\varphi} + \tau\varphi = 0 \qquad \tau > 0 \tag{3.39}$$

Using equations (3.38) to solve the system (3.37) with the evolution condition (3.39), then we can have

$$M\left(Ax(t) + Bu(t)\right) = -\tau\varphi + M\,\dot{x}_d \tag{3.40}$$

Therefore, the synergetic control input formula is denoted as

$$u(t) = -\left(M\,B\right)^{-1}\left[M\,Ax(t) + \tau\varphi - M\,\dot{x}_d\right] \tag{3.41}$$

According to the fuzzy system (3.35), let the drive system, Lorenz hyperchaotic system [53], can be expressed exactly by the following inferred Takagi-Sugeno fuzzy output

$$\dot{x}(t) = \sum_{i=1}^{2} \xi'_i(x_i) A'_i\, x(t) \tag{3.42}$$

The following fuzzy rule structure is utilized to design and develop the law of the synergetic control input signal which synchronizes the mentioned hyperchaotic systems

$$\begin{aligned}
&\text{Rule1: if } y_1(t) \text{ is } \xi_1 \text{ and } x_1(t) \text{ is } \xi'_1,\\
&\quad \text{Then } \dot{y}(t) = A_1 y(t) + B u_1(t) \text{ and } u_1(t) = -\left(M\,B_1\right)^{-1}\left[M\,A_1\,y(t) + \tau_1\varphi - MA'_1\,x(t)\right]\\
&\text{Rule2: if } y_1(t) \text{ is } \xi_2 \text{ and } x_1(t) \text{ is } \xi'_2,\\
&\quad \text{Then } \dot{y}(t) = A_2 y(t) + B u_2(t) \text{ and } u_2(t) = -\left(MB_2\right)^{-1}\left[M\,A_2\,y(t) + \tau_2\varphi - MA'_2\,x(t)\right]
\end{aligned} \tag{3.43}$$

Therefore, the overall fuzzy model and the general controller are conceivably presented by

$$\dot{y}(t) = \sum_{i=1}^{2} \xi_i(y_i) A_i y(t) + \sum_{i=1}^{2} \xi_i(y_i) B_i u(t) \tag{3.44}$$

$$u(t) = \sum_{i=1}^{2} \xi_i(y_i) u_i(t) - M \sum_{i=1}^{2} \xi_i(x_i) A'_i\, x(t) \tag{3.45}$$

where

$$u_i(t) = -\left(M\,B_i\right)^{-1}\left[M\,A_i\,y(t) + \tau_i\varphi)\right] \tag{3.46}$$

The following theorems for synchronization and stabilization of the hyperchaotic systems are verified based on the Lyapunov stability analysis.

Theorem 3.1

Take into consideration the hyperchaotic synchronization problem, between the hyperchaotic Lu system (1.33) and the hyperchaotic Lorenz system [53], the driven and the drive systems are asymptotically synchronized if the fuzzy SC law (3.46) is used and $M\,B_i = M\,B_j = M\,B$ for $i \neq j$.

Proof

To check the stability of the SC, we consider $Z = 0.5\,\varphi^T\varphi$ as the Lyapunov function candidate. The derivation of this function must be calculated, therefore

$$\dot{Z} = \varphi^T\dot{\varphi} = \varphi^T M\,(\dot{y} - \dot{x}) \tag{3.47}$$

Substituting (3.44) into (3.47) yields

$$\begin{aligned}
\dot{Z} &= \varphi^T M \left(\sum_{i=1}^{2} \xi_i(y_1) A_i y(t) + M\,B \sum_{i=1}^{2} \xi_i(y_1) u_i(t) \right)\\
&\leq -2 \sum_{i=1}^{2} \xi_i(y_1)\tau_i Z(t) \leq 0
\end{aligned} \tag{3.48}$$

Since $(M\,B)^{-1} \neq 0$, $\xi_i(y_i) > 0$ and $\tau_i > 0$, hence (3.48) implies that the driven system's states, x_i, and the slave system's states, y_i, are synchronized asymptotically.

3.3.3 Analysis of Robustness

When the above theorem conditions $M\,B_i = M\,B_j = M\,B$ for $i \neq j$ are not easily applicable, the imposed fuzzy synergetic control's robustness approach is improved.

Theorem 3.2

If we take into consideration the hyperchaotic synchronization problem, between the hyperchaotic Lu system (1.33) and the hyperchaotic Lorenz system [53], the driven and the drive systems are asymptotically synchronized if the fuzzy synergetic control action (3.46) is used and $M\,B_i = M\,B_j = M\,B$ for $i \neq j$.

$$\begin{aligned} u_i(t) &= u^k(t) \\ &= -\left(M\,B_k\right)^{-1}\left[M\,A_k\,y(t) + \tau_k\varphi - M\,\dot{x})\right] \\ k &= \left\{i : \max\left[\xi_1, \cdots, \xi_r\right]\right\} \end{aligned} \tag{3.49}$$

such that, $u^k(t)$ represents control law that dominates in the fuzzy rules (3.43) and the control τ_k satisfies

$$\tau_k > \tau_i \tag{3.50}$$

such that

$$\tau_i = \frac{\left\| MA_i - MB_i(MB_k)^{-1}MA_k \right\|}{\|M\| Q_{\min}\left(MB_i(MB_k)^{-1} + \left(MB_i(MB_k)^{-1}\right)^T\right)} > 0 \tag{3.51}$$

Hence, the considered hyperchaotic systems are asymptotically synchronized.

Proof

Let us choose $Z = 0.5\,\varphi^T\varphi$ as a Lyapunov function candidate. Therefore, its time derivative is

$$\dot{Z} = \varphi^T\varphi \tag{3.52}$$

hence

$$\begin{aligned} \dot{Z} &= \varphi^T M\left(\sum_{i=1}^{2}\xi_i(y_1)A_i y(t) + \sum_{i=1}^{2}\xi_i(y_1)u_i(t) - \sum_{i=1}^{2}\xi'_i(x_1)A_i x(t)\right) \\ &= \varphi^T\left(\sum_{i=1}^{2}M\,\xi_i(y_1)A_i y(t) - \sum_{i=1}^{2}\xi_i(y_1)MB_i\left((MB_k)^{-1}\left[MA_k y(t) + \tau_k\varphi\right]\right)\right) \\ &= \sum_{i=1}^{2}\xi_i(y_1)\varphi^T\left(\left(MA_i - MB_i(MB_k)^{-1}MA_k\right)y(t) - MB_i(MB_k)^{-1}\tau_k\varphi\right) \end{aligned} \tag{3.53}$$

Let $Q_{\min} > 0$ be the smallest eigenvalue of the matrix $\left(\left(MB_i(MB_k)^{-1}\right)^T + MB_i(MB_k)^{-1}\right)$. Hence, the minimization of (3.52) can be determined as

$$\begin{aligned}\dot{Z} \le -\sum_{i=1}^{2}\xi_i(y_1)\|y(t)\|\Big(Q_{\min}\left(MB_i(MB_k)^{-1}\right)^T \\ +MB_i(MB_k)^{-1}\tau_k\|M\| - \left\|MA_i - MB_i(MB_k)^{-1}MA_k\right\|\Big)\|\varphi\| \\ \le 0\end{aligned} \tag{3.54}$$

where the gain condition (3.50) has been implemented. Since (3.54) implies $\dot{Z} \le 0$, it can be inferred that the global stability and the asymptotical synchronization are guaranteed.

3.3.4 Simulation Results

Intending to validate the effectiveness and benefits of the suggested strategy, we provide an application example proceeded from the hyperchaotic Lorenz system. Figure 3.8 depicted a simplified schematic of the proposed synchronization approach, as well as the interconnections of the used techniques.

The following form represents the hyperchaotic Lorenz system [53]

$$\begin{cases}\dot{x}_1 = a'(x_2 - x_1) \\ \dot{x}_2 = b'x_1 - x_2 - x_1x_3 + x_4 \\ \dot{x}_3 = c'x_1 + x_1x_2 \\ \dot{x}_4 = k_1x_1 + k_2x_2\end{cases} \tag{3.55}$$

where x_1, x_2, x_3 and x_4 symbolize the state variables. The system (3.55) exhibits hyperchaotic behavior for the following parameter values $k_1 = -9.3, k_2 = 1, a' = 10, b' = 28$ and $c' = 8/3$.

The Takagi-Sugeno fuzzy model for the hyperchaotic Lorenz system (3.55) is presented in [54]. where

$$A'_1 = \begin{bmatrix}-a' & a' & 0 & 0 \\ b' & -1 & -\alpha & 1 \\ -c' & \alpha & 0 & 0 \\ k_1 & k_2 & 0 & 0\end{bmatrix},\ A'_2 = \begin{bmatrix}-a' & a' & 0 & 0 \\ b' & -1 & \alpha & 1 \\ -c' & -\alpha & 0 & 0 \\ k_1 & k_2 & 0 & 0\end{bmatrix},\ \xi'_1 = \frac{1}{2}\left(1 + \frac{x_1(t)}{\alpha}\right) \text{and } \xi'_2 = \frac{1}{2}\left(1 - \frac{x_1(t)}{\alpha}\right).$$

To achieve effective synchronization between the above hyperchaotic systems using the fuzzy synergetic technique, the control gain is set to be $\tau_k = 9$. Also $Q_{\min} > 0$ is satisfied for all i and k. Also, in order to verify the simulation results of the proposed synchronization

approach, we have tested this scheme with the results of the SMC technique [13]. Such that, the control input signal is disabled for $t < 6s$ and is enabled otherwise.

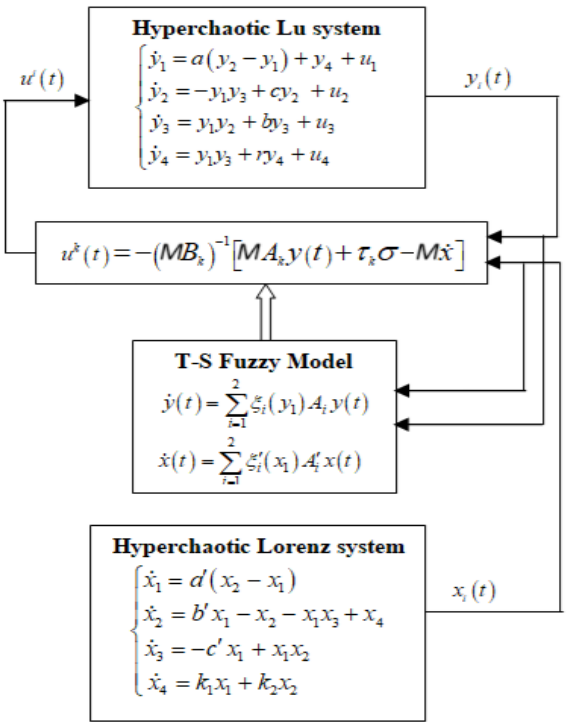

Figure 3.8 The fuzzy synergetic controller scheme.

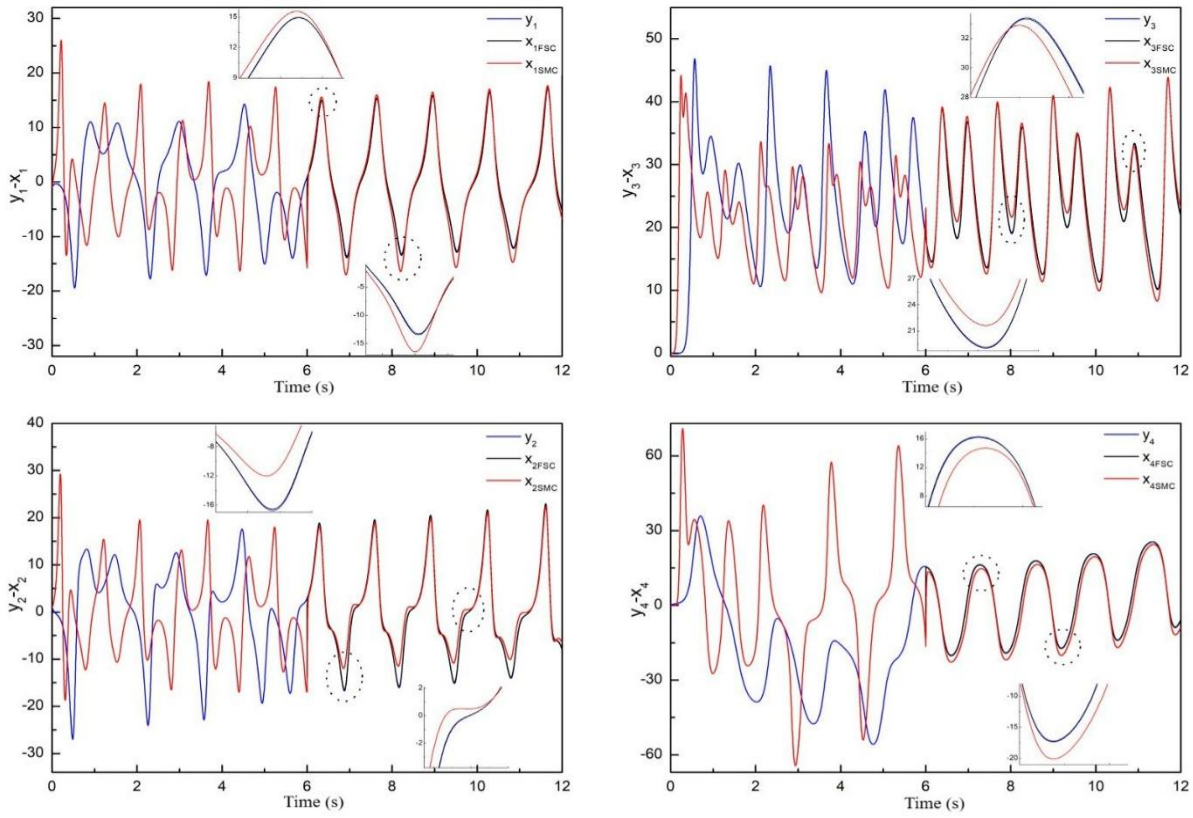

Figure 3.9 Synchronization results for the first proposition.

To begin, the Lu system is proposed to act as the master system. Let $y(0) = x(0) = [-1 \quad 1 \quad -0.1 \quad 0.1]$ be the initial conditions for the master and the response systems.

The variable states of the synchronized dynamics, between the hyperchaotic Lu (y_i , master) and Lorenz (x_i , driven) systems, are clearly achieved through chaos synchronization. The zoomed time frames in Figure 3.9 show the fuzzy synergetic control technique converges drive states faster and more accurately than the other method.

For the second proposition, the hyperchaotic Lorenz system is viewed as a master system. The initial conditions are chosen as $x(0) = y(0) = [5,8,-1,-2]$ for both systems, the drive and the response systems.

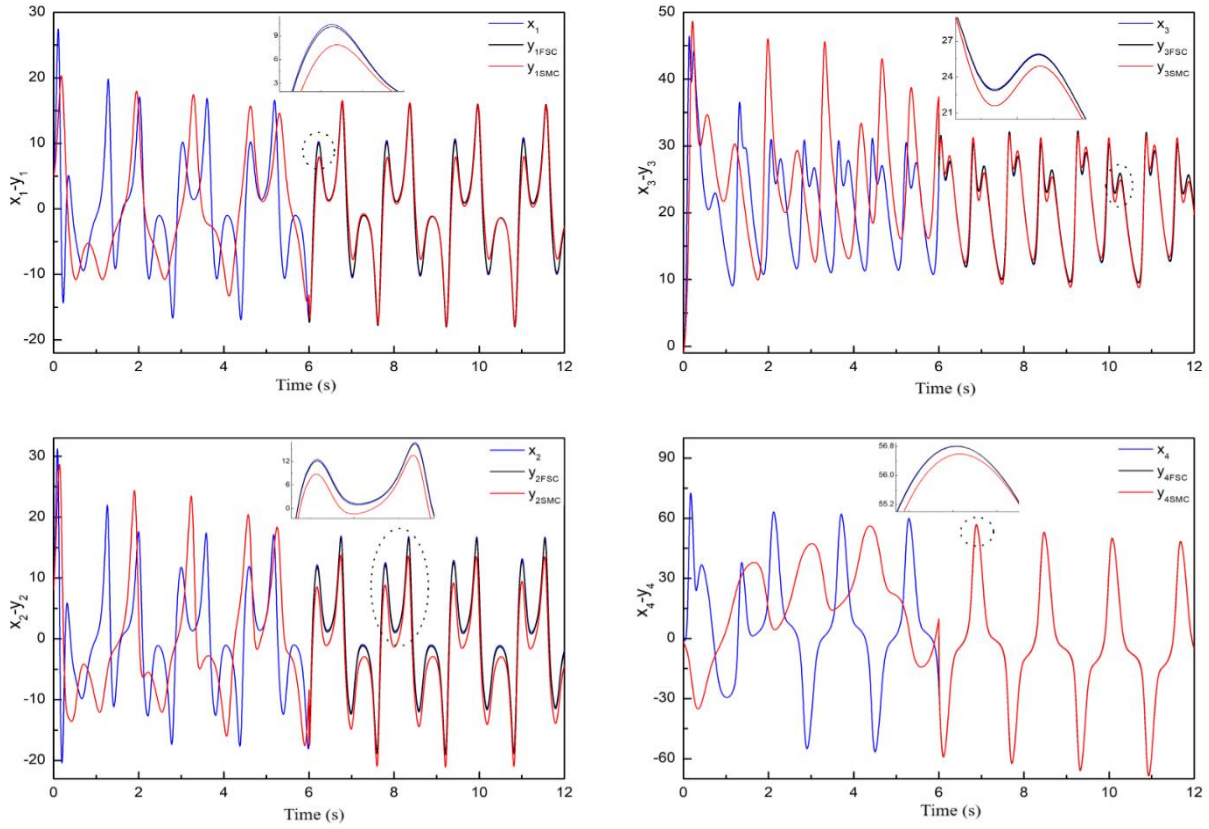

Figure 3.10 Synchronization results for the first proposition.

Numerical simulation results are shown in Figure 3.10, which illustrates that the suggested technique is effective in synchronizing the two systems contrasted with the results of the sliding mode control method. From all the simulations, we achieved very satisfactory results and they show that this control procedure works well.

3.4 Conclusion

In conclusion, a fuzzy logic system is a methodology based on an experienced operator for managing or modeling a system utilizing fuzzy terms that fetch up from our natural language through a set of rules that may be applied in a variety of contexts.

In this part of the work, we discussed that the hyperchaotic systems can be exactly modeled using the Takagi-Sugeno fuzzy modeling technique. Also, we have presented a robust controller for hyperchaotic systems' synchronization with the aid of a synergetic control approach cooperated with Takagi-Sugeno fuzzy properties. The stability analysis has been carried out using Lyapunov stability theory. Finally, the simulation results using MATLAB have been illustrated to demonstrate the effectiveness of the FSC method.

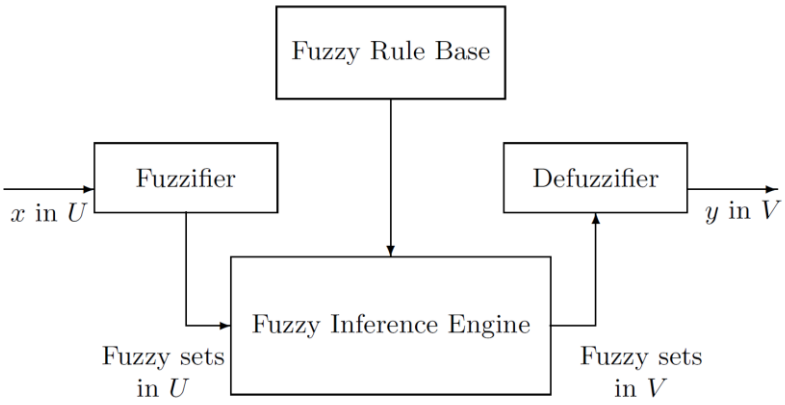

Figure 3.11 Block diagram of fuzzy system.

Chapter 4. Synchronization of Chaotic Oscillator Systems Based on Adaptive Synergetic Control Theory

4.1 Introduction

A non-autonomous dynamical system has more complex dynamical behavior compared to an autonomous system due to its vector fields change over time [55]. The dynamics of non-autonomous systems is an interesting and significant subject for research. Numerous studies have been conducted to investigate, for example, a non-autonomous chaotic system with no equilibrium [56], a novel non-autonomous chaotic system with an infinite 2-D lattice of attractors and bursting oscillations [57], a simple nonautonomous hidden chaotic system with a switchable stable node-focus [58].

With the aim of tracking a desired path under uncertain parameters and external disturbances, the control of uncertain chaotic systems has attracted increasing attention from research communities and has been extensively studied [18], [59]. furthermore, different methods for uncertain chaotic systems synchronization have been presented, including adaptive control methods, back-stepping control methods, sliding mode methods, and many others [60]–[63].

The sensitivity to initial conditions is the main problem with chaotic systems. Therefore, for practical plans, the systems suffer from external disturbances and parameter uncertainties. On the other hand, the system states attain the desirable references in undesired infinite time. To handle this important issue, our hamble work, synchronization of chaotic oscillator systems based on adaptive synergetic control theory [15], deals effectively with the influence produced by the system uncertainties and external noise even when their upper bounds are unknown. This work is inspired by the terminal sliding mode techniques and by finite-time stability theory [64], [65].

This section presents an adaptive finite-time synergetic controller for chaotic synchronization between two distinct chaotic systems, Van der Pol and Duffing oscillators. The controller is fed with synchronization error signals and has an adaptive controller gain. The suggested adaptive controller can ensure synchronization and anti-synchronization processes even in the presence of system parameters uncertainties and external disturbances. The Lyapunov stability theorem is used to establish the necessary criteria for stable synchronization. Furthermore, numerical simulations are performed to evaluate the efficiency of the provided approach.

4.2 System Descriptions and Objective of The Study

It is well-known that mathematically simple nonlinear systems of ordinary differential equations can result in chaos. A variety of dynamical systems are modeled as self-excited forced oscillators [66], [67]. Duffing oscillators and Van der Pol are the most widely studied systems; They represent a range of nonlinear dynamical behaviors such as chaos, elementary bifurcations, and quasi-periodic oscillations. These oscillators exposed to harmonic parametric stimulation are defined by the nonautonomous second-order differential equations (4.1) and (4.2), respectively.

$$\ddot{y} + \mu(1-y^2)\dot{y} + \frac{dV(y)}{dy} = f(t) \tag{4.1}$$

$$\ddot{y} + \lambda\dot{y} + \frac{dV(y)}{dy} = f(t) \tag{4.2}$$

where, y is the state variable, μ and λ are damping parameters, and $f(t) = f_0\cos(wt)$ is the external excitation with amplitude f_0 and angular frequency w. $V(y)$ represents the potential. It is approximated by a finite Taylor series. Three distinct potentials $V(y)$ were introduced in [68], [69] are

$$V_2(y) = \frac{1}{2}\alpha y^2 \tag{4.3}$$

$$V_4(y) = \frac{1}{2}\alpha y^2 + \frac{1}{4}by^4 \tag{4.4}$$

$$V_6(y) = \frac{1}{2}\alpha y^2 + \frac{1}{4}by^4 + \frac{1}{6}cy^6 \tag{4.5}$$

where, α, b and c are the potentials' positive constant parameters.

When α is strictly positive, the potential $V_2(y)$ in (4.3) is a single well. The potential $V_4(y)$ in (4.4) has three conditions, that are, single well when both α and b are strictly positive, double well for $\alpha < 0, b > 0$, and double-hump when $\alpha > 0, b < 0$. The potential $V_6(y)$ in equation (4.5) is double well when α, b and c are strictly negative, double-hump when $\alpha > 0, b < 0, c < 0$, triple well for $\alpha > 0, b < 0, c > 0$, and triple-hump for $\alpha < 0, b > 0, c < 0$ [70].

By substituting the potential $V_6(y)$ in (4.5) into (4.1) and (4.2), the mathematical models of the described oscillators are represented by the general forms of nonautonomous differential equations as

$$\ddot{y} + \mu(1-y^2)\dot{y} + ay + by^3 + cy^5 = f(t) \tag{4.6}$$

$$\ddot{y} + \lambda\dot{y} + ay + by^3 + cy^5 = f(t) \tag{4.7}$$

respectively.

This study aims to develop an adaptive controller for synchronizing and anti-synchronizing chaotic oscillators, taking into consideration external disturbances and system uncertainties. Let us define the Van der Pol equation as the drive system

$$\begin{cases} \dot{y}_1 = y_2 \\ \dot{y}_2 = \mu(1-y_1^2)y_2 - ay_1 - by_1^3 - cy_1^5 + f(t) \end{cases} \tag{4.8}$$

Consider the following Duffing oscillator as the response system

$$\begin{cases} \dot{x}_1 = x_2 \\ \dot{x}_2 = -\lambda x_2 - ax_1 - b'x_1^3 - c'x_1^5 + f'(t) + d(t) + \Delta(x_1, x_2) + u(t) \end{cases} \tag{4.9}$$

where $y = [y_, y_2]$ and $x = [x_1, x_2]$ are the state variables of the drive and response systems, respectively. $\Delta(x_1 x_2)$ represents the parameter uncertainties. $d(t)$ denotes the external disturbance. $u(t)$ is the control input signal to be designed.

The system uncertainty and the external noise are assumed to be bounded and satisfy the following condition

$$0 < \left| d(t) + \Delta(x_1, x_2) \right| < D \tag{4.10}$$

where D represents a positive constant that has not been predetermined for the design of the proposed adaptive controller.

let the synchronization error states between the master (4.8) and the slave system (4.9) be

$$e_i(t) = x_i(t) - \Lambda y_i(t) \tag{4.11}$$

Λ is a scaling factor that determines the relationship between the two systems, taking the value of 1 for synchronization and -1 for anti-synchronization.

Combining (4.8) and (4.9), the synchronization tracking error dynamic system can be expressed as

$$\begin{cases} \dot{e}_1(t) = e_2(t) \\ \dot{e}_2(t) = \eta e_2(t) - a e_1(t) + g(x,y) + \Delta(x_1, x_2) + d(t) + u(t) \end{cases} \tag{4.12}$$

such that, $\eta = \mu - \lambda$ and the function $g(x,y)$ is a continuous nonlinear function that can be found mathematically.

In this application, it is assumed to be unknown and has an upper bound, as given in the following condition

$$\left| g(x,y) \right| < F \tag{4.13}$$

System uncertainties, external disturbances, and nonlinear terms, which may not be suitable for practical applications, have to be compensated by the designed controller.

4.3 Synchronization Controller Design

A Terminal Adaptive Synergetic Controller (TASC) is suggested in this part to overcome both synchronization and the previously mentioned drawbacks. The proposed method involves selecting a suitable macro-variable σ that fulfills the required dynamic evolution and constructs a robust controller to drive any state trajectories to converge to the manifold $\sigma = 0$ and then move along it toward the origin. Now, the terminal synergetic macro-variable has been formed as a nonlinear function of the tracking error and can be represented as follows

$$\sigma(t) = e_1(t) + \frac{1}{\alpha} e_2(t)^{\gamma} \tag{4.14}$$

where $1 < \gamma = \frac{p_1}{p_2} < 2$ and p_1, p_2 are positive odd integers.

With the aim to guarantee the stability and to ensure the convergence of the state trajectories to their corresponding target manifolds and stick on it for afterward time, the macro-variable, shown in equation (4.14), evolves with a desired dynamic evolution chosen as

$$\dot{\sigma}(t) + \tau \sigma(t) = 0 \quad , \quad \tau > 0 \tag{4.15}$$

where τ express the rate of convergence of the macro-variable to manifold $\sigma(t) = 0$. When the system achieves the terminal attractor $\sigma = 0$, the equation (4.14) can be expressed as

$$\dot{e}_1(t) = -\left[\alpha e_1(t)\right]^{\frac{1}{\gamma}} \tag{4.16}$$

Therefore, we can get

$$dt = -\frac{1}{\alpha^{\frac{1}{\gamma}}} e_1(t)^{-\frac{1}{\gamma}} de_1 \tag{4.17}$$

Integrating both sides of (4.17) over the closed interval from $e_1(t_s) \neq 0$ to $e_1(t_f) = 0$, it yields the following equation

$$t_f = \frac{\gamma \alpha^{-\frac{1}{\gamma}}}{(\gamma - 1)} \left|e_1(t_s)\right|^{\frac{\gamma-1}{\gamma}} \tag{4.18}$$

where t_f is finite, indicating convergence within a finite time frame, as opposed to the asymptotic infinite-time convergence to the attractor $\sigma = 0$.

With the goal of establishing synchronization and anti-synchronization among chaotic oscillators (4.8) and (4.9), this TASC approach is inspired by sliding mode techniques, which will be used to develop the suggested adaptive terminal synergetic control rule given in the following theorem.

Theorem 4.1

Consider the synchronization problem of the chaotic oscillators (4.8) and (4.9). If the control action $u(t)$ is designed using the terminal synergetic manifold function (4.14). the control input is described by the following specified equation

$$u(t) = ae_1(t) - \eta e_2(t) - \Gamma e_2(t)^{2-\gamma} - \hat{\tau}(t) - \sigma(t) \tag{4.19}$$

and the control gain $\hat{\tau}(t)$ is adjusted according to the adaptive law defined as follows

$$\dot{\hat{\tau}}(t) = r\left|e_2(t)\right|^{\gamma-1} \sigma(t)^2 \tag{4.20}$$

where $\Gamma = \frac{\alpha}{\gamma}$. r is designed finite positive constant. Then, the synchronized error states will converge to zero in a finite-time.

Proof

Let us select the following Lyapunov function candidate

$$V(t) = \frac{1}{2}\sigma(t)^2 + \frac{1}{2\Gamma r}\left(\hat{\tau}(t) - \hat{\tau}^0\right)^2 \tag{4.21}$$

where $\hat{\tau}^0$ is the optimal parameter value that satisfies the following condition

$$\hat{\tau}^0 > F + D \tag{4.22}$$

Taking the first-time derivative of the equation (4.21) and substituting (4.20) into it, while considering (4.10) and (4.13), gives

$$\begin{aligned} \dot{V} &= \sigma(t)\dot{\sigma}(t) + \frac{1}{\Gamma r}(\hat{\tau}(t) - \hat{\tau}^0)\dot{\hat{\tau}}(t) \\ &\le \sigma(t)^2 \frac{1}{\Gamma} e_2(t)^{\gamma-1}(F + D - \hat{\tau}(t)) - \frac{1}{\Gamma}\hat{\tau}^0\sigma(t)^2 e_2(t)^{\gamma-1} + \frac{1}{\Gamma}\hat{\tau}\sigma(t)^2 e_2(t)^{\gamma-1} \end{aligned} \tag{4.23}$$

Here, if considering that $e_2(t) \neq 0$ in this case, and according to γ, there exists $e_2(t)^{\gamma-1} > 0$, then the Lyapunov condition is satisfied as follows

$$\dot{V} \le \sigma(t)^2 \frac{1}{\Gamma} e_2(t)^{\gamma-1}\left[\hat{\tau}^0 - (F + D)\right] \le 0 \tag{4.24}$$

Now consider the opposite of the above case, i.e. $e_2(t) = 0$, and taking the time derivative of $\sigma(t) = e_2$ with a constant controller gain in the equation (4.19), i.e. $\hat{\tau}(t) = \hat{\tau}^0$, one can obtain

$$\dot{\sigma}(t) = \dot{e}_2(t) = -g(x, y) + \Delta(x_1, x_2) + d(t) - \hat{\tau}^0\sigma(t) \tag{4.25}$$

In this case, choosing the Lyapunov function candidate as $V_1 = \frac{1}{2}\sigma(t)^2$, and taking its derivative yields

$$\dot{V}_1 = \sigma(t)\dot{\sigma}(t) \le \sigma(t)^2\left[F + D - \hat{\tau}^0\right] \le 0 \tag{4.26}$$

Fulfilling requirements (4.24) and (4.26) ensures Lyapunov stability analysis and synchronized error states converge to zero in a finite time.

4.4 Numerical simulation

The main simulation results of the proposed TASC controller are presented in this section. First, for the parameter values $\mu = 0.4$, $a = 1$, $b = -0.7$, $c = 0.1$ and $f(t) = 9\cos(\pi t)$, we plot the Van der Pol phase space and show that it exhibits chaotic dynamics, as depicted in Figure 4.1. Similarly, the Duffing oscillator demonstrates chaotic dynamics in the phase space, as

depicted by the chaotic attractor in Figure 4.2, For the parameter values $\lambda = 0.01$, $a = 1$, $b' = -0.495$, $c' = 0.05$ and $f'(t) = 0.78\cos(\frac{\pi}{6}t)$.

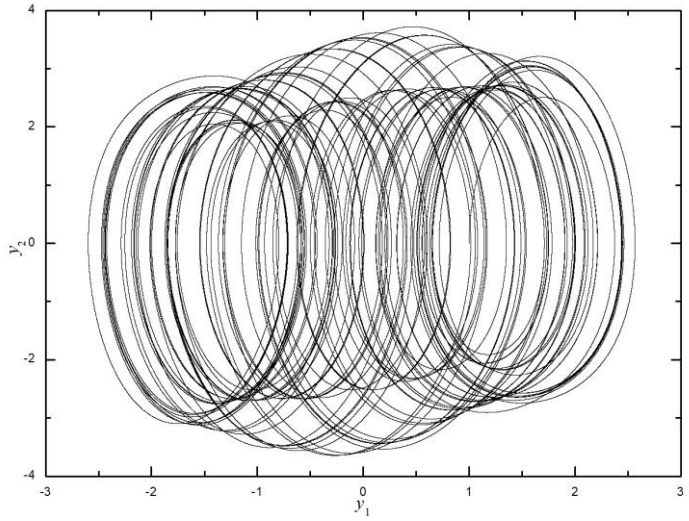

Figure 4.1 Van der pol oscillator.

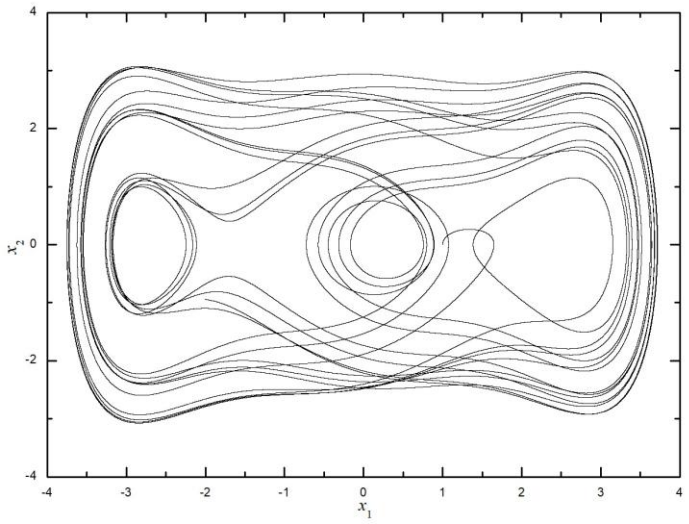

Figure 4.2 Duffing oscillator.

Next, to examine convergence time and rapid response, the proposed control algorithm's trajectory performance responses are compared to those of an adaptive synergetic controller (ASC) design in both synchronization and anti-synchronization cases.

The ASC design is performed using the same steps as in constructing the TASC controller and with the same controller parameters, except for the parameters p_1 and p_2, which are equal. In all numerical simulations, the initial value of the adaptive parameter in equation (4.20) is chosen as $\hat{\tau}(0) = 0$.

The external disturbance and system uncertainty are assumed to be $d(t)=\sin(\pi t)$ and $\Delta(x_1,x_2)=\sin(x_1)\sin(x_2)$, respectively. The TASC controller parameter values are set to be as $\gamma=\frac{5}{3}$, $\alpha=0.9$ and $r=1/10$.

Case 1: In this case, a synchronization test is carried out. Two distinct sets of initial conditions are chosen as $y(0)=[0,0]$ for the master system (4.8) and $x(0)=[1,0]$ for the slave system (4.9). The control action switched on at $t=15\ s$.

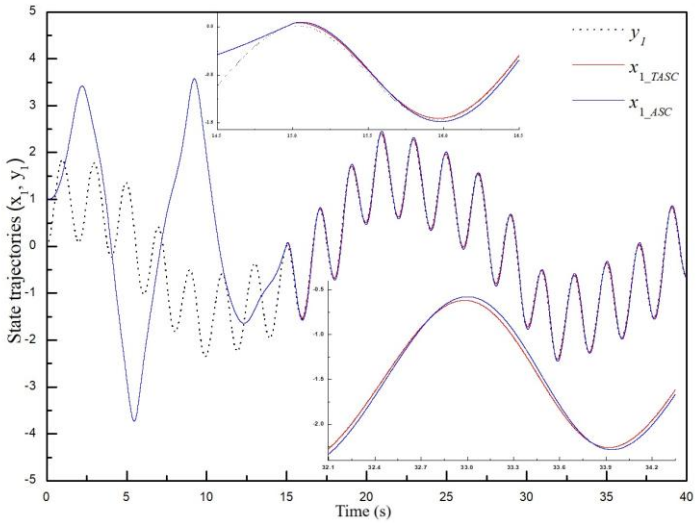

Figure 4.3 Dynamic evolution of variable states $x_1(t)$ and $y_1(t)$ for Case 1.

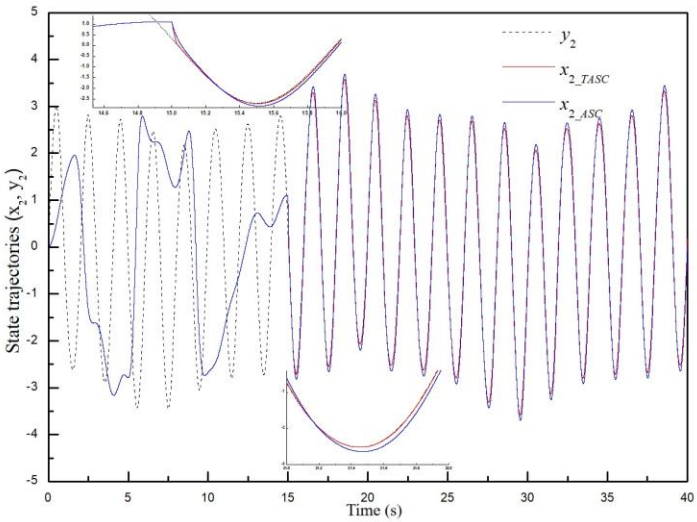

Figure 4.4 Dynamic evolution of variable states $x_2(t)$ and $y_2(t)$ for Case 1.

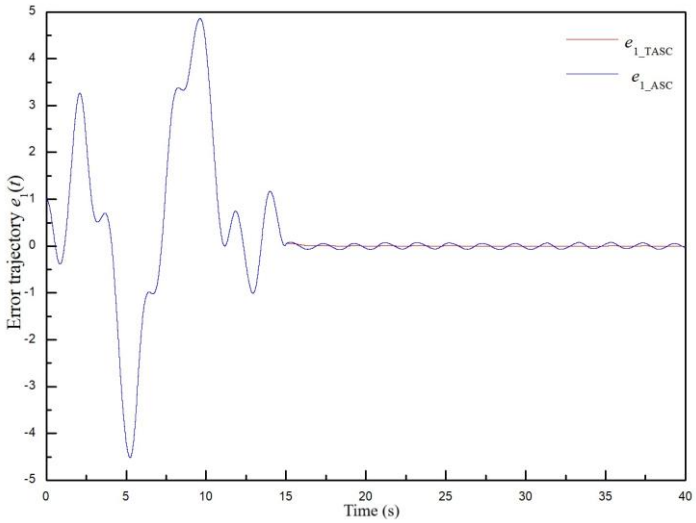

Figure 4.5 Dynamics evolution of tracking error $e_1(t)$ for Case 1.

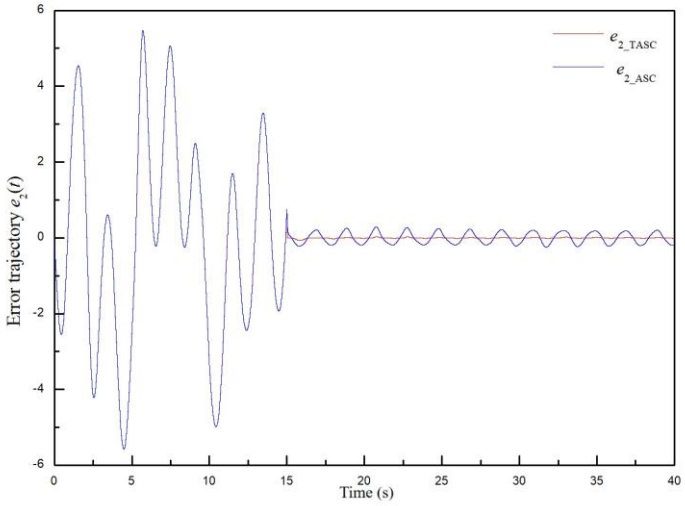

Figure 4.6 Dynamics evolution of tracking error $e_2(t)$ for Case 1.

Figure 4.3 and Figure 4.4 illustrate state trajectories of the master-slave systems. It is easy to conclude that the suggested controller effectively demonstrates and confirms superior performance in enhancing finite-time convergence and high-precision tracking with smooth signal management, without overestimating the controller gain, as shown in Figure 4.5 and Figure 4.6, respectively. From Figure 4.7, we can see the time history of the control gain $\hat{\tau}(t)$. The control signal generated by TASC to synchronize the systems is shown in Figure 4.8.

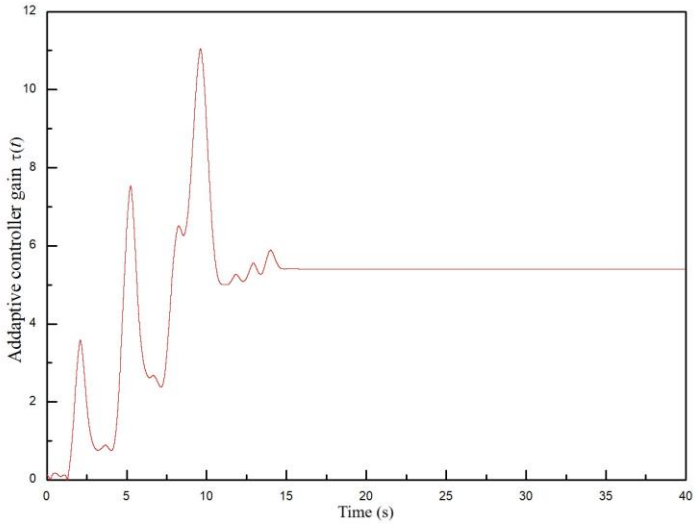

Figure 4.7 Evolution of the terminal adaptive synergetic controller gain for Case 1.

Case 2: with the same initial conditions and parameter values as given in the above case, an anti-synchronization test is simulated in this second case.

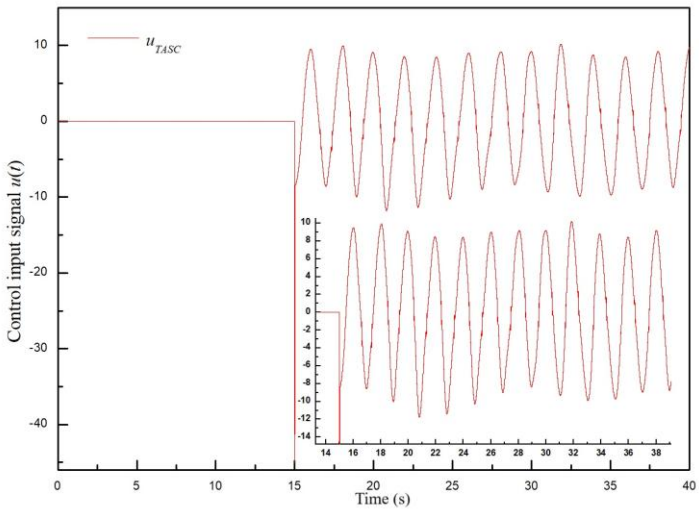

Figure 4.8 Evolution of the terminal adaptive synergetic control input signal for Case 1.

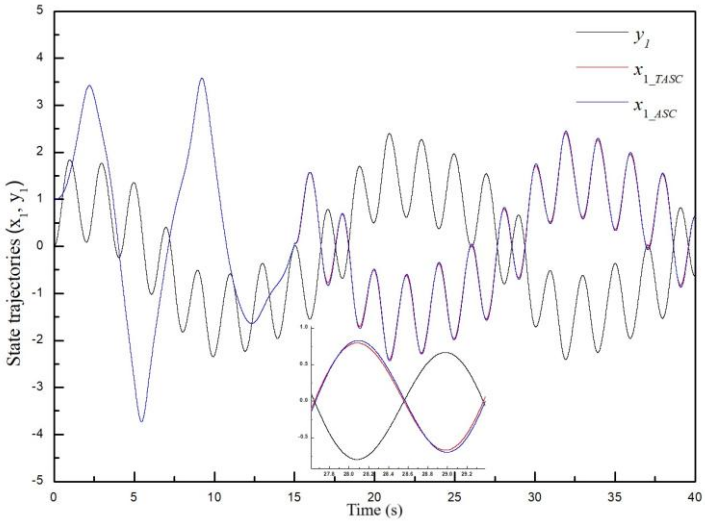

Figure 4.9 Dynamic evolution of variable states $x_1(t)$ and $y_1(t)$ for the Case 2.

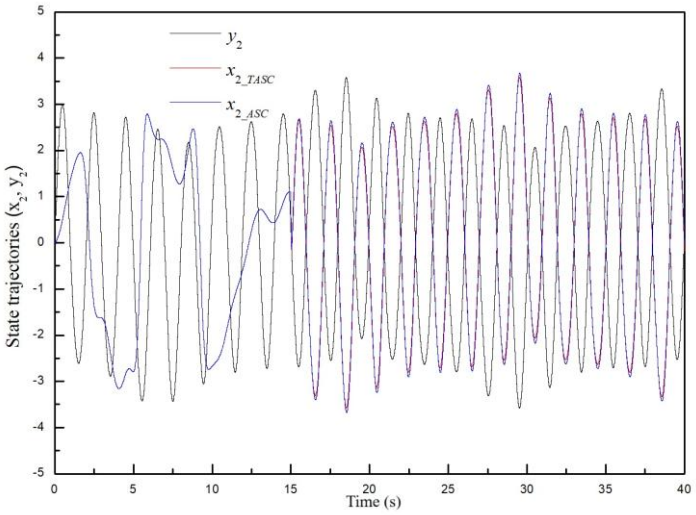

Figure 4.10 Dynamic evolution of variable states $x_2(t)$ and $y_2(t)$ for the Case 2.

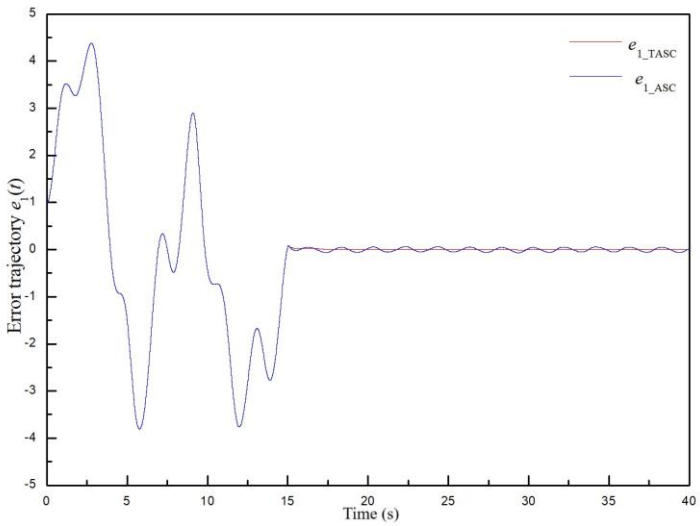

Figure 4.11 Dynamic evolution of tracking error $e_1(t)$ for the Case 2.

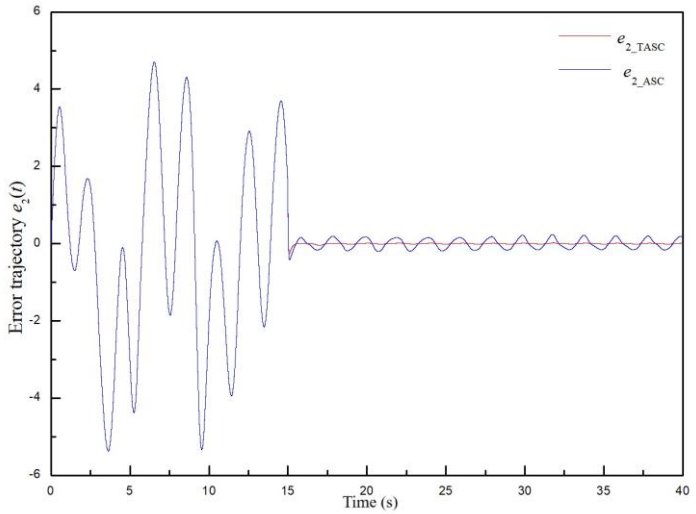

Figure 4.12 Dynamic evolution of tracking error $e_2(t)$ for the Case 2.

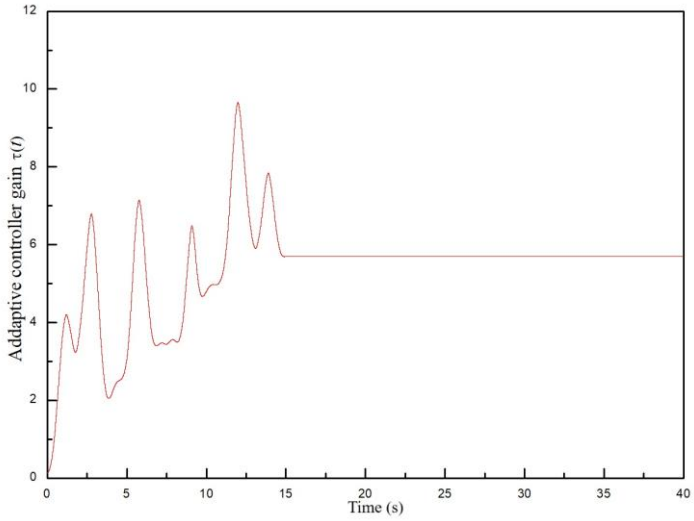

Figure 4.13 Evolution of the terminal adaptive synergetic controller gain for the Case 2.

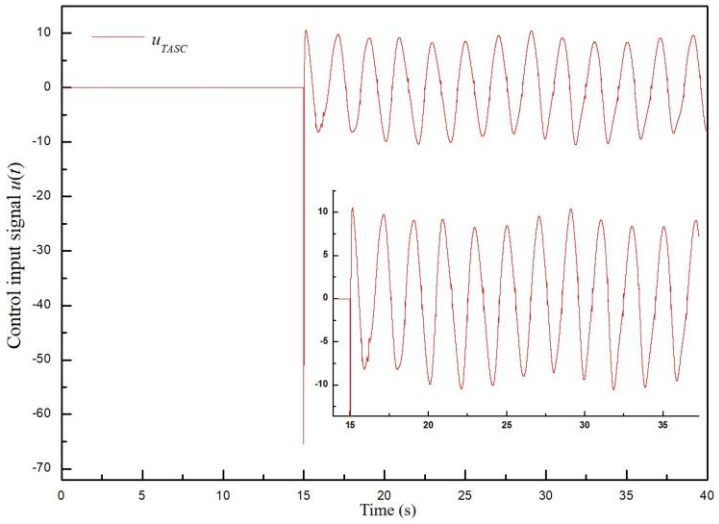

Figure 4.14 Evolution of the terminal adaptive synergetic control input signal for Case 2.

Figure 4.9 and Figure 4.10 depict the state trajectories of the anti-synchronization process. Figure 4.11 and Figure 4.12 display the tracking errors in the TASC's anti-synchronization reaction as compared to the ASC; They indicate that the TASC performs better tracking and better error variance than that based on ASC. Figure 4.13 and Figure 4.14 show the TASC's adaptive controller feedback gain and input control signal respectively. The simulation results show that the suggested method meets control objectives and provides good control performance. In comparison to the ASC, the TASC improves control response speed and provides a more desirable feedback gain controller.

4.5 Conclusion

This section discusses a terminal adaptive synergetic controller designed to achieve synchronization and anti-synchronization between two distinct chaotic oscillator systems. Unlike methods that actively suppress the nonlinear dynamic of the synchronized error systems, the suggested approach takes into consideration system uncertainties and external disturbances without requiring their boundaries to be defined in advance. Based on the Lyapunov stability theorem, sufficient conditions are provided to guarantee stable synchronization along with suitable controller gain in practical applications. Furthermore, numerical simulations are carried out in the corresponding part to validate the effectiveness and robustness of the proposed systems.

Conclusion and Perspectives

This thesis addresses three main objectives: the modeling, analysis, and control of nonlinear dynamical chaotic systems. Each chapter is dedicated to tackling specific challenges associated with these complex systems.

In the first chapter, we present the foundational concepts necessary for the qualitative and quantitative analysis of the behavior of dynamical systems. We employ both continuous-time and iterated map examples to illustrate the fundamental principles of dynamical systems theory. Through these examples, we explore key concepts such as stability, bifurcations, and chaos, setting the groundwork for understanding the more advanced topics covered in subsequent chapters.

The second chapter focuses on the control problem of synchronizing two hyperchaotic systems, where one system has unknown parameters. Hyperchaotic systems, characterized by having more than one positive Lyapunov exponent, pose significant challenges due to their complex and unpredictable behavior. To address this, we apply an adaptive terminal sliding mode control technique. This approach not only ensures robust control of the system but also guarantees finite-time convergence, a crucial property for ensuring fast and efficient synchronization. We provide a detailed analysis of the control strategy, demonstrating its effectiveness in overcoming parameter uncertainties and external disturbances.

In the third chapter, we shift our attention to chaos modeling and synchronization. We introduce a fuzzy rule-based Takagi-Sugeno model, which provides an efficient representation of a hyperchaotic system. The advantage of this model lies in its ability to capture the system's nonlinear behavior while offering a structure that is amenable to control design. Building on this model, we apply a fuzzy control-based synergetic control technique to synchronize two different hyperchaotic systems. The synergy between fuzzy logic and synergetic control enables us to develop a robust control strategy that can handle the inherent complexities of hyperchaotic systems.

The fourth chapter is dedicated to addressing the control of chaotic systems that are subject to external disturbances and parametric uncertainties. One of the main challenges with chaotic systems is their extreme sensitivity to initial conditions, which makes them particularly vulnerable to disturbances and uncertainties. To tackle this issue, we investigate a terminal adaptive synergetic control approach. This method is designed to handle the nonlinear terms in the synchronization error system, account for system uncertainties, and mitigate the effects of

external noise. The result is a control strategy that offers improved robustness and reliability in the presence of uncertainties and disturbances.

Furthermore, we explore the potential of using non-integer order (fractional) differential equations to model chaotic systems with greater accuracy. Fractional-order systems have shown promise in capturing the complex dynamics of chaotic systems more precisely. In future work, we aim to extend this research by developing robust controllers specifically tailored for time-delayed fractional-order chaotic systems. The incorporation of fractional-order dynamics introduces additional flexibility and precision, opening up new paths for controlling complex systems in real-world applications.

Bibliography

[1] R. Devaney, *An introduction to chaotic dynamical systems*. CRC press, 2018.

[2] S. H. Strogatz, *Nonlinear Dynamics and Chaos With Applications to Physics, Biology, Chemistry, and Engineering*, 2nd ed. CRC Press, 2018. doi: https://doi.org/10.1201/9780429492563.

[3] G. Kaddoum, "Wireless Chaos-Based Communication Systems: A Comprehensive Survey," *IEEE Access*, vol. 4, pp. 2621–2648, 2016, doi: 10.1109/ACCESS.2016.2572730.

[4] A. Korolj, H. T. Wu, and M. Radisic, "A healthy dose of chaos: Using fractal frameworks for engineering higher-fidelity biomedical systems," *Biomaterials*, vol. 219, no. February, p. 119363, 2019, doi: 10.1016/j.biomaterials.2019.119363.

[5] S. Eshaghi, N. Kadkhoda, and M. Inc, "Chaos Control and Synchronization of a New Fractional Laser Chaotic System," *Qual. Theory Dyn. Syst.*, vol. 23, no. 5, p. 241, 2024.

[6] R. J. Field, *Chaos in chemistry and biochemistry*. World Scientific, 1993.

[7] L. Minati, L. V. Gambuzza, W. J. Thio, J. C. Sprott, and M. Frasca, "A chaotic circuit based on a physical memristor," *Chaos, Solitons and Fractals*, vol. 138, 2020, doi: 10.1016/j.chaos.2020.109990.

[8] A. Chen, J. Lu, J. Lü, and S. Yu, "Generating hyperchaotic Lü attractor via state feedback control," *Phys. A Stat. Mech. its Appl.*, vol. 364, pp. 103–110, 2006, doi: 10.1016/j.physa.2005.09.039.

[9] M. Bernal, A. Sala, Z. Lendek, and T. M. Guerra, *Analysis and synthesis of nonlinear control systems*. Springer, 2022.

[10] L. Lu, R. Fu, J. Zeng, and Z. Duan, "On the domain of attraction and local stabilization of nonlinear parameter-varying systems," *Int. J. Robust Nonlinear Control*, vol. 30, no. 1, pp. 17–32, 2020.

[11] A. R. Gaiduk, N. N. Prokopenko, A. V Bugakova, and M. J. Almashaal, "On the Global Stability of Nonlinear Hurwitz Control Systems," *IEEE Trans. Autom. Sci. Eng.*, vol. 21, no. 1, pp. 502–511, 2024, doi: 10.1109/TASE.2022.3225763.

[12] A. Silani, M. Cucuzzella, J. M. A. Scherpen, and M. J. Yazdanpanah, "Output regulation for voltage control in DC networks with time-varying loads," *IEEE Control Syst. Lett.*, vol. 5, no. 3, pp. 797–802, 2020.

[13] J.-J. E. Slotine and W. Li, *Applied nonlinear control*, vol. 199, no. 1. Prentice hall Englewood Cliffs, NJ, 1991.

[14] K. Behih, S. E. Saadi, and Z. Bouchama, "Hyperchaos Synchronization Using T-S Fuzzy Model Based Synergetic Control Theory," *Int. J. Intell. Eng. Syst.*, vol. 14, no. 6, pp. 588–595, 2021, doi: 10.22266/ijies2021.1231.52.

[15] S. E. Saadi, K. Behih, Z. Bouchama, N. Essounbouli, and K. Zehar, "Synchronization of chaotic oscillator systems based on adaptive synergetic control theory," *South Florida J. Dev.*, vol. 5, no. 9, p. e4352, 2024, doi: 10.46932/sfjdv5n9-014.

[16] V. I. Arnold, V. S. Afrajmovich, Y. S. Il'yashenko, and L. P. Shil'nikov, *Dynamical systems V: bifurcation theory and catastrophe theory*, vol. 5. Springer Science & Business Media, 2013.

[17] E. N. Lorenz, "Deterministic Nonperiodic Flow," *J. Atmos. Sci.*, vol. 20, no. 2, pp. 130–148, 1963, doi: 10.1175/1520-0469(1963)020<0130:DNF>2.0.CO;2.

[18] Z. Lu, L. S. Shieh, and G. R. Chen, "On robust control of uncertain chaotic systems: A sliding-mode synthesis via chaotic optimization," *Chaos, Solitons and Fractals*, vol. 18, no. 4, pp. 819–827, 2003, doi: 10.1016/S0960-0779(03)00033-X.

[19] L. Chen and G. Chen, "Fuzzy modeling, prediction, and control of uncertain chaotic systems based on time series," *IEEE Trans. Circuits Syst. I Fundam. Theory Appl.*, vol. 47, no. 10, pp. 1527–1531, 2000, doi: 10.1109/81.886983.

[20] L. A. Zadeh, "Fuzzy sets," *Inf. Control*, vol. 8, no. 3, pp. 338–353, 1965, doi: https://doi.org/10.1016/S0019-9958(65)90241-X.

[21] R. Grimshaw, "Nonlinear ordinary differential equations," *Nonlinear Ordinary Differ. Equations*, pp. 1–328, 2017, doi: 10.1201/9780203745489.

[22] W. M. Haddad and V. S. Chellaboina, *Nonlinear Dynamical Systems and Control: A Lyapunov-Based Approach*. Princeton University Press, 2011. [Online]. Available: https://books.google.dz/books?id=bUQN6Ph7YEIC

[23] H. K. Khalil, "Lyapunov stability," *Control Syst. Robot. Autom.*, vol. 12, p. 115, 2009.

[24] Y. Li, M. Yuan, and Z. Chen, "Multi-parameter analysis of transition from conservative to dissipative behaviors for a reversible dynamic system," *Chaos, Solitons & Fractals*, vol. 159, p. 112114, 2022, doi: https://doi.org/10.1016/j.chaos.2022.112114.

[25] U. Parlitz, "Estimating Lyapunov Exponents from Time Series," in *Chaos Detection and Predictability*, C. (Haris) Skokos, G. A. Gottwald, and J. Laskar, Eds. Berlin, Heidelberg: Springer Berlin Heidelberg, 2016, pp. 1–34. doi: 10.1007/978-3-662-48410-4_1.

[26] P. Frederickson, J. L. Kaplan, E. D. Yorke, and J. A. Yorke, "The liapunov dimension of strange attractors," *J. Differ. Equ.*, vol. 49, no. 2, pp. 185–207, 1983, doi: 10.1016/0022-0396(83)90011-6.

[27] R. M. May, "Simple mathematical models with very complicated dynamics," *Nature*, vol. 261, no. 5560, pp. 459–467, 1976, doi: 10.1038/261459a0.

[28] T.-Y. Li and J. A. Yorke, "Period Three Implies Chaos," *Am. Math. Mon.*, vol. 82, no. 10, pp. 985–992, Jun. 1975, doi: 10.2307/2318254.

[29] Y. Li, W. K. S. Tang, and G. Chen, "Hyperchaos evolved from the generalized Lorenz equation," *Int. J. Circuit Theory Appl.*, vol. 33, no. 4, pp. 235–251, 2005, doi: https://doi.org/10.1002/cta.318.

[30] O. E. Rossler, "An equation for hyperchaos," *Phys. Lett. A*, vol. 71, no. 2, pp. 155–157, 1979, doi: https://doi.org/10.1016/0375-9601(79)90150-6.

[31] J. LÜ and G. CHEN, "A NEW CHAOTIC ATTRACTOR COINED," *Int. J. Bifurc. Chaos*, vol. 12, no. 03, pp. 659–661, 2002, doi: 10.1142/S0218127402004620.

[32] S. Čelikovský and G. Chen, "On the generalized Lorenz canonical form," *Chaos, Solitons & Fractals*, vol. 26, no. 5, pp. 1271–1276, 2005, doi: https://doi.org/10.1016/j.chaos.2005.02.040.

[33] G. CHEN and T. UETA, "YET ANOTHER CHAOTIC ATTRACTOR," *Int. J. Bifurc. Chaos*, vol. 09, no. 07, pp. 1465–1466, 1999, doi: 10.1142/S0218127499001024.

[34] C. Friedrich and H. Braun, "Linear viscoelastic behaviour of complex polymeric materials: a fractional mode representation," *Colloid Polym. Sci.*, vol. 272, no. 12, pp. 1536–1546, 1994, doi: 10.1007/BF00664721.

[35] Y. A. Rossikhin and M. V Shitikova, "Application of fractional derivatives to the

analysis of damped vibrations of viscoelastic single mass systems," *Acta Mech.*, vol. 120, no. 1, pp. 109–125, 1997, doi: 10.1007/BF01174319.

[36] M. Rivero, J. J. Trujillo, L. Vázquez, and M. Pilar Velasco, "Fractional dynamics of populations," *Appl. Math. Comput.*, vol. 218, no. 3, pp. 1089–1095, 2011, doi: https://doi.org/10.1016/j.amc.2011.03.017.

[37] M. K. Shukla and B. B. Sharma, "Stabilization of a class of fractional order chaotic systems via backstepping approach," *Chaos, Solitons & Fractals*, vol. 98, pp. 56–62, 2017, doi: https://doi.org/10.1016/j.chaos.2017.03.011.

[38] C. A. Monje, Y. Q. Chen, B. M. Vinagre, D. Xue, and V. Feliu-Batlle, *Fractional-order Systems and Controls: Fundamentals and Applications*. Springer London, 2010. [Online]. Available: https://books.google.dz/books?id=c4fV9WeCiEwC

[39] K. Diethelm, N. J. Ford, and A. D. Freed, "A Predictor-Corrector Approach for the Numerical Solution of Fractional Differential Equations," *Nonlinear Dyn.*, vol. 29, no. 1, pp. 3–22, 2002, doi: 10.1023/A:1016592219341.

[40] M. Rivero, S. V Rogosin, J. A. Tenreiro Machado, and J. J. Trujillo, "Stability of Fractional Order Systems," *Math. Probl. Eng.*, vol. 2013, p. 356215, 2013, doi: 10.1155/2013/356215.

[41] W. Perruquetti and J. P. Barbot, *Sliding mode control in engineering*, vol. 11. Marcel Dekker New York, 2002.

[42] U. Itkis, *Control systems of variable structure*. New-York: Wiley, 1976.

[43] X. Yu, Y. Feng, and Z. Man, "Terminal Sliding Mode Control - An Overview," *IEEE Open J. Ind. Electron. Soc.*, vol. 2, no. September 2020, pp. 36–52, 2021, doi: 10.1109/OJIES.2020.3040412.

[44] A. Kolesnikov, G. Veselov, and A. Kolesnikov, "Modern applied control theory: synergetic approach in control theory," *TRTU, Moscow, Taganrog*, pp. 4477–4479, 2000.

[45] A. T. Azar and S. Vaidyanathan, *Chaos modeling and control systems design*, vol. 581. Springer, 2015.

[46] J. Zaqueros-Martinez, G. Rodriguez-Gomez, E. Tlelo-Cuautle, and F. Orihuela-Espina, "Fuzzy Synchronization of Chaotic Systems with Hidden Attractors," *Entropy*, vol. 25,

no. 3, pp. 1–23, 2023, doi: 10.3390/e25030495.

[47] T. Weng, H. Yang, J. Zhang, and M. Small, "Modeling chaotic systems: Dynamical equations vs machine learning approach," *Commun. Nonlinear Sci. Numer. Simul.*, vol. 114, p. 106452, 2022, doi: 10.1016/j.cnsns.2022.106452.

[48] T. Takagi and M. Sugeno, "Fuzzy identification of systems and its applications to modeling and control," *IEEE Trans. Syst. Man. Cybern.*, vol. SMC-15, no. 1, pp. 116–132, 1985, doi: 10.1109/TSMC.1985.6313399.

[49] L. X. Wang, *A course in fuzzy systems and control*. Prentice-Hall, 1997. [Online]. Available: https://books.google.dz/books?id=nh1SPgAACAAJ

[50] Y.-H. Song and A. T. Johns, "Applications of fuzzy logic in power systems. I. General introduction to fuzzy logic," *Power Eng. J.*, vol. 11, no. 5, pp. 219–222, 1997, doi: 10.1049/pe:19970505.

[51] Y.-L. Kuo and I. E. Citra Resmi, "Model predictive control based on a Takagi–Sugeno fuzzy model for nonlinear systems," *Int. J. Fuzzy Syst.*, vol. 21, pp. 556–570, 2019.

[52] M. T. Yassen, "Synchronization hyperchaos of hyperchaotic systems," *Chaos, Solitons and Fractals*, vol. 37, no. 2, pp. 465–475, 2008, doi: 10.1016/j.chaos.2006.09.045.

[53] Q. Yang, K. Zhang, and G. Chen, "Hyperchaotic attractors from a linearly controlled Lorenz system," *Nonlinear Anal. Real World Appl.*, vol. 10, no. 3, pp. 1601–1617, 2009, doi: 10.1016/j.nonrwa.2008.02.008.

[54] J. Wang, X. Xiong, M. Zhao, and Y. Zhang, "Fuzzy stability and synchronization of hyperchaos systems," *Chaos, Solitons and Fractals*, vol. 35, no. 5, pp. 922–930, 2008, doi: 10.1016/j.chaos.2006.05.087.

[55] X. Zhang and G. Chen, "Chaotic and non-chaotic strange attractors of a class of non-autonomous systems," *Chaos*, vol. 28, no. 2, 2018, doi: 10.1063/1.5006284.

[56] C. Li, K. Rajagopal, F. Nazarimehr, and Y. Liu, "A non-autonomous chaotic system with no equilibrium," *Integration*, vol. 79, no. October 2020, pp. 143–156, 2021, doi: 10.1016/j.vlsi.2021.04.001.

[57] M. Wang *et al.*, "A Novel Non-Autonomous Chaotic System with Infinite 2-D Lattice of Attractors and Bursting Oscillations," *IEEE Trans. Circuits Syst. II Express Briefs*, vol. 68, no. 3, pp. 1023–1027, 2021, doi: 10.1109/TCSII.2020.3020816.

[58] B. Bao, J. Luo, H. Bao, C. Chen, H. Wu, and Q. Xu, "A Simple Nonautonomous Hidden Chaotic System with a Switchable Stable Node-Focus," *Int. J. Bifurc. Chaos*, vol. 29, no. 12, 2019, doi: 10.1142/S0218127419501682.

[59] J. Zhou and M. J. Er, "Adaptive output control of a class of uncertain chaotic systems," *Syst. Control Lett.*, vol. 56, no. 6, pp. 452–460, 2007, doi: 10.1016/j.sysconle.2006.12.002.

[60] M. P. Aghababa and B. Hashtarkhani, "Synchronization of unknown uncertain chaotic systems via adaptive control method," *J. Comput. Nonlinear Dyn.*, vol. 10, no. 5, p. 51004, 2015.

[61] J. Sun, Z. Shan, P. Liu, and Y. Wang, "Backstepping Synchronization Control for Three-Dimensional Chaotic Oscillatory System via DNA Strand Displacement," *IEEE Trans. Nanobioscience*, vol. 22, no. 3, pp. 511–522, 2023, doi: 10.1109/TNB.2022.3213946.

[62] Q. Yao, "Synchronization of second-order chaotic systems with uncertainties and disturbances using fixed-time adaptive sliding mode control," *Chaos, Solitons and Fractals*, vol. 142, no. xxxx, p. 110372, 2021, doi: 10.1016/j.chaos.2020.110372.

[63] A. S. TEWA KAMMOGNE, V. FOPA MAWAMBA, and J. KENGNE, "Robust prescribed-time stabilization for fuzzy sliding mode synchronization for uncertain chaotic systems," *Eur. J. Control*, vol. 59, pp. 29–37, 2021, doi: 10.1016/j.ejcon.2021.01.007.

[64] A. Modiri and S. Mobayen, "Adaptive terminal sliding mode control scheme for synchronization of fractional-order uncertain chaotic systems," *ISA Trans.*, vol. 105, pp. 33–50, 2020, doi: 10.1016/j.isatra.2020.05.039.

[65] N. Zerroug, M. N. Harmas, S. Benaggoune, Z. Bouchama, and K. Zehar, "DSP-based implementation of fast terminal synergetic control for a DC–DC Buck converter," *J. Franklin Inst.*, vol. 355, no. 5, pp. 2329–2343, 2018, doi: 10.1016/j.jfranklin.2018.01.004.

[66] J.-M. Ginoux and J. Llibre, "A family of periodic orbits for the extended Hamiltonian system of the Van der Pol oscillator," *J. Geom. Phys.*, vol. 183, p. 104705, 2023.

[67] O. M. Njimah, J. Ramadoss, A. N. K. Telem, J. Kengne, and K. Rajagopal, "Coexisting oscillations and four-scroll chaotic attractors in a pair of coupled memristor-based

Duffing oscillators: Theoretical analysis and circuit simulation," *Chaos, Solitons & Fractals*, vol. 166, p. 112983, 2023.

[68] M. S. Siewe, F. M. M. Kakmeni, and C. Tchawoua, "Resonant oscillation and homoclinic bifurcation in a Φ6-Van der Pol oscillator," *Chaos, Solitons & Fractals*, vol. 21, no. 4, pp. 841–853, 2004.

[69] A. N. Njah and U. E. Vincent, "Chaos synchronization between single and double wells Duffing–Van der Pol oscillators using active control," *Chaos, Solitons & Fractals*, vol. 37, no. 5, pp. 1356–1361, 2008.

[70] A. N. Njah, "Synchronization via active control of identical and non-identical Φ6 chaotic oscillators with external excitation," *J. Sound Vib.*, vol. 327, no. 3–5, pp. 322–332, 2009.